MSc. Thesis – B. Patterson

McMaster University – Biochemistry and Biomedical Sciences

Paternal obesity is associated with hypoxia and angiogenesis in female placentae and mediates placental development

McMaster University – Biochemistry and Biomedical Sciences

Paternal obesity is associated with hypoxia and angiogenesis in female placentae and mediates placental development

By

Brendan Patterson, BSc. (Honours)

A thesis submitted to the School of Graduate Studies in partial fulfillment of the requirements for the degree Master of Science

McMaster University Master of Science (2018) Hamilton, Ontario (Biochemistry and Biomedical Sciences)

TITLE:	Paternal obesity is associated with hypoxia and angiogenesis in female placentae and mediates placental development
Author:	Brendan Patterson, BSc. (Honours)
Supervisor:	Dr. Deborah M. Sloboda
Number of pages:	116

Abstract

While the impacts of maternal obesity on placental development have been extensively studied, the role of the father's health in regulating placentation is less understood. Paternal obesity is associated with offspring metabolic dysfunction, but the mechanism regulating this association is unclear. We investigated how paternal diet-induced obesity impacted placental vascular development, associated cellular stress pathways, and markers of placental endocrine function and macronutrient transport across gestation in a murine model. We found that paternal obesity is associated with placental hypoxia as measured by CAIX and HIF1α at E14.5 which persisted to E18.5. Hypoxia was associated with increased VEGF protein levels, as well as its pro-angiogenic receptor, VEGFR2 in male and female E14.5 placentae, although, this increase was apparent only in females at E18.5. The proportion of placental tissue that was immunopositive for the endothelial cell marker CD31 was increased in female but not male E18.5 placentae. Paternal obesity was associated with cellular stress as measured by the three branches of the unfolded protein response (UPR): ATF6, PERK, and IRE1α. However, despite increased phosphorylation of PERK and IRE1α in placental tissue derived from obese fathers, there was no impact on downstream signal transducers. Pro-apoptotic Bcl2 family members' transcript levels were reduced at E18.5 in placentae from obese fathers, but this did not correspond to any changes in cleaved casp-3 protein levels. Placental lactogen and macronutrient transporter transcript levels were similar between groups across gestation, although *Igf2* transcripts were increased in female placenta from obese fathers at both mid and late gestation. Thus, paternal obesity results in placental hypoxia and VEGF mediated sex specific changes in vascularization with a pro-angiogenic response occurring in females. Future studies will

investigate whether paternal obesity impairs early placental implantation, resulting in poor vascularization and hypoxia at E18.5.

Acknowledgements

First, to my supervisor Dr. Deborah Sloboda, thank you for your tremendous amount of help over these past three and a half years of volunteering and working in your lab. I know I wouldn't be close to half the scientist I am today without your guidance and supervision. I'd also like to thank my committee members, Dr. Alison Holloway and Dr. Sandy Raha in addition to Dr. Deborah Sloboda for pushing me further than I thought was possible, leading to my academic success and scientific achievement in the Sloboda lab

I'd like to thank every past and current member of the Sloboda lab for their support and kindness during my time here. Thank you Leon, Haider, and Kennedy for making my Sloboda lab undergrad life as fun as it was. Thank you Wajiha, Jessica W., and Tati for guiding me in my early time in the Sloboda lab, without you I would have been so helplessly lost. Thank you Kate, you not only made all my presentations much prettier than they had any right to be, but also always knew what I needed to hear, and somehow managed to help me keep my head on straight even when I freaked out in the lab (which definitely happened much more than it needed to). Thank you Patrycja for helping me with (every?) animal collection I ever had and for always being there when I needed help with GTTs. Thank you Christian and Jessica B. for all your encouragement and support and for helping me make my presentations and experiences at conferences that much better. Thank you Dr. Luseadra Mckerracher for all your stats wisdom.

Last but not least, I'd like to thank two of my dearest friends, TJ Poplar and Ella Hantho. Thank you TJ for sharing your magical gift of making everyone around you smile, and also for assisting with lab work from time to time. Thank you Ella for your absurd amounts of compassion and support, and for everything you've taught me. Thank you both for everything.

Table of contents

List of figures and tables

Abbreviations

ANOVA	Analysis of variance
APS	Ammonium persulfate
ATF	Activating transcription factor
AUC	Area under the curve
B2m	Beta-2-microglobulin
Bad	Bcl2-associated death promoter
Bax	Bcl2-associated X protein
BCA	Bicinchoninic acid assay
Bcl2	B-cell lymphoma 2
Bid	BH3 interacting-domain death agonist
Bim	Bcl2-like protein 11
BLAST	Basic local alignment search tool
BMI	Body mass index
bp	Base pair
BSA	Bovine serum albumin
CAIX	Carbonic anhydrase IX
Casp-3	Caspase 3
CDK	Cyclin-dependent kinase
CD31	Cluster of differentiation 31
cDNA	Complimentary DNA
CHOP	DNA damage-inducible transcript 3
Con	Controls
CO_2	Carbon dioxide
Csh	Chorionic somatomammotropin hormone (placental lactogen)
DAB	3,3'-diaminobenzidine
DNA	Deoxyribonucleic acid
dNTP	Deoxyribose nucleoside triphosphate
DOHaD	Developmental origins of health and disease
DTT	Dithiothreitol
E	Embryonic day
ECL	Enhanced chemiluminescence
ECM	Extracellular matrix
Edem1	ER degredation-enhancing alpha-mannosidase-like protein 1
EDTA	Ethylenediaminetetraacetic acid
eIF2α	Eukaryotic initiation factor 2 alpha
ELISA	Enzyme-linked immunosorbent assay
ERK	Extracellular signal-related kinase
FABP	Fatty acid binding protein
FABPpm	Plasma membrane associated fatty acid binding protein
FAS	Fatty acid synthase
FAT	Fatty acid translocase
FATP	Fatty acid transport protein
g	Grams

Gadd34	Growth arrest and DNA-damage inducible protein
GLUT	Glucose transporter
GRP78	Glucose-regulated protein 78
Gusb	Beta-glucuronidase
H_2O	Water
H_2O_2	Hydrogen peroxide
H19	Imprinted maternally expressed transcript
HBSS	Hank's balanced salt solution
HCl	Hydrochloric acid
HEPES	4-(2-hydroxyethyl)-1-piperazineethanesulfonic acid
HF	High fat
HIF1α	Hypoxia-inducible factor 1 alpha
HMOX1	Heme oxygenase 1
HOMA-IR	Homeostatic model of insulin resistance
Hprt	Hypoxanthine-guanine phosphoribosyltransferase
hr	Hour
HRP	Horseradish peroxidase
HSD	Honestly significant difference
IGF	Insulin-like growth factor
IGFBP3	Insulin-like growth factor binding protein 3
IGFR	Insulin-like growth factor receptor
IgG	Immunoglobulin G
IHC	Immunohistochemistry
IL-1β	Interleukin 1 beta
IL-6	Interleukin 6
IPGTT	Intraperitoneal glucose tolerance test
Ipo8	Importin 8
IR	Insulin receptor
IRE1α	Inositol-requiring enzyme 1 alpha
IRS	Insulin receptor substrate
IUGR	Intrauterine growth restriction
JNK	c-Jun N-terminal kinase
kcal	Kilocalorie
KCl	Potassium chloride
kDa	KiloDalton
LAT	Large amino acid transporter
LGA	Large for gestational age
m/s	Meters per second
MAPK	Mitogen-activated protein kinase
MDF	Modified Davidson's fixative
$MgCl_2$	Magnesium chloride
mins	Minutes
miRNA	Micro RNAs
mmol/L	Millimoles per liter

MMP	Matrix metalloproteinase
MRI	Magnetic resonance imaging
mRNA	Messenger RNA
mTOR	Mechanistic target of rapamycin
mU/L	Milliunits per liter
N_2	Nitrogen
NaCl	Sodium chloride
NF-κB	Nuclear factor kappa-light-chain-enhancer of activated B cells
nm	Nanometer
NONO	Non-POU domain-containing octamer-binding protein
O_2	Oxygen
OR	Odds ratio
Pat obs	Paternal obesity
PBS	Phosphate-buffered saline
PDI	Protein disulfide isomerase
Peg	Paternally-expressed gene
PERK	Protein kinase R-like ER protein kinase
PFA	Paraformaldehyde
pg/mL	Picograms per milliliter
pH	Presence of hydrogen
Phlda	Pleckstrin homology-like domain family A
Phospho-	Phosphorylated
PI3K	Phosphoinositide-3-kinase
PKB	Protein kinase B
PL	Placental lactogen
Plpp1	Lipid phosphate phosphohydrolase 1
PolyA	Polyadenosine
Ppia	Cyclophilin
PVDF	Polyvinylidene fluoride
RNA	Ribonucleic acid
ROS	Reactive oxygen species
rpm	Rotations per minute
RT-qPCR	Reverse transcriptase quantitative polymerase chain reaction
S6K1	Ribosomal protein S6 kinase beta-1
SDS	Sodium dodecyl sulfate
SEM	Standard error of the mean
SGA	Small for gestational age
SHBG	Sex hormone-binding globulin
SNAT	Sodium-linked neutral amino acid transporter
Sry	Testis-determining factor
sXBP1	Spliced XBP1
T2D	Type 2 diabetes mellitus
TBS	Tris-buffered saline
TBST	Tris-buffered saline with 0.1% Tween 20

TBP	TATA-box binding protein
TEMED	Tetramethylethylenediamine
TGFβ1	Transforming growth factor beta 1
TNF	Tumour necrosis factor
Traf6	TNF receptor associated factor
Tuba1a	Tubulin alpha-1A chain
tXBP1	Total XBP1
Ubc	Ubiquitin C
UP-H2O	Ultra pure water
UPR	Unfolded protein response
V	Volts
v/v	Volume per volume
VEGF	Vascular endothelial growth factor
VEGFR	Vascular endothelial growth factor receptor
Wnt	Wingless-type MMTV integration site family
w/v	Weight per volume
XBP1	X-box binding protein 1
YWHAG	14-3-3 protein gamma
µL	Microliter
µm	Micrometer
µM	Micromolar

Declarations of academic achievement

The present study was designed, conducted, analyzed, and written by the author of thesis under the supervision and guidance of Dr. Deborah M. Sloboda with the following exceptions: animal handling, sacrifice, and tissue collection for the E18.5 cohort (with the exception of a few animals added to increase the sample size), as well as the Nanostring nCounter gene expression assay, was completed jointly by Dr. Tatianne Ribeiro, and Wajiha Gohir. Dr. Johanna S. Selvaratnam, Dr. Kevin P. Foley, Patrycja Jazwiec, Katherine Kennedy, Christian Bellissimo, Jessica Breznik, and Jessica G. Wallace assisted with animal metabolic tests and tissue collection. Dr. Tatianne Ribeiro, Andrew de Jong, Wajiha Gohir, Jessica G. Wallace, Christian Bellissimo, and Katherine Kennedy assisted with primer design for RT-qPCR analyses. Wajiha Gohir, Bronte Johnston, and Debbie Kao assisted with fixed placental tissue processing. Debbie Kao and Lyn Li assisted with E14.5 fetal genotyping. All immunostaining with the exception of cleaved caspase 3 staining was performed by our collaborator, Dr. Jim Petrik and his lab. Andrew de Jong, Justine Mayne, Erica Yeo, Lyn Li, Danielle Penney, Bronte Johnston, Debbie Kao, Emily Moon, Gabriella Paniccia, and Anja Kandic assisted with data collection and recording. Dr. Deborah M. Sloboda, Dr. Kevin P. Foley, Wajiha Gohir, Jessica G. Wallace, Katherine Kennedy, Jessica Breznik, and Christian Bellissimo assisted with teaching new laboratory procedures. Dr. Deborah M. Sloboda, Dr. Alison Holloway, and Dr. Sandy Raha contributed significantly to the study design, analysis, and interpretation of the results.

Chapter 1.0 Introduction

Canadian obesity rates have reached epidemic proportions. Approximately 46% of adult females and 62% of adult males are classified as overweight or obese [1]. Obesity is an immunometabolism disorder that results in changes to glucose metabolism [2] and adipose accumulation [3]. Obese individuals have impaired glucose clearance, resulting in poorer regulation of blood glucose. This is associated with increased insulin secretion and progressively poorer β cell function [4]. Over time, this leads to insulin resistance and ultimately β cell dysfunction, a key physiological characteristic of type 2 diabetes mellitus (T2D) [5]. In healthy individuals, insulin signaling inhibits lipolysis through protein kinase B (PKB), as insulin is associated with glucose uptake and increased glycolysis (glucose breakdown for energy) [6]. However, in obese individuals with insulin resistance, the chronic elevated insulin levels due to β cell dysfunction maintain this lipolysis inhibition, and lead to an accumulation of triglycerides (stored fatty acids), promoting lipid accumulation and increasing adiposity [7,8]. Lipid accumulation triggers a pro-inflammatory response [9], by promoting nuclear factor kappa B (NF-κB) activation, which increases pro-inflammatory cytokine secretion [10,11]. These pro-inflammatory cytokines, such as tumour necrosis factor (TNF), interleukin 6 (IL-6) and IL-1β may be the underlying cause of some obesity-associated diseases such as chronic inflammation, T2D, and hypertension/cardiovascular problems [12].

Pregnancy is also associated with insulin resistance [13], and increased inflammation [14]. While these metabolic changes are normal during healthy pregnancy, in pregnancies complicated by maternal obesity, there are adverse impacts on the developing fetus, resulting in increased offspring disease risk [15]. This concept that metabolic stressors during pregnancy alter fetal

development and increase disease risk forms the basis for the Developmental Origins of Health and Disease (DOHaD) hypothesis [16].

The DOHaD hypothesis was established based on epidemiological data correlating the birth weight of children with a risk of developing hypertensive disorders later in life [17,18]. Barker et al. found that infant birth weights at the extrema were at the greatest risk for dying from cardiovascular disease [18]. They hypothesized that there are critical windows of development where adverse events occurring in the intrauterine environment will have lasting effects on the developmental trajectory of offspring [17,19]. Obesity during pregnancy is one such event where the fetus is exposed to adversity, and thus makes adaptations that often lead to postnatal disease risk [20,21].

Maternal obesity is associated with increased circulating lipids [7,8], glucose [2], and insulin [4], which influence placental nutrient transport via changes in placental macronutrient transporter expression [22–24]. The placenta receives environmental stimuli, (i.e. heighted macronutrient availability), and makes the adaptive response of increasing macronutrient transport to the fetus to increase fetal growth. In the context of maternal obesity, the fetus is preparing for a nutrient-rich postnatal environment [25], however, in a proper nutritionally-supported postnatal environment, fetal adaptations prove to be maladaptive and lead to increased risk of metabolic disorders like T2D [26,27]. Although a number of intrauterine adversities may exist, including caloric restriction [28], stress [29], and micronutrient deficiencies [30], this review will concentrate on obesity and its effects on fetoplacental development. The placenta is of particular interest in the field of DOHaD as this is the main site for maternal-fetal exchange, and adapts to the maternal environment to mediate fetal growth [31].

1.1 Placental development

The placenta is of particular interest in the field of DOHaD as it controls maternal-fetal exchange, and adapts to the maternal environment to mediate fetal growth [31]. The placenta is the principal mediator of fetal development, and must itself grow alongside the fetus to regulate fetal growth [32–35]. The placenta is a highly metabolic organ composed of two primary regions: the maternal region where endocrine signaling occurs, and the fetal region where nutrient transport from the placenta to the fetus occurs. In humans these regions are called the intervillous space (filled with maternal blood perfusing from maternal arteries) and chorion respectively [36]. In mice, these regions are called the junctional zone and labyrinth zone respectively. This review will primarily focus on mouse placentae.

In the mouse placenta, the junctional zone is largely avascular [37], and is the primary site of hormone production, directly influencing fetal growth and development [38]. The junctional zone contains three types of trophoblast cells: parietal trophoblast giant cells, spongiotrophoblast cells, and glycogen trophoblast cells [39,40]. Conversely, the labyrinth zone is highly vascularized [37], and is the primary site of maternal nutrient transport from mother to fetus [41]. This layer contains spiral artery trophoblast giant cells, maternal blood canal trophoblast giant cells, syncytiotrophoblast cells, and fetal capillary endothelium cells [39,40]. These placental cell types have specific functions based on their location, gene expression, and environmental signals [42] (Figure 1.1.1, adapted from [39]).

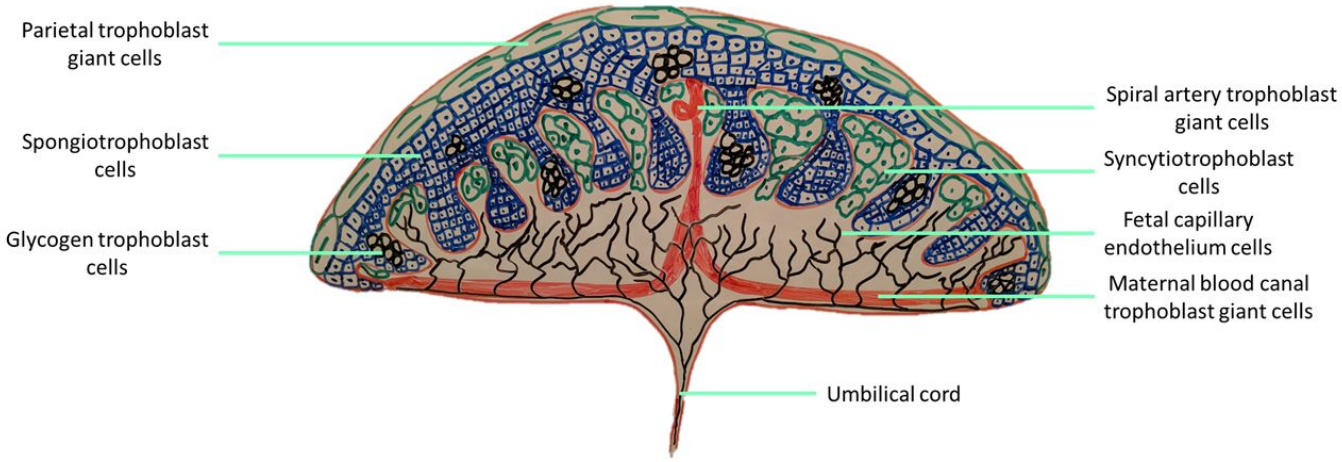

Figure 1.1.1: Mouse cross section of placental tissue. Artistic representation of a mouse placenta. The mouse placenta has two primary placental zones: the junctional zone and labyrinth zone. The junctional zone contains parietal trophoblast giant cells (green), spongiotrophoblast cells (blue), and glycogen trophoblast cells (black). The labyrinth zone contains spiral artery trophoblast giant cells and maternal blood canal trophoblast cells (red), syncytiotrophoblast cells (green), and fetal capillary endothelium cells (black). The junctional and labyrinth zones are marked by a separation between spongiotrophoblast cells and syncytiotrophoblast cells.

Trophoblast giant cells, which are present in both the junctional and labyrinth zones regulate a number of processes, including implantation and early placental vasculogenesis (*de novo* blood vessel development), vascular remodeling and angiogenesis (blood vessel development from preexisting blood vessels), and mediate maternal spiral artery remodeling and growth factor/hormonal secretion [43]. The junctional zone parietal trophoblast giant cells primarily line the implantation site and are necessary during early embryonic development for proper placental implantation, and early vasculogenesis [44]. These trophoblast giant cells are the first cells to invade the maternal uterine lining, and promote vascular remodeling to facilitate adequate placental perfusion [43,45]. This process is regulated by vascular endothelial growth factor

(VEGF) to promote vasculogenesis and decidual invasion into the uterus [45,46]. VEGF promotes vascular mitogenic signaling by increasing cyclin dependent kinase (CDK) expression, which initiates mitosis, promoting cell proliferation [47] thus facilitating proper placental implantation [45].

In the labyrinth, spiral artery trophoblast giant cells and maternal blood canal trophoblast giant cells regulate spiral artery remodelling [48] and maternal vascular remodelling [49] respectively. Spiral artery remodelling involves the breakdown of the extracellular matrix (ECM) [50], which allows for blood vessel widening to increase perfusion [51], which is regulated by heme oxygenase 1 (HMOX1) [50]. HMOX1 promotes matrix metalloproteinases (MMPs) [52], to degrade the ECM basement membrane [53], facilitating blood vessel widening [50,52]. While the exact function of the maternal blood canal trophoblast cells is unknown [54], they are believed to play a structural role in maternal vascular remodeling [49,54]. Similar to the junctional zone, labyrinth vascular remodeling is regulated by VEGF, and is required to for proper placental vascular development [46,55,56].

Spongiotrophoblasts in the junctional zone work together with glycogen trophoblasts to maintain placental glycogen stores for quick access to glycogen as a reserve energy source. Placental glycogen can be broken down to produce energy for the placenta via glycogenolysis and subsequent glycolysis [57,58], and this reserve capacity is key for mediating fetal growth as it facilitates constant glucose supply to the fetus, in the absence of constant maternal glucose intake (i.e. between meals) [59,60]. Syncytiotrophoblast cells and fetal capillary endothelial cells both regulate maternal blood flow to the fetus [61,62], and form the fetal capillary network that makes up the majority of the labyrinth zone [62]. This fetal capillary network is regulated by hypoxia-inducible factor 1 alpha (HIF1α). During placental development, the placenta is in a state of hypoxia [63], which activates HIF1α, a transcription factor that binds to the *Vegf* promoter

to increase placental vasculogenesis and angiogenesis forming a fetoplacental capillary network through CDK-regulated cell proliferation [64]. It is in this capillary network that nutrient transport occurs [62].

The transport of macronutrients (glucose, fatty acids, and amino acids) [32], micronutrients [23,24], gases (O_2, CO_2) [65], and waste products [65], is essential for fetal development [35]. While all macronutrients are necessary [66], glucose is the most important fuel source as it is required to not only ensure fetal growth but also to maintain placental glycogen stores in the glycogen trophoblast cells of the junctional zone [59]. These glycogen stores give the placenta its reserve capacity to supply the fetus with glucose in the absence of a glucose gradient between mother and fetus [59,60].

Glucose transport across the mouse placenta is regulated primarily by glucose transporter 1 (GLUT1), GLUT3, and GLUT4, with GLUT1 levels increasing across gestation [67]. Placental glucose transport is regulated at two key locations: maternal to placental transport [68], and placental to fetal transport [69]. Maternal to placental glucose transport sustains placental glucose levels, required for maintaining placental growth and reserve energy from placental glycogen stores [68]. Unique to the maternal side of placental glucose transport is the presence of the GLUT4 transporter [67], which is insulin-dependent [67,70]. This glucose transporter is advantageous for placental growth as the mother is in a state of insulin resistance during pregnancy, leading to increased circulating insulin [13] and subsequently increased GLUT4 translocation to the cell membrane, promoting placental glucose uptake [67]. These glucose transporters are regulated by a key placental growth factor, insulin-like growth factor 2 (IGF2) [71], which promotes placental growth via mitogenic pathways, promoting trophoblast proliferation [72]. Glucose is then rapidly

broken down with glycolysis for energy to maintain cell proliferation, or stored as glycogen for future use in glycogen trophoblast cells [72–74]. Conversely, placental to fetal glucose transport is primarily regulated by insulin independent glucose transporters, GLUT1 and GLUT3 [68], maintaining a constant glucose transport to the developing fetus, promoting fetal growth by providing the energy required for fetal organogenesis and mitogenic development [74,75].

Amino acids are transported by sodium-coupled neutral amino acid transporters (SNATs) and large amino acid transporters (LATs). Mouse placentae express SNAT1, 2, and 4 [76], and LAT1 [77] and 2 [78]. The SNATs transport neutral amino acids including serine, threonine, alanine, glycine, cysteine, asparagine, methionine, and glutamine [75,79,80]. SNATs are particularly important for fetal development as they transport glucogenic amino acids to the developing fetus, which can be converted to glucose if needed [81]. Fetal glycolysis is very high while endogenous gluconeogenesis is very low [82] to maintain a high glucose gradient between mother and fetus [83]. While gluconeogenesis is low, it is predominantly mediated by glucogenic amino acid transport to the developing fetus as an alternative fuel source [84]. Conversely, LATs transport branched amino acids including phenylalanine, proline, valine, leucine, isoleucine, tryptophan, and tyrosine [85,86]. Of particular note are the essential amino acids isoleucine, leucine, phenylalanine, valine, and tryptophan transported by LATs. These amino acids cannot be synthesized in mice and must be consumed from food sources [87]. Since the fetus receives all nutrients from maternal sources, fetal protein synthesis is dependent on placental transport of essential amino acids [81].

While the exact mechanism of fatty acid transport across the placenta is not fully known, it has been established to be mediated by fatty acid binding proteins (FABPs): plasma membrane associated FABP (FABPpm), FABP1, 3, 4, and 5 [88,89], fatty acid translocase (FAT) [90], and fatty

acid transport proteins (FATP1, 2, 3, 4, and 6) [91–93]. Maternal triglycerides are hydrolyzed via lipase proteins (lipoprotein lipase, endothelial lipase, and hormone sensitive lipase) [94,95] into free fatty acids after which, FABPpm, FATPs, and FAT facilitate their transport to the cytosol of placental trophoblast cells [96]. Here, fatty acids bind to FABPs, and promote mitochondrial β oxidation of fatty acids for placental energy production [97], or shuttle fatty acids to labyrinth trophoblast FATPs and FAT enzymes. These are located on labyrinth endothelial and trophoblast cells, where fatty acids are transferred to the developing fetus [41].

Macronutrient transport and availability are regulated by factors including maternal glucose [98], fatty acids [99], and endocrine signaling (insulin) [100]. During pregnancy increased levels of maternal circulating fatty acids promote increased fatty acid transport via upregulation of placental FAT [7]. Maternal hyperglycemia and hyperinsulinemia [13,101] increase placental glucose uptake from passive diffusion through GLUT1 and GLUT3, and insulin-dependent transport via GLUT4 [67]. The placenta also secretes endocrine factors to mediate maternal pregnancy adaptations and regulate fetoplacental development [98]. The placenta secretes a number of hormones that regulate maternal metabolic adaptations [102]. In mice, placental lactogen 1 and 2 are produced in the first half and second half of pregnancy respectively [102]. Placental lactogen 1, and prolactin secretion promote fetal growth through stimulating IGF2 secretion [103], leading to the insulin-sensitive anabolic state in the first half of pregnancy to prepare for the nutrient demands of later fetal development and lactation [104]. This insulin-sensitive state shifts to an insulin resistant state, as fetal growth rapidly increases in late pregnancy [105], promoting increased glucose transport to the placenta and fetus [98], as glucose is the primary fuel source for the developing fetus [106]. The fetus facilitates this increased glucose transport by maintaining low

levels of gluconeogenesis and high rates of glycolysis [82,107], establishing a large glucose gradient between mother and fetus, keeping glucose transport to the fetus high [83], and promoting placental and fetal growth [108].

IGF1 and IGF2 are key hormones involved in placental growth and signaling [109]. IGF1 and IGF2 promote placental growth through increased placental perfusion rates [110], and mediate fetal macronutrient uptake from the placenta by regulating glucose and amino acid transport through GLUT3 and SNAT4 respectively [111]. IGFs are shuttled to their receptors by binding to IGF binding protein 3 (IGFBP3) [112], facilitating binding to insulin receptors (IR), IGF receptor 1 (IGFR1), and IGFR2 (though they have the strongest affinity for their respective receptors), all of which are present in the placenta [109]. Elevated levels of IGF1 and IGF2 stimulate IGFBP3 synthesis, which can target excess IGFs for degradation [113]. Binding of both IGF1 and IGF2 to IGFR1 results in signal transduction (though this is stronger with binding of IGF1 binding than IGF2), while binding to IGFR2 inhibits signal transduction by degradation of excess IGF1 and IGF2 [106]. Ligand binding to IGFR1 promotes the recruitment of insulin receptor substrate (IRS) 1 and 2 [72,114], inducing phosphoinositide-3-kinase (PI3K) and PKB [114]. PKB promotes GLUT1 translocation to the cell membrane [115], and also inhibits glycogen synthase beta, leading to the transcriptional activation of glycolysis-regulating genes hexokinase and pyruvate kinase [116]. PKB also activates mechanistic target of rapamycin (mTOR) [114] to regulate fatty acid and amino acid uptake through FAT [117] and SNATs [118] respectively. mTOR promotes vasculogenesis and angiogenesis by inducing the transcriptional activation of HIF1α, which in turn promotes VEGF activation [119]. This pathway is intimately involved with placental growth and vascular development, via mitogenic CDK-mediated signaling [47,120].

Proper placental vascularization [37] is key for facilitating nutrient and gas exchange between mother and fetus [34,121,122]. It begins in mice at approximately embryonic day (E)8.0 and persists until E9.5, where angiogenesis begins and continues until term [123]. Placental vasculogenesis is mediated VEGF, beginning with the development of angioblasts, which differentiate into endothelial cells [124]. In the hypoxic environment of early pregnancy [63], this promotes the expression of HIF1α, a transcription factor that induces *Vegf* transcription [64]. This activates Wnt/β-catenin signaling [125], which further promotes *Vegf* transcription due the presence of Wnt-specific promoter sites in the *Vegf* gene [126]. Wnt/β-catenin signaling is also mitogenic by activation of CDK which promotes endothelial cell proliferation to facilitate vasculogenesis [47]. This increases VEGF protein levels, where its paracrine signaling induces a shift from angioblasts (primordial endothelial cells) to endothelial cells, and facilitates the development of a primitive fetal capillary network [62,127]. From this primitive capillary network, placental angiogenesis expands to establish the mature placental vasculature [124,127].

VEGF paracrine signaling is also required for branching angiogenesis (villi maturation) and elongation of mature villi [124,127] through binding of two primary receptors, VEGFR1 and VEGFR2 [128]. These are transmembrane receptors when active, however, soluble VEGFR1 (in the cytosol) binds VEGF but does not provide signal transduction, essentially inhibiting VEGF to reduce vasculogenesis or angiogenesis [129]. Conversely, membrane-bound VEGFR1 and VEGFR2 are pro-angiogenic receptors located primarily on endothelial cells, and facilitate rapid endothelial cell expansion required for blood vessel formation (vasculogenesis), branching, and elongation (angiogenesis) [130].

Under typical, healthy pregnancy conditions, vasculogenesis and angiogenesis lead to the development of sufficient placental vasculature to support fetal growth [131]. These pathways are regulated by IGF2 promoting vascularization through proliferation and mitogenic activity [47,120]. Of note, IGF2 is also regulated by paternal genomic inheritance, where paternally inherited genes (such as *Igf2*) promote fetoplacental growth, while maternally inherited genes (such as *Igfr2*) work antagonistically to ensure maternal survival [111]. Despite this fact, the role of the father in placental development is often overlooked.

1.1.1 Paternal contributions to placental development

Paternal contributions to placental development occur primarily through genomic imprinting, [132] when one parental allele of a gene is silenced, via DNA or histone methylation [133], or activated via DNA or histone acetylation [134]. These imprinted genes are epigenetically modified in the oocyte (maternal inheritance) [135] and in the sperm (paternal inheritance) [136] which regulate genomic activity by altering access to transcriptional machinery [137]. These epigenetic modifications often target genes that are maintained through cell divisions that persist throughout gestation and in the postnatal environment [137]. Thus, epigenetic regulation of these target genes could be modified by stressors during development [138].

Several paternally inherited genes including *Igf2* [139], *Peg1*, and *Peg3* promote fetal growth [111]. While the exact function of *Peg1* and *Peg3* is not known, they have been suggested to play a role in placental vasculogenesis and angiogenesis because of their appearance at E8.0 in placental labyrinth trophoblast and endothelial cells (coinciding with the initiation of vasculogenesis) [140–142]. Conversely, maternally inherited genes including *H19* [133], *Igfr2*, and

Phlda2 reduce fetal growth [111]. *H19* is expressed ubiquitously in the placenta and regulates trophoblast cell proliferation by inhibiting CDK, preventing cell proliferation [143,144]. *Phlda2* is located in the spongiotrophoblast and glycogen trophoblast cells of the junctional zone, and regulates the size and growth of these trophoblast cells [145]. *Phlda2* knockout mice show increased junctional zone size and glycogen trophoblast cell hyperplasia and hypertrophy [145]. Deletions of *H19* and *Igf2* are associated with fetal overgrowth (in the case of maternal gene allele silencing) [146] and fetal undergrowth (in the case of paternal gene allele silencing) respectively [71]. IGF2 promotes feto-placental growth and development by maximizing trophoblast proliferation [139], while H19 works antagonistically to minimize trophoblast proliferation and protect the mother from excessive fetal growth [133,143]. These genomic imprints work together to regulate fetoplacental development. Although methylation is commonly thought of when epigenetics is considered, paternal genes are also tightly regulated by the inheritance of microRNAs (miRNAs) from the paternal spermatozoa.

MicroRNAs are short (19-24 nucleotides) single strand non-coding RNAs that function by forming complementary base pairing to the mRNA of specific genes, leading to either reduced mRNA stability, or direct promotion of mRNA degradation [147]. MicroRNAs are formed when RNA polymerase II transcribes an elongated pri-miRNA which contains a hairpin loop on one end, and a 5' cap and 3' polyA tail on the other. The 5' cap and 3' polyA tail are cleaved from this pri-miRNA by RNase III, Drosha, forming a pre-miRNA [148]. The hairpin loop is then removed by an RNase III enzyme, Dicer, forming two sets of mature miRNA complementary sequences [149], one of which is incorporated into the RNA-induced silencing complex, where it can now target mRNA for post-transcriptional regulation. If the miRNA forms exact

complementarity to the target gene, then the mRNA will be targeted for degradation, if the complementarity is not exact however, then the mRNA will undergo translation inhibition [147]. In spermatozoa, these miRNAs play roles in embryo development, specifically mediating embryo preimplantation development [150].

Spermatozoa miRNAs are integral to fetal survival. Conditional knockouts of Drosha/Dicer complexes result in miRNA changes that reduced testis weight, sperm motility, and number [151]. These altered miRNA profiles are also associated with reduced preimplantation potential, and increased risk of embryonic lethality [151]. Paternally inherited miRNAs also regulate placental development and function [152,153], and disruptions in miRNAs are associated with pregnancy complications. The C19MC cluster of paternal miRNAs, is associated with preeclampsia (improper placental implantation into the uterine wall) and fetal growth restriction [152]. This cluster contains 15 unique miRNAs which regulate the transcription of hundreds of placental genes, however, of particular interest is miR-520h, which regulates placental vascular development [152], and is predicted to transcriptionally regulate up to 462 different genes in the developing placenta, including VEGF and HIF1α [152,154].

1.2 Prenatal adversity and endoplasmic reticulum stress activation

It is well established that the developing organism is vulnerable to adversity and makes physiological adaptations to this adversity in a manner that maximizes postnatal fitness at the expense of increased disease risk [17,18,27,29,155]. Although many studies have reported that early life adversity increases postnatal disease risk [17,156,157], the signaling pathways are still unclear. Given

that cellular stress is often associated with metabolic dysfunction [29,158–160], this has become a prime target of investigation.

Endoplasmic reticulum (ER) stress is the cellular response to dysregulated homeostasis, in order to remove the stressor and restore cell functionality [161]. ER stress is often initiated in response to hypoxia or obesity [25,162]. This occurs through hypoxia-mediated HIF1α activation. HIF1α binds to the *Vegf* gene, mediating placental mitogenesis through CDK [47]. This rapid cell expansion leads to an accumulation of misfolded proteins [25,163], triggering the unfolded protein response (UPR). There are three branches of UPR signaling: protein kinase R-like ER protein kinase (PERK) [164], activating transcription factor 6 (ATF6) [165], and inositol-requiring enzyme 1 α (IRE1α) [164,166]. Under homeostatic conditions, glucose-regulated protein 78 (GRP78) binds to each of these transmembrane proteins, preventing their signal transduction [164–166]. However, under ER stress conditions, the binding affinity of GRP78 to misfolded proteins is greater than to each of the UPR mediators, promoting GRP78 dissociation and subsequent UPR activation [167].

The ATF6 branch primarily promotes the transcriptional activation of pro-survival genes during the early stages of UPR activation [168]. ATF6 signaling is mediated by protein disulfide isomerase (PDI), which breaks disulfide bonds in misfolded proteins to facilitate proper protein folding [169]. The PERK branch of ER stress further attempts to restore cellular homeostasis through phosphorylation of eukaryotic initiation factor 2 alpha (eIF2α). eIF2α attenuates translation of complex proteins by altering ribosomal conformation to prevent further translation [170], and can initiate apoptosis via activation of ATF4 and DNA damage-inducible transcript 3 (CHOP), which activate transcription of the pro-apoptotic B cell lymphoma 2 (Bcl2) family members [158]. Bcl2-mediated apoptosis is initiated by weakening of the mitochondrial membrane

by Bcl2-associated X protein (Bax) and BH3 interacting-domain death agonist (Bid) [171], this promotes the release of cytochrome C from the mitochondria, activating caspase-3 (casp-3) [172]. Casp-3 is a protease that cleaves proteins indiscriminately leading to cell death [173]. Lastly, IRE1α functions as a kinase, promoting pro-inflammatory signaling via phosphorylation of c-Jun N-terminal kinase (JNK) which promotes NF-κB transcription [174]. IRE1α also has RNase activity, cleaving X-box binding protein 1 (XBP1) to produce the active transcript [175], which is a transcription factor that promotes transcriptional activity of pro-survival UPR-associated genes, including *Pdi* and *Grp78* [176]. In addition to regulating cell stress responses, the PERK [55] and IRE1α [56] branches of ER stress are also associated with placental vascular development. While the exact mechanism is unclear, placental PERK and IRE1α are associated with increased VEGF activation through the unconventional signaling of ATF4 and XBP1 respectively [55,56].

1.2.1 Maternal obesity

1.2.1.1 Epidemiological studies

Maternal obesity has been well established to negatively impact pregnancy and placental outcomes. Three main impacts are increased incidence of pregnancy complications [21,177], impaired placental vascular development during gestation [178], and dysregulated placental insulin signaling and IGF2-mediated growth [179]. These developmental and functional disruptions to the placenta are associated with adverse outcomes for the offspring later in life [20,180,181], such as increased risk of developing obesity [180], T2D [182], and cardiovascular disease [183]. These poor

offspring outcomes are due to the combination of impaired placental development, and altered fetal growth trajectory [121].

Maternal obesity contributes to pregnancy complications including preeclampsia [1], gestational diabetes [21], and increases risk of caesarean delivery [177]. Maternal obesity and preeclampsia are thought to impair placental vascular development [178] through increased maternal circulating insulin [184] and reduced placental lactogen secretion from the placenta respectively [185,186]. These disruptions occur through impairment of proper endothelial cell proliferation, resulting in placental lesions in the fetal capillary network [187], reducing placental perfusion and fetal growth [188].

Maternal obesity is associated with disrupted vascular circulation and blood flow in the developing placenta [178]. This impaired vascularization and blood circulation increases the risk of fetal blood supply abnormalities [178], and can promote fetal hypoxia [189]. In hypoxic environments, the placentae promotes increased angiogenesis [190] to compensate for the reduced oxygen and nutrient availability for the fetus. However, during gestation this compensatory angiogenesis may not develop properly and prove insufficient in maintaining nutrient and oxygen transport to the fetus [191,192]. These hypoxic conditions mediate fetal metabolic adaptations during pregnancy, and predispose the fetus to negative metabolic outcomes such as cardiovascular disease [193]. A contributing factor to this hypoxic environment is the risk of poor placental implantation, resulting in preeclampsia which further limits fetal growth [1].

Studies have shown that in cases of preeclampsia [102,186], there is reduced placental lactogen secretion [102,186]. Placental lactogen mediates maternal pregnancy adaptations, and facilitates increased placental uptake of maternal nutrients, showing a positive correlation

between placental lactogen secretion and offspring birth weight [194]. Preeclampsia is a common pregnancy complication occurring in up to 10% of pregnancies [195] and is characterized by improper placental implantation, causing exacerbated placental hypoxia and fetal growth restriction. This poor intrauterine environment is associated with increased risk of stillbirth (OR 1.3; 95% CI 1.1-1.7) [196], increased risk of offspring stroke later in life (OR 1.9; 95% CI 1.2-3.0) [197], and increased offspring blood pressure (2.39 mm Hg; 95% CI 1.74-3.05) [157]. In cases of impaired placental growth, it is also very common for macronutrient transport to be significantly impacted possibly due to disrupted placental vascularization, especially in the context of maternal obesity [32,198]. Maternal obesity increases risk of macrosomia through increased macronutrient transport (Figure 1.2.1.1.1, adapted from [199]), and in the offspring is associated with obesity, cardiovascular disease, and T2D [15,32,33]. This increased macronutrient transport has been implicated to be associated with ER stress and the UPR [25].

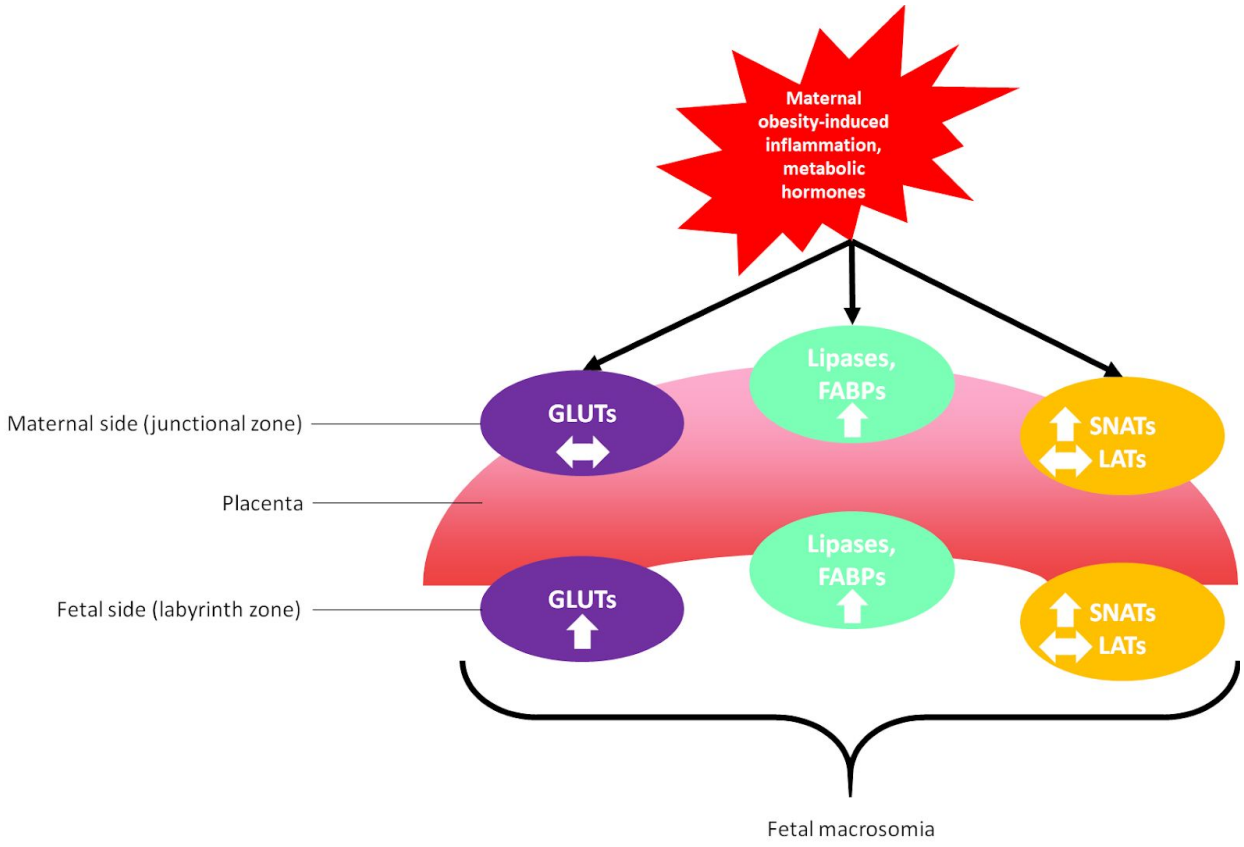

Figure 1.2.1.1.1: Obesity-induced changes in placental macronutrient transport. Schematic image showing how maternal obesity promotes increased glucose (left), fatty acid (middle), and amino acid (right) transport through changes in macronutrient transporters on the fetal side of the placenta. Increased macronutrient transport directly contributes to fetal growth and increases macrosomia risk.

1.2.1.2 Experimental studies

Animal models are an effective method for analyzing pathways and mechanisms behind adverse outcomes, such as offspring metabolic disease risk. Maternal obesity has been shown to impair vascularization and placental development [35,200], increase placental macronutrient transport [32,200], and subsequently increase offspring risk of developing metabolic disease [15], possibly mediated through changes in placental ER stress and UPR-mediated signaling [25,55,56].

Maternal obesity impairs placental vasculature through increased VEGF signaling [201], similar to human pregnancies complicated by preeclampsia [195], and is associated with hypoxia-mediated factors, carbonic anhydrase IX (CAIX) [202], and HIF1α [203]. VEGF regulation has also been demonstrated to be mediated by the IRE1α and PERK branches of the UPR [55,56]. In conditional knockout studies, both IRE1α and PERK have been shown to be directly associated with VEGF activity, although the exact mechanism is unclear. The evidence suggests that these branches of the UPR mediate VEGF activity through unconventional signaling via XBP1 [56] and ATF4 [55]. Under ER stress conditions, such as hypoxia [159], placental perfusion is compromised [204] which limits fetal access to maternal blood and nutrients [52].

Fetal macronutrient supply is integral for regulating fetal growth [121], and is upregulated in pregnancies complicated by maternal obesity [22,32,200]. Maternal obesity increases glucose and amino acid transporters, GLUT1 and SNAT2 respectively [32], which may be an adaptive response to the vascularization changes and placental hypoxia. Similar outcomes are found in hypoxic placentae from non-obese mothers with increases in GLUT3 [205] and LATs [206]. Excess nutrient transport to the fetus is harmful as it greatly increases the risk of the offspring being born large for gestational age (LGA), and these offspring have a greater risk for developing metabolic disorders later in life [15,32].

1.2.2 Paternal obesity

Paternal impacts on perinatal development are equally as important as maternal mediators, however, are much more frequently overlooked. While mechanistic links between

paternal obesity and offspring disease risk are not fully understood, a few studies have correlated paternal obesity with increased risk of obesity, T2D, hypertensive disorders [20], fetal growth restriction, and increased placental GLUT1 and SNAT2 transporter levels in rodent models [32]. Whether these impairments are associated with poor placental development and function has been suggested [32,34], but the signalling pathways are unclear.

1.2.2.1 Epidemiological studies

Overweight and obese men are significantly more likely to experience infertility compared to healthy weight individuals (OR 1.20; 95% CI 1.04-1.38 and OR 1.36; 95% CI 1.13-1.63 respectively) even when controlling for other parameters such as maternal BMI, smoking, age, and coital frequency [207]. This outcome worsens when both partners are obese, even with assisted reproduction such as *in vitro* fertilization (OR 1.37; 95% CI 0.90-2.08) [208]. This reduced fertility is largely mediated by obesity-induced changes in spermatozoa health and function. Spermatozoa quality is reduced by paternal obesity showing reduced motility, reduced concentration, and increased DNA fragmentation [209]. These negative impacts are believed to be mediated by endocrine differences in obese males compared to healthy males [210,211].

Sex hormone-binding globulin (SHBG) is a glycoprotein that binds to the sex hormones testosterone and estradiol, inhibiting their activity [211]. An inverse correlation exists between SHBG and circulating insulin levels, and evidence suggests this relationship may be mediated by fat mass [211,212]. In obese males, hyperinsulinemia leads to lower SHBG levels, increasing the amount of bioavailable testosterone [211], which is converted into estradiol in adipocytes by aromatase, increasing circulating estradiol levels [213]. This increased circulating estradiol signals

the pituitary gland to reduce follicle stimulating hormone secretion, impairing Sertoli cell proliferation, negatively affecting spermatogenesis [214], and reducing spermatozoa number [214]. Furthermore, mature sperm in this obese environment are exposed to elevated levels of circulating lipids [7,8], which increases sperm oxidative stress by triggering pro-inflammatory signaling [9,215].

Although studies investigating male obesity and spermatozoon health are still somewhat controversial; some studies show paternal obesity has a negative impact [209,216], while others report that it has no effect [217,218]. While the debate of paternal obesity on spermatozoa health continues, this review will focus on studies showing paternal obesity negatively impacting spermatozoa parameters and impairing male fertility.

One key impairment in spermatozoa health is the impact on spermatozoon epigenetic inheritance, specifically, DNA methylation [219] and miRNA profiling [220]. Two key imprinted genes in the spermatozoa, *Igf2* and *H19*, which are paternally expressed and silenced respectively, have decreased methylation in obese humans compared to healthy controls [219]. This hypomethylation of *Igf2*, a key factor regulating fetoplacental growth has been shown to be associated with increased risk of macrosomia and offspring birth weight [221]. López et al. (2018) found that two miRNAs, miR-155 and miR-122 were significantly elevated in obese men compared to healthy controls. miR-155 is known to promote a shift to the M1 macrophage phenotype, increasing pro-inflammatory macrophages [222], while miR-122 mediates iron metabolism [223]. Based on López et al.'s findings, this would suggest developing embryos from obese fathers are more pro-inflammatory and have disruptions in micronutrient metabolism.

These preimplantation changes may dictate how the fetoplacental unit develops postimplantation, and form the framework for the harmful postnatal outcomes.

1.2.2.2 Experimental studies

Paternal obesity impacts embryo viability largely through disruptions in spermatozoa, including increased DNA damage [224], and aberrant miRNA inheritance [225]. In animal studies, obesity in males has been shown to reduce fertility through reduced embryo viability and changes to embryo development [32,224], and to induce impairments as early as the 2-cell stage in the preimplantation embryo by increasing mitochondrial lipids [32]. This accumulation of lipids in the mitochondria predisposes the developing embryo to ER stress, and increases reactive oxygen species (ROS), promoting oxidative stress [32].

In male mice, obesity results in reduced fertility by reducing spermatozoa motility, increasing spermatozoa mitochondrial ROS, and increasing spermatozoa DNA damage. Spermatozoa motility is regulated by mitochondrial production of energy via the Krebs cycle [226]. In obese males, the accumulation of circulating lipids disrupts this signaling pathway, reducing spermatozoa motility by preventing sufficient energy production required for flagellar movement [226–229]. Dysregulation of the Krebs cycle increases spermatozoa ROS levels as the Krebs cycle produces many antioxidant intermediates (pyruvate, oxaloacetate, and α-ketoglutarate) [230]. These intermediates contain a keto acid group (carboxylic acid and ketone) which can be reduced by ROS and protect mitochondrial energy output [230]. These functional impairments of sperm health due to paternal obesity directly influence embryo development and mediate changes in fetoplacental growth [32].

Paternal obesity impacts spermatozoa epigenetic regulators, such as DNA methylation [225,231], and miRNAs [225,232], impairing tightly regulated epigenetic inheritance patterns [225] (Figure 1.2.2.2.1, adapted from [233]). In high fat-fed mice, these are associated with altered DNA methylation [136,232]. Paternal obesity-induced DNA methylation is associated with increased miRNA let-7c in the spermatozoa, as well as in the offspring [225]. The miRNA let-7c regulates glucose homeostasis and has been associated with a predisposition to T2D in mouse models [234]. While the full extent of this miRNA has not been studied in the developing fetus, in offspring, it has been shown to be strongly expressed in adipose tissue targeting lipid synthesis genes such as *Plpp1* [235]. Frost et al. (2011) found that overexpression of let-7c results in impaired glucose clearance and reduced insulin secretion [234]. Taken together with the correlation of paternal obesity and elevated offspring let-7c levels [225], this suggests that paternal obesity may mediate offspring metabolism and disease risk through epigenetic inheritance.

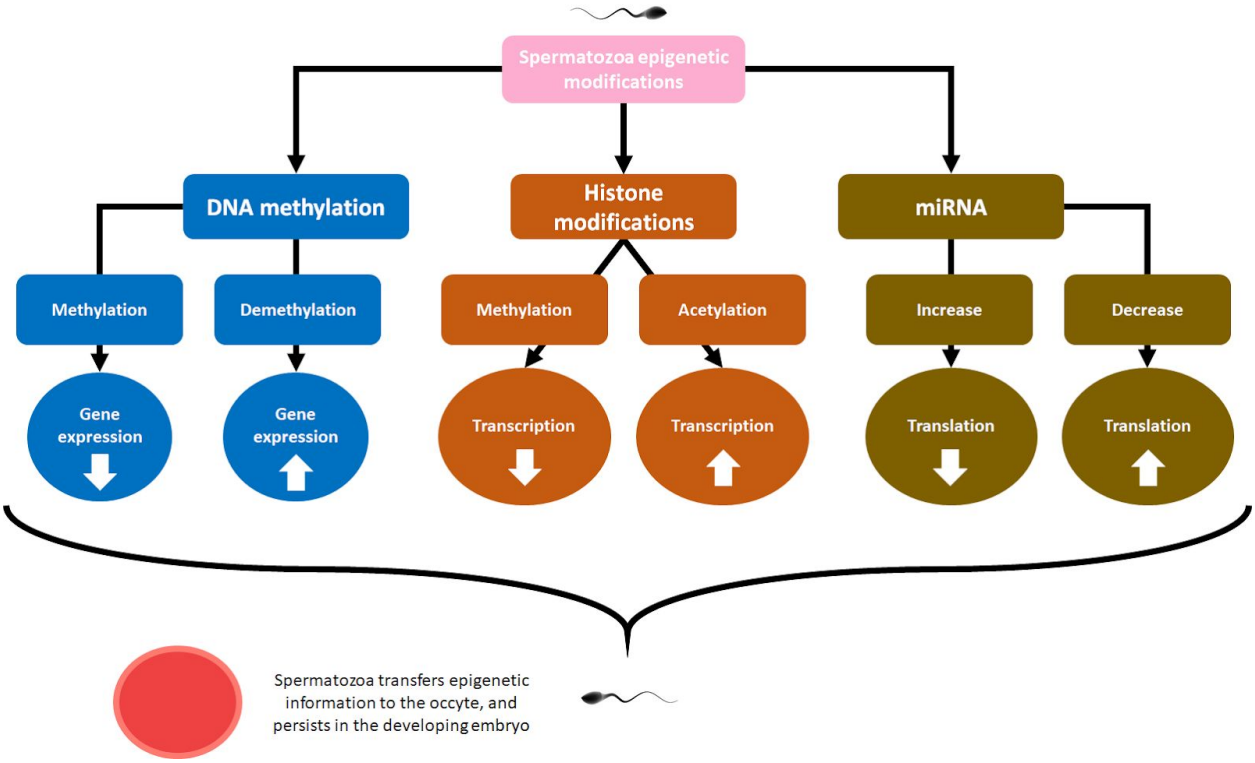

Figure 1.2.2.2.1: Spermatozoa epigenetic modifications. Schematic showing three examples of paternal epigenetic transference from spermatozoa. Three methods of epigenetic inheritance are DNA methylation (left), histone modifications (middle), and miRNAs (right). These are examples of pre- and post-transcriptional modifications to mediate gene expression and embryonic development. Disruptions in this conserved mechanism alter fetoplacental development and program offspring disease risk.

1.2.2.3 Fetoplacental development

Paternal obesity increases spermatozoa DNA damage [224,236], oxidative stress [32], and alters epigenetic inheritance [232]. In mice, these obesity-regulated changes in spermatozoa have been correlated with reduced placental growth [32], and increased apoptosis [34]. Paradoxically, paternal obesity in mice has been shown to decrease placental weight and growth [32,34], while maternal obesity has been shown to increase placental weight and growth in mice [32,38]. Despite this

reduction in fetoplacental growth, evidence suggests increased glucose and amino acid transport through elevated GLUT1 and SNAT2 transporter levels respectively [32]. This paternal obesity-mediated reduction in placental growth could be partially mediated by oxidative stress, which impairs placental development by promoting apoptotic signaling through UPR-mediated PERK and IRE1α activity in the developing placenta [34,132,237]. Increased placental apoptosis is associated with small for gestational age (SGA) offspring, and often with postnatal catch-up growth, leading to increased risk of obesity, T2D, and cardiovascular disease later in life [28]. Conversely, increased placental weight and growth is correlated with excessive gestational weight gain and LGA offspring, and increased risk of pregnancy complications [15,32]. This is an interesting observation as it shows that maternal and paternal obesity predispose poor offspring metabolic outcomes later in life through apparently different pathways.

While paternal obesity has often been overlooked in the context of fetoplacental development, some evidence suggests that paternal obesity mediates fetal growth through increased macronutrient transport [32]. This is similar to what occurs in pregnancies complicated by maternal obesity [32], although, the mechanisms and related developmental pathways in the context of paternal obesity, are poorly understood.

1.3 Rationale

The negative effects of maternal obesity on the developing offspring have been well established to increase disease risk later in life [15,20,21,32,33,177]. Maternal obesity is known to impair placental function [17,25,32,132], and alter the growth trajectory of the developing fetus. However, the effects of paternal obesity are not as well understood.

Paternal obesity is known to disrupt spermatozoa health through increased DNA damage, altered DNA methylation [224], and altered miRNA inheritance [220,222,234], however, the specific interactions between spermatozoa damage and placental health and growth have not been thoroughly studied, apart from correlational studies [32,34]. It has been shown that increased global DNA methylation in spermatozoa is correlated with increased placental DNA methylation [34,224]. These changes in placental DNA methylation status have been shown to be correlated with impaired placental development and function [32,34]. Conversely, paternal obesity has also been correlated with hypomethylation of the paternally-inherited gene, *Igf2* [219], leading to increased fetoplacental growth [221]. This increased risk for fetoplacental over- and undergrowth is similar to cases of maternal obesity [22,32]. Associated with this upregulated placental growth, paternal obesity is correlated with increased macronutrient transport across the placenta [32] and increased placental apoptosis [34], but the signalling pathways are not clear and have not been characterized. While maternal obesity-induced inflammation [35,38] has been suggested to act through the UPR and placental ER stress, it has not been studied in the context of paternal obesity.

Since male obesity results in increased mitogenic dysfunction and ROS inducing epigenetic changes in sperm [32,224,225], and is associated with poor placental development [32], this study set out to investigate whether paternal obesity alters placental vascular development through hypoxia-mediated ER stress signaling at two key time points during mouse gestation, E14.5 (when the placenta is maximally efficient) and E18.5 (term). These time points were selected as placental development persists until approximately E12.5-E14.5, at which point angiogenesis remodelling continues for the rest of gestation [122].

1.4 Hypothesis

We hypothesize that paternal obesity impairs placental vascular development and growth through UPR-mediated signaling in the placenta. This dysregulated vascular development impairs placental growth, and is associated with apoptosis and inflammation. As a result, placental macronutrient transport and endocrine function will be impaired. These effects will be sex and gestational age-dependent.

1.5 Aims

Aim 1 – To determine the impacts of paternal obesity on placental vasculogenesis and angiogenesis and to determine whether these changes are associated with increased endoplasmic reticulum stress.

Aim 2 – To determine whether paternal obesity-induced impairments in placental vasculature negatively impact placental macronutrient transporter expression and endocrine function.

Aim 3 – To establish whether the negative impacts of paternal obesity on placental development are sex specific and worsen with advancing gestation.

Chapter 2.0 Materials and methods

2.1 Animal model assessment and tissue collection

2.1.1 Diet-induced obesity model

All experiments were approved by the Animal Ethics Committee at McMaster University (Animal Utilization Protocol #: 16-09-35). Six week old wild type C57BL/6J male mice were fed a control (Con; n = 31, 17% kcal from fat; Harlan 8640 Teklad 22/5 Rodent diet; Appendix Table 9.1.1 [238]) or high fat (Pat obs; n = 30, 60% kcal from fat; Research Diets Inc. D12492; Appendix Table 9.1.2 [239]) diet for 10 weeks (two cycles of mouse spermatogenesis [224]) prior to mating with nine-week-old, control-fed females (Figure 2.1.1.1). Prior to mating males and females, and throughout gestation, mice were weighed and food intake recorded to confirm adequate food consumption and proper weight gain.

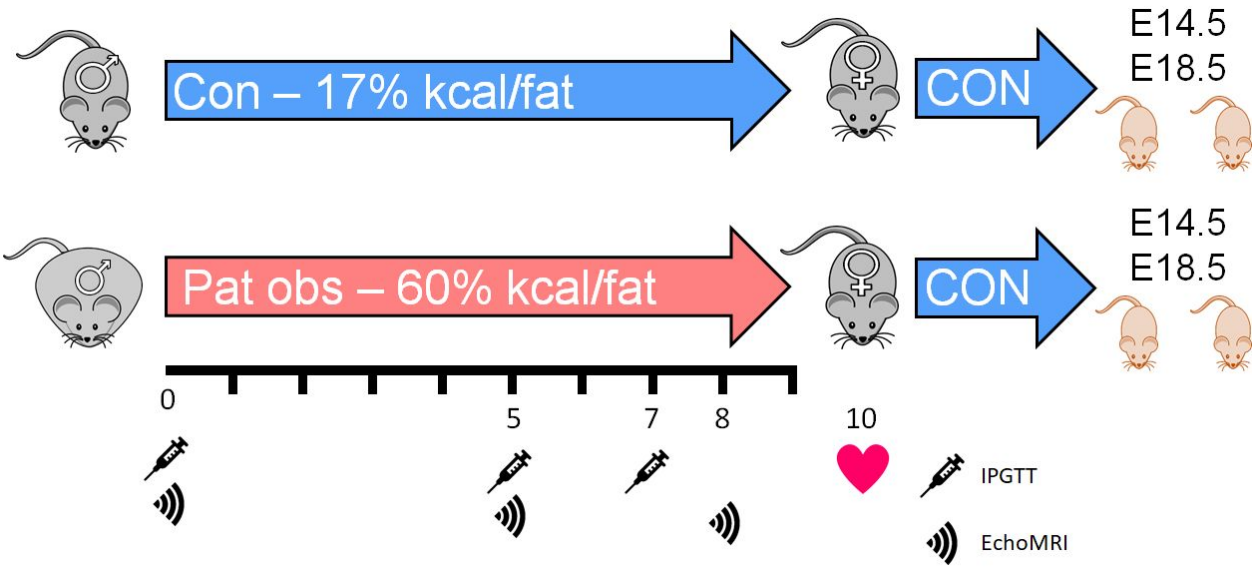

Figure 2.1.1.1: Experimental design. Six week old C57BL/6J male mice (n = 61) were randomly assigned to one of two groups: 1) control diet (Con; n = 31, 17% kcal/fat, blue) or 2) high fat diet (Pat obs; n = 30, 60% kcal/fat, pink), and fed their respective diet for 10 weeks. Weight and caloric intake were measured weekly. Male metabolic phenotype was assessed using an intraperitoneal glucose tolerance test (IPGTT; 2 g/kg glucose [240]) on weeks 0, 5, and 7 of the dietary intervention (syringe). Adiposity was measured via echoMRI on weeks 0, 5, and 8 (wave symbol). After 10 weeks of diet, males were housed overnight with control-fed female C57BL/6J mice (heart). Pregnant females were individually housed and given *ad libitum* access to standard control chow and water during pregnancy, and were sacrificed at E14.5 or E18.5, where placental tissues were collected.

2.1.2 Male in vivo metabolic testing

In males, intraperitoneal glucose tolerance tests (IPGTT) were performed at 0, 5, and 7 weeks of intervention. Mice were fasted overnight for 9h and injected with 2g/kg of glucose (G5767-500G, Sigma-Aldrich) in 0.9% saline (LC234602, Thermo Fisher) [240] at 9 am using a 26G x ½ inch needle (305111, BD). Whole blood glucose was measured at 0, 20, 30, 40, 60, 90, and 120 minutes post-injection using a glucometer (Accu-Chek Performa). Adiposity was measured via echoMRI (Bruker Minispec LF90-II) at weeks 0, 5, 8, and 13 (Figure 2.1.1.1).

2.1.3 Mating and pregnancy

At week 10 of dietary intervention, males were housed with control-fed females overnight. The presence of a vaginal plug the following morning was defined as embryonic day (E)0.5. Two cohorts of pregnant females were generated: E14.5 (CON-M, n = 9; HF-M, n = 8) and E18.5 (CON-T, n = 9; HF-T, n = 6). In both cohorts, pregnant females were housed individually and fed standard control chow diet and water *ad libitum* throughout pregnancy. Maternal pregnancy weight gain and food intake was measured at E0.5, E10.5, and E14.5 for CON-M and HF-M females, and at E0.5, E10.5, E15.5, and E18.5 for CON-T and HF-T females.

2.1.4 Collection of male tissues

After confirmation of successful pregnancy (approximately 11-14 weeks of dietary intervention), males were sacrificed via cervical dislocation, and body weight and overnight (12hr) fasting blood glucose levels were recorded. Whole blood was collected using heparinized capillary tubes (22-362566, Thermo Fisher), incubated at room temperature for 30 minutes then centrifuged at 7500 rpm for 5 minutes where the serum fraction was collected and stored to measure fasting blood insulin levels. Liver, gonadal fat, mesenteric fat, and gonadal tissues (testes, epididymides, and empty seminal vesicles) were dissected, weighed, and banked for use in other studies.

2.1.5 Collection of maternal, placental, and fetal tissues

Females were sacrificed via cervical dislocation at either E14.5 or E18.5, and body weight and overnight (12 hr) fasting blood glucose levels were recorded. Serum was collected as in males (see above). Maternal liver, gonadal fat, and mesenteric fat were weighed and collected as above

and banked for use in other studies. For the collection of fetal and placental tissues, the gravid uterus was removed from the maternal abdominal cavity, and placed in a petri dish containing Hank's balanced salt solution (HBSS, 14025-134, Thermo Fisher). The fetuses were removed from the uterus, the amniotic sac was opened, and fetuses were separated from their placentae. The fetal tail was collected and snap frozen in liquid N_2 and stored at - 80 °C for subsequent genotyping to determine fetal sex (see below). Placentae were separated from maternal decidual tissue, and cut sagittally where one half was snap frozen in liquid N_2 and stored at - 80 °C, and the other half was fixed either in Modified Davidson's fixative (MDF; E14.5; 50% distilled H_2O, 30% of 37-40% formaldehyde, 15% anhydrous ethanol, 5% glacial acetic acid) for 8h and transferred to 70% ethanol, or in 4% paraformaldehyde (PFA; E18.5) for 24h and transferred to 70% ethanol.

2.2 Fetal genotyping

Fetal tails were thawed and placed in lysis buffer (100 mM Tris-HCl pH 8-8.5, T5941-1KG, Sigma-Aldrich; 5 mM EDTA pH 8.0, E478-500, Thermo Fisher; 200 mM NaCl, S671-3, Thermo Fisher; 0.2% w/v SDS, SDS001.500, BioShop; 0.5% proteinase K, EO0491, Thermo Fisher) and incubated at 37 °C overnight. The samples were shaken to mix and centrifuged at 13 000 rpm for 20 minutes at 4 °C, the supernatant was removed and transferred to 500 µL 100% isopropanol. The tubes were gently shaken to precipitate DNA and centrifuged for 13 000 rpm for 15 minutes at 4 °C. The solution was decanted and 75% ethanol was added to wash the samples. The solution was decanted and the ethanol wash was repeated, the samples were incubated at room temperature for 10 minutes and 50 µL ultra-pure RNase/DNase-free distilled water (UP-H_2O,

10977015, Thermo Fisher) was added. The samples were added to a PCR mixture prepared following the Thermo Fisher iTaq manual (#EP402, Thermo Fisher). In brief, PCR buffer, 50 mM $MgCl_2$, 10 mM dNTP mix, 10 µM forward primer, 10 µM reverse primer, Redi Load, and 5 U/µL Taq DNA polymerase were mixed as per kit specifications and placed in a BioRad C1000 Touch thermal cycler (1851148, BioRad). The forward and reverse primer sequences used for the *Sry* gene were 5' TTGTCTAGAGAGCATGGAGGGCCATGTC 3' and 5' CCACTCCTCTGTGACACTTTAGCCCTCCG 3' respectively (Table 2.3.3.1). The samples were incubated for 3 minutes at 95 °C, then the following 3 steps were repeated 30 times: 95 °C for 30 seconds, 58 °C for 30 seconds, and 72 °C for 1 minute. The samples were then incubated at 72 °C for 5 minutes. The samples were analyzed using electrophoresis through a 1% agarose gel at 110 V for 25 minutes, with an adult male and adult female DNA sample included as a positive and negative control respectively. Bands imaged using a ChemiDoc MP Imaging System (1708280, BioRad) with Sybr Safe DNA gel stain (S33102, Thermo Fisher), and males were identified by the presence of a band at ~900 bp, females by the absence of a band (data not shown). From this point forward, one male and one female placenta from each litter were used for all analyses.

2.3 Gene expression analyses

2.3.1 RNA isolation

Total RNA was isolated using Trizol (15596018, Ambion). Approximately one quarter of a frozen placenta was homogenized in 900 µL Trizol with 0.2 g glass acid-washed homogenizing beads (G4640-100G, Sigma-Aldrich) for 60 seconds at 5 m/s. The homogenate was centrifuged

at 12 000 g for 10 minutes at 4 °C, the supernatant was removed and washed in 300 µL chloroform, then incubated for 3 minutes. Tubes were centrifuged again as before and the aqueous supernatant was added to 500 µL 100% isopropanol. Samples were mixed and incubated for 20 minutes at room temperature. Tubes were centrifuged again as above, the supernatant was discarded and pellet washed in 75% ethanol, samples were mixed and centrifuged at 12 000 g for 5 minutes at 4 °C. The supernatant was removed and samples washed again as before in 75% ethanol, then centrifuged at 12 000 g for 10 minutes at 4 °C. The supernatant was removed and the samples were dried in a fume hood for 5 minutes, 20 µL pre-heated UP-H_2O was added and concentration was determined on a NanoDrop 2000 spectrophotometer (ND2000, Thermo Fisher).

2.3.2 Complementary (c)DNA synthesis

For cDNA generation, placental RNA (2000 ng) was added to 1 µL 10X ezDNase Buffer and 1 µL ezDNase enzyme. The samples were incubated at 37 °C for 2 minutes, then 4 µL SuperScript IV VILO Master Mix and 6 µL UP-H_2O was added. The samples were incubated in a BioRad C1000 Touch thermal cycler (1851148, BioRad) at 25 °C for 10 minutes, 50 °C for 10 minutes, and 85 °C for 5 minutes. The cDNA was diluted 1:100 for reverse transcriptase quantitative polymerase chain reaction (RT-qPCR) analysis (see below).

2.3.3 Primer design for reverse transcriptase quantitative polymerase chain reaction (RT-qPCR)

Primer pairs were designed using the primer basic local alignment search tool (Primer-BLAST, NCBI) [241] and purchased from Invitrogen (custom DNA oligos). Primer conditions were

optimized as follows: 50-150 base pair PCR product size, primer melting temperatures between 58 °C and 62 °C with up to a 2 °C difference between forward and reverse primers, and primer pairs spanned exon-exon junctions within the target gene. Primer pairs were then analyzed using NetPrimer [242] to determine the spontaneity of hairpin loops, primer dimers, and other non-specific binding. Only primers with a ΔG value greater than or equal to -8.00 for each non-specific binding possibility were used. NCBI's nucleotide BLAST [243] was used to automatically detect the highest affinity targets of the primers generated. This was referenced to the gene of interest to confirm that the target gene for each primer was the highest affinity binding target (Table 2.3.3.1).

Table 2.3.3.1: Primer sequences used in RT-qPCR and PCR analyses.

Gene	Accession number	Forward primer (5' to 3')	Reverse primer (5' to 3')
B actin	NM_007393.5	AGATCAAGATCATTGCTCCT	ACGCAGCTCAGTAACAGTC
Hprt	NM_013556.2	CAGTCCCAGCGTCGTGATTA	TCGAGCAAGTCTTTCAGTCCT
Ipo8	NM_001081113.1	AGACGGAGCTTAACCAGTCCT	GCAAGCTGGGGGCAAAAT
Ywhag	NM_018871.3	GTGACCGAGCTGAACGAAC	GATGCTCCTGATGACCCTCC
Ppia	NM_008907.1	CTTCGAGCTGTTTGCAGACA	TGGCGTGTAAAGTCACCAC
B2m	NM_009735.3	CTCGGTGACCCTGGTCTTTC	TTGAGGGGTTTTCTGGATAGCA
Nono	NM_001252518.1	GCCAGAATGAAGGCTTGACTAT	TATCAGGGGGAAGATTGCCCA
Sry	NM_011564.1	TTGTCTAGAGAGCATGGAGGGCCATGTC	CCACTCCTCTGTGACACTTTAGCCCTCCG
Igf2	NM_010514.3	CCAGCCCTAAGATACCCTAAAGA	GAAGCACCAACATCGACTTCC
Igfbp3	NM_008343.2	TAAGAAGAAGCAGTGCCGCC	TTTCCCCTTGGTGTCGTAGC
Irs1	NM_010570.4	GGACATCACAGCAGAATGAAGAC	AGACGTGAGGTCCTGGTTGT
Irs2	NM_001081212.2	TCCAGGCACTGGAGCTTTG	CTTCACTCTTTCACGACTGTGG
Wnt4	NM_009523.2	GAAGGTGGTGACACAAGGGAC	TGTTGTCCGAGCATCCTGAC
Csh1	NM_001205322.1	TGGAGCCTACATTGTGGTGGA	CATTCCTGCGGAGCCTGAAAG

Csh2	NM_008865.3	GTCCACCAGACAACATCGGA	CTGCTGCCACCATGTGTTTC
Hmox1	NM_010442.2	AGGCTTTAAGCTGGTGATGGC	GGGGCATAGACTGGGTTCTG
Tgfb1	NM_011577.2	CCCGAAGCGGACTACTATGC	CTCATAGATGGCGTTGTTGCG
Hif1α	NM_010431.2	ACTAGACAAAGTTCACCTGAGAGAC	AGGCTGGGAAAAGTTAGGAGTG
Vegf	NM_001317041.1	GCAGACTATTCAGCGGACTCA	CCTCAAACCGTTGGCACGAT
Vegfr2	NM_010612.2	GCATACCGCCTCTGTGACTT	AAATCGCCAGGCAAACCCAC
Mmp2	NM_008610.3	AACGGTCGGGAATACAGCAG	GGTAAACAAGGCTTCATGGGG
Mmp14	NM_008608.4	GATAAGCCCAAAAACCCCGC	AACCATCGCTCCTTGAAGACA
Grp78	NM_001163434.1	TTCAGCCAATTATCAGCAAACTCT	TTTTCTGATGTATCCTCTTCACCAGT
Atf6	NM_001081304.1	AGAAAGCCCGCATTCTCCAG	CTCACTCCCAGAATTCCTACTGAT
Pdi	NM_007952.2	AGAGGCGGCTCAGATTGTTC	GAAGTGTACCTTCCGAGCTTTT
Gadd34	NM_008654.2	CCAGCGTTGTCTACCAGGAG	AGTGTACCTTCCGAGCTTTTAGA
Edem1	NM_138677.2	CTACCTGCGAAGAGGCCG	GTTCATGAGCTGCCCACTGA
Atf4	NM_009716.3	GGGTTCTGTCTTCCACTCCA	AAGCAGCAGAGTCAGGCTTTC
Chop	NM_007837.4	CCACCACACCTGAAAGCAGAA	AGGTGAAAGGCAGGGACTCA
Bcl2	NM_009741.5	CACTCTGGGTGCATACCTGG	GTTTGGGGCAGGTTTGTCG
Bax	NM_007527.3	GATCCAAGACCAGGGTGGCT	CCTTCCCCCATTCATCCCAG
Bad	NM_007522.3	CAGGATCCAAATGGGAACCCC	GGAACATACTCTGGGCTGCTG
Bid	NM_007544.4	CGCAAACCTTTGCCTTAGCC	CAGGGAATCACCACGCAGA
Bim	NM_207680.2	GTGCAATGGCTTCCATACGAC	CAGCTCCTGTGCAATCCGTA
sXbp1	NM_001271730.1	CTGAGTCCGAATCAGGTGCAG	GTCCATGGGAAGATGTTCTGG
tXbp1	NM_013842.3	TGGCCGGGTCTGCTGAGTCCG	GTCCATGGGAAGATGTTCTGG
Traf6	NM_009424.3	GCACGGAAACTTGGGTCTT	CTCTGTTGTCAGTCGACTTG
Tnf	NM_013693.3	TAGCCACGTCGTAGCAAAC	ACAAGGTACAACCCATCGGC
Il6	NM_001314054.1	GGGACTGATGCTGGTGACAA	ACAGGTCTGTTGGGAGTGGT
Il1β	NM_008361.4	GCCACCTTTTGACAGTGATGAG	GACAGCCCAGGTCAAAGGTT
Glut1	NM_011400.3	GGCTTGCTTGTAGAGTGACG	TGTAGAACTCCTCAATAACCTTCTG
Glut3	NM_011401.4	AATAGGTAGGCTGGGCTTCG	AGAGATGGGGTCACCTTCGTT
Fabp4	NM_024406.3	AAGCTGGTGGTGGAATGTGTTA	CCTCTTCCTTTGGCTCATGC
Snat2	NM_175121.3	GCAGTGGAATCCTTGGGCTT	TAAAGATCCTCCTTCGTTGGCAG

2.3.4 Quantitative (q)PCR assays

Quantitative PCR was carried out in 384-well plates with 10 µL reaction volumes, prepared under sterile fume hood conditions to minimize contamination. Each reaction consisted of 2.5 µL of template cDNA (1:100 dilution) prepared from placental tissue samples, 1 µL of 5 µM forward and reverse oligonucleotide primers for the gene of interest (Invitrogen), 0.5 µL UP-H_2O, and 5 µL Lightcycler 480 SYBR Green I Master (Roche, 04887352001, Canada). Each RT-qPCR plate consisted of the placental samples of interest, non-template control (consisting of 2.5 µL UP-H_2O instead of template cDNA), and 5 standards (generated from a serial 1:10 dilution from placental cDNA made by pooling cDNA from all samples, see below) for quantification purposes, all samples were plated in triplicate.

2.3.5 Standard curve generation and sample analysis

An equal portion of each sample was collected and pooled to generate a standard that was used to construct a standard curve. The standard was serially diluted (1:10, 1:100, 1:1 000, 1:10 000, 1:100 000) along with a negative control (UP-H_2O). The standard curve and diluted samples were centrifuged at 3000 rpm for 2 minutes at 4 °C, and incubated at 95 °C for 5 minutes, followed by these cycling conditions (LightCycler 480 II, 05015243001, Roche), 45 successive cycles of 95 °C for 10 seconds, 60 °C for 10 seconds, and 72 °C for 10 seconds. Following which, samples were incubated at 95 °C for 5 seconds, 65 °C for 1 minute, and 97 °C for 5 minutes, and 40 °C for 30 seconds.

2.3.6 RT-qPCR data analysis and verification

An absolute amplification [244] and melting point analysis [245] were performed on all placental cDNA samples for each gene of interest. The geometric mean of constitutively activated genes (housekeeping genes) was used as a correction factor for all genes of interest. All housekeeping genes showed no difference with diet or placental sex (data not shown). The housekeeping genes used for E14.5 placentae were beta actin (*β actin)*, cyclophilin (*Ppia*), beta-2-microglobulin (*B2m*), 14-3-3 protein gamma (*Ywhag*), and non-POU domain containing octamer binding protein (*Nono*). The housekeeping genes used for E18.5 placentae were *β actin*, hypoxanthine-guanine phosphoribosyltransferase (*Hprt*), and importin 8 (*Ipo8*). Data from genes of interest were expressed as the ratio of the gene of interest to the geometric mean of the housekeeping genes. A melting point analysis was used to identify the heterogeneity of the genomic products amplified by RT-qPCR. Only samples which generated a single melting curve peak (homogenous, amplifying a single genomic target) [245] were used.

2.3.7 nCounter Nanostring

In order to investigate novel pathways, a custom nCounter reporter codeset (designed by Dr. Kjetil Ask, McMaster University) was used to analyze the transcript levels of 184 genes associated with ER stress, apoptosis, inflammation, and placental growth (Table 2.3.7.1) in a subset of E18.5 placental tissues (n = 4 per group). One hundred ng RNA was incubated overnight with the nCounter reporter codeset, capture probeset, and hybridization buffer. The samples were then processed with the nCounter prep-station. Raw data were normalized to six

housekeeping genes (*Ubc*, *Tuba1a*, *Hprt*, *Ipo8*, *Gusb*, and *β actin*). Fold change from controls was automatically determined using nSolver analysis software version 2.5.

Table 2.3.7.1: Genes used in the Nanostring custom nCounter codeset.

Metabolism	Inflammatory markers		ER stress and autophagy	EMT and vascular development		Other
Acc1	*Arg1*	*Il4*	*Ap1*	*Angpt1*	*sfrp1*	*C myc*
Enpp1	*Arg2*	*Il1a*	*Ask1*	*Angpt2*	*sfrp2*	*Coli*
Fas	*B2m*	*Il1b*	*Pkb*	*Bdnf*	*sfrp4*	*Fn1*
Irs1	*Baff*	*Il2*	*Atf4*	*Bmp2*	*snail1*	*Gata4*
Irs2	*C1qc*	*Il6*	*Atf6*	*Bmp4*	*snail2*	*Mmp1*
Mapk14 P38	*Ccl20*	*Il6ra*	*Bak1*	*Bmp7*	*Scf*	*Mmp2*
Pcsk9	*Ccr3*	*Il13*	*Bax*	*Bmpr1a*	*Ror2*	*Mmp3*
Pparg	*Ccr4*	*Il15*	*Bbc3*	*Bmpr2*	*Tie1*	*Mmp7*
Ppia	*Ccr5*	*Il17a*	*Bim*	*Cd44*	*Timp3*	*Mmp9*
Srebp1 c	*Ccr8*	*Il21*	*Bcl2*	*Col3a1*	*Twist*	*Mmp14*
	Cxcl1	*Il23*	*Bad*	*Dkk1*	*TrkA*	*Rab9*
	Cxcl17	*Nos2*	*Beclin 1*	*E Cadherin*	*TrkB*	*Tac1*
	Cd8	*Ido1*	*Bid*	*Fzd1*	*TrkC*	*Tacr1*
	Cd11b	*Ip10*	*Calnexin*	*Fzd3*	*Trp53*	*Taok3*
	Cd11c	*Lys6g*	*Calreticulin*	*Gremlin*	*Vip*	*Tbp*
	Cd23	*Cd206*	*Chop*	*Hmox1*	*Vpac1*	*Timp1*
	Cd68	*Mapk8*	*Edem1 Perk*	*Hsp 27*	*Vpac2*	
	Cd103	*Mcp1*	*Faslg*	*Hsp47*	*Vegf*	
	Cxcr3	*Myd88*	*Fkbp13*	*Lrp5/6*	*Wnt1*	
	Cxcr6	*Nfkb1*	*Fkbp65*	*Lgals1*	*Wnt10b*	
	Cgrp	*Nlrp3*	*Grp78*	*Lgals3*	*Wnt11*	
	Csf2	*Nod1*	*P4h*	*Lgals9*	*Wnt2*	
	Emr1	*Nod2*	*Xbp1*	*Loxl2*	*Wnt3a*	
	Foxp3	*Ngf*	*Vps34*	*Lrp6*	*Wnt4*	
	Gp130	*Stat3*	*Vps15*	*Osm*	*Wnt5a*	
	Ifng	*Tgfb1*		*OsmRb*	*Wnt7b*	
	Traf2	*Tgfbr1*		*Ntf3*	*Wnt8a*	
	Tlr2	*Tlr4*				
		Tnf				

2.4 Immunoblotting analyses

2.4.1 Total protein extraction

Total protein was extracted by taking approximately one quarter of placental tissue and adding two 2.8 mm ceramic homogenization beads (19-646-3, Omni International) and 300 µL extraction buffer (50 mM HEPES, H3375-100G, Sigma-Aldrich; 150 mM NaCl, S671-3, Thermo Fisher; 100 mM NaF, S299-500, Thermo Fisher; 10 mM sodium pyrophosphate, P8010-500G, Sigma-Aldrich; 5 mM EDTA, E478-500, Thermo Fisher; 250 mM sucrose, SUC507.500, BioShop; 1% Triton-X, X100-500ML, Sigma-Aldrich; 1 mM sodium orthovanadate, S6508-10G, Sigma-Aldrich; 1% protease inhibitor tablet, 04693159001, Roche). Samples were homogenized for 30 seconds at 4.5 m/s, centrifuged at 14 000 g for 15 minutes at 4°C and the lysate was pipetted into fresh tubes and protein concentration determined using a BCA protein assay (detection range of 0.025-2 mg/mL). Using a Pierce BCA protein assay kit (23225, Thermo Fisher), a standard curve was generated with BSA concentrations from 0 to 2 mg/mL (0, 0.025, 0.125, 0.250, 0.500, 0.750, 1.0, 1.5, 2) from a 2 mg/mL stock. Placental protein samples were diluted 1:25, 2:25, and 3:25 in distilled H_2O. For each BSA standard and placental sample, 25 µL was added to a 96-well plate (07-200-95, Thermo Fisher) in triplicate. The working reagent was prepared as per kit specifications (50:1 ratio of reagent A to B), and 200 µL was added to each well. The plate was lightly shaken to mix the samples and incubated at 37 °C for 30 minutes. The sample absorbance was measured at 562 nm using a BioTek Synergy H4 Hybrid microplate reader (BioTek). Placental protein sample absorbance was used to calculate protein concentration, all samples were normalized to 1 µg/µL using extraction buffer

(above) as a diluent. Protein samples were aliquoted and stored at - 80 °C for immunoblotting and ELISA analyses.

2.4.2 Nuclear protein extraction

This protocol was adapted from [246] and used on E14.5 placental samples only - no E18.5 tissue was available for nuclear protein extraction. Nuclear protein was extracted from half of a frozen E14.5 placenta, washed twice in 1 mL phosphate-buffered saline (PBS) and then re-suspended in 500 µL hypotonic lysis buffer (10 mM HEPES, pH 7.9, H3375-100G, Sigma-Aldrich; 1.5 mM $MgCl_2 \cdot 6\ H_2O$, 242964, Sigma-Aldrich; 10 mM KCl, PX1405-1, EMD Millipore; 1% protease inhibitor tablet, 04693159001, Roche). Three 2.8 mm ceramic homogenization beads (19-646-3, Omni International) were added and the samples were homogenized at 4.5 m/s for 60 seconds then centrifuged at 11 000 g for 20 minutes. The supernatant was discarded (cytoplasmic fraction) and the nuclei pellet was resuspended in 70 µL of extraction buffer (20 mM HEPES, pH 7.9, H3375-100G, Sigma-Aldrich; 1.5 mM $MgCl_2 \cdot 6\ H_2O$, 242964, Sigma-Aldrich; 420 mM NaCl, S671-3, Thermo Fisher; 0.2 mM EDTA E478-500, Thermo Fisher, 25% v/v glycerol, 5350-1, Caldeon; 1% protease inhibitor tablet, 04693159001, Roche), and the samples were homogenized again as above. The samples were incubated at room temperature for 30 minutes on a rotating platform at 60 rpm then centrifuged for 5 minutes at 21 000 g. The supernatant was transferred to fresh tubes and the protein concentration was determined using a BCA assay as above.

2.4.3 Immunoblotting

Protein from each sample was denatured as follows: 10 µg of protein was mixed with loading buffer (4% w/v sodium dodecyl sulfate, SDS, SDS001.500, BioShop; 20% v/v glycerol, 5350-1, Caldeon; 120 mM Tris-HCl, T5941-1KG, Sigma-Aldrich; 0.02% w/v bromophenol blue, 114391-5G, Sigma-Aldrich; and 50 mM dithiothreitol, DTT, 646563-10X.5ML, Sigma-Aldrich) in a 1:3 protein to loading buffer ratio and incubated at 55 °C for 10 minutes. The samples were loaded into an acrylamide (1610148, BioRad) gel. The stacking gel was 12.5% acrylamide, 125 mM Tris-HCl pH 6.8, 10% SDS, 10% ammonium persulfate (APS, 161-0700, BioRad), and 1% tetramethylethylenediamine (TEMED, 161-0801, BioRad). The separating gel was 7.5-15% acrylamide (based on protein size; Table 2.4.3.1), 250 mM Tris HCl pH 8.8, 10% SDS, 10% APS, 1% TEMED. The samples were separated using electrophoresis at 100 V for at least 105 minutes using a running buffer (0.3 % w/v Tris base, BP152-5 Thermo Fisher; 14.4% w/v glycine, BP38-1, Thermo Fisher; 1% w/v SDS). Polyvinylidene fluoride (PVDF, 1620177, BioRad) membranes were incubated in 100% methanol for 5 minutes, then the membranes, filter paper (1703959, BioRad), and the separating gels were incubated in transfer buffer (25 mM Tris, 192 mM glycine, 10% v/v methanol) for 10 minutes. The proteins were then transferred to the PVDF membranes using the semi-dry transfer method with a Trans-Blot® Turbo™ Transfer System (1704150, BioRad), and blocked in 5% bovine serum albumin (BSA, A2153-1KG, Sigma-Aldrich) in tris-buffered saline with 0.1% v/v tween 20 (TBST; twn508.500, BioShop) for 1 hour. The membranes were incubated overnight with a rabbit anti-mouse primary antibody (Table 2.4.3.1). The following day, the membranes were washed for 4x15 minutes in TBST, incubated in goat anti-rabbit IgG secondary antibody (ab6721, Abcam) for one hour at room

temperature, and washed 4x15 minutes in TBST. The membranes were rinsed in distilled water, and incubated for 5 minutes in Clarity Western ECL Blotting Substrate (1705061, BioRad). The membranes were imaged using a ChemiDoc MP Imaging System (1708280, BioRad). In the case of phosphorylated proteins, membranes were then washed 2x15 minutes in TBST, incubated in stripping buffer (21059, Thermo Fisher) for 5 minutes, and washed for 2x15 minutes in TBST, then blocked in 5% BSA in TBST for 1 hour. The membranes were then probed with the primary antibody binding to the total (phosphorylated and non-phosphorylated) protein of interest, and repeated as above. Beta actin (5125S, CST) was used as a positive internal control in each gel; TATA-box binding protein (TBP, 8515S, CST) was used as a positive internal control for nuclear protein extracts. All protein data are expressed as a relative concentration to the internal controls. All immunoblotting data were analyzed using ImageLab software (Image Lab™ Software for PC Version 6.0.1 SOFT-LIT-170-9690-ILSPC).

Table 2.4.3.1: Immunoblotting antibodies and gel conditions.

Target protein	Primary antibody dilution	Secondary antibody dilution	Gel %	Primary antibody product code	Primary antibody supplier
GRP78	1:2000	1:100 000	10	ab21685	Abcam
Phospho-PERK	1:500	1:150 000	7.5	MA-01533	Thermo Fisher
PERK	1:1000	1:150 000	7.5	3192	CST
Phospho-IRE1α	1:1000	1:200 000	7.5	ab48187	Abcam
IRE1α	1:1000	1:150 000	7.5	ab37073	Abcam
Phospho-eIF2α	1:1000	1:100 000	12	9721	CST
eIF2α	1:1000	1:100 000	12	9722	CST
Cleaved casp-3	1:1000	1:50 000	12	9661	CST
Total casp-3	1:1000	1:100 000	12	9662	CST
GLUT1	1:1000	1:100 000	12	12939	CST
HIF1α[#]	1:1000	1:100 000	7.5	NB100-479	Novus Biologicals
β-actin*	1:5000	N/A	(based on protein of interest)	5125	CST
TBT*[#]	1:1000	1:20 000	(based on protein of interest)	8515	CST

* Indicates a positive internal control

[#] Indicates these antibodies were only used on samples of nuclear protein extracts, all others were used on samples from total protein extracts.

2.5 Enzyme-linked immunosorbent assays (ELISAs)

2.5.1 Insulin ELISA

Serum insulin levels were measured using a high sensitive mouse insulin immunoassay kit (32380, Toronto Bio Sciences). In brief, 10 µL of sample or standard (detection range of 200-7000 pg/mL) was added to each well, then 100 µL of detection antibody was added. The plate was incubated at room temperature for 90 minutes at 600 rpm. The wells were washed 4 times with wash buffer, and 100 µL of substrate solution was added to each well. The plate was protected from light and incubated at room temperature for 15 minutes. 100 µL of the stop solution was added to each well and the absorbance of 450 nm was measured using a BioTek Synergy H4 Hybrid microplate reader (BioTek) the sample concentrations were determined by log-log curve fitting and linear regression (GraphPad Prism 6.0 © GraphPad Software Inc. 1994-2013).

2.5.2 NF-κB ELISA

NF-κB protein levels were measured using a TransAM NF-κB p65 transcription factor assay kit (40096, Cedarlane). In brief, 30 µL of complete binding buffer and 20 µg of total placental protein was added to each well. 10% v/v of Jurkat nuclear extract in complete lysis buffer was used as a positive control, and complete lysis buffer was used as a negative control. The samples were then incubated at room temperature for one hour at 300 rpm. The wells were then washed three times with wash buffer and 1:1000 NF-κB primary antibody was added to each well. The samples were incubated for one hour at room temperature and then washed again as above. 1:1000 HRP-conjugated secondary antibody was added and the plate was incubated at room

temperature for one hour, and then washed as above. The developing solution was added to each well, then the samples were incubated in the dark for 5 minutes, and lastly, stop solution was added. The absorbance of 450 nm light was measured using a BioTek Synergy H4 Hybrid microplate reader (BioTek), absorbance at 655 nm was used as a reference.

2.6 Immunohistochemical analyses

2.6.1 Fixed tissue processing

Fixed placental tissues were incubated in 70% ethanol for 4x1h, then 95% ethanol 2x1 hr, and incubated overnight in 95% ethanol. Samples were then incubated in 100% ethanol for 2x1 hr, then 1:1 100% ethanol:histoclear for 1h, followed by 2x1h histoclear. Lastly, the samples were incubated in 1:1 histoclear:paraffin overnight. In preparation for the paraffin embedding, the samples were incubated in pre-heated paraffin wax at 60 °C 3x1 hr and embedded in paraffin wax using a standard tissue embedding machine (EG1160, Leica Biosystems). The samples were then placed on a cold plate for the wax to solidify and stored at room temperature for immunohistochemistry.

2.6.2 Immunohistochemistry

Placental tissues were cut (4 µm except for cleaved caspase-3 staining where 7 µm sections were used; Microm HM325, Thermo Fisher), placed on microscope slides (12-550-15, Thermo Fisher), and incubated overnight at 37°C. Sections (3 per placenta) were immunostained with anti-carbonic anhydrase IX (CAIX) as a hypoxia marker (1:600; ab15086, Abcam), anti-CD31 as an endothelial cell marker (1:25; ab24590, Abcam; only used for E18.5 placentae),

anti-vascular endothelial growth factor (VEGF, 1:400; sc152, Santa Cruz), and anti-VEGFR2 antibody (1:200; sc6251, Santa Cruz) as angiogenesis markers, and anti-cleaved caspase-3 as an apoptosis marker (1:100; 9661, CST). In brief, the sections were deparaffinized (3x5 mins histoclear, 50-329-50, Thermo Fisher; 2x2 mins anhydrous ethanol, 2x2 mins 90% ethanol, 2x2 mins 70% ethanol, and 2x5 mins tris buffered saline, TBS, pH 7.4). Antigen retrieval was performed with citrate buffer (pH 6.0, incubated at 95°C for 20 minutes and washed 2x5 mins in TBS). The sections were blocked with 1% BSA in TBST (pH 7.4) and 5% goat serum (ZC0620, Vector) in a humidified chamber for one hour. The blocking reagent was removed and each section was incubated with each primary antibody (diluted in 1% BSA/TBST) overnight at 4°C and washed the next day in TBS for 2x5 mins. Endogenous peroxidases were inhibited by incubating sections in 0.2% v/v H_2O_2 (H324-500, Thermo Fisher) diluted in TBS and next washed in TBS for 2x5 mins. The sections were incubated for one hour in a humidified chamber with a biotinylated secondary antibody (1:100 in TBST, PK6101, Vector), and washed in TBS for 2x5 mins. Each section was labeled with avidin-biotin peroxidase complex following VectaStain ABC kit protocols (PK-4000, Vector) for one hour and then washed in TBS for 2x5 mins. Protein was visualized via incubation with 3,3' diaminobenzidine (DAB) peroxidase (HRP; SK-4100, Vector). The sections were counterstained with Meyer's hematoxylin (MHS32-1L, Sigma-Aldrich), washed in running water and dehydrated (2x2 mins 70% ethanol, 2x2 mins 90% ethanol, 2x2 mins anhydrous ethanol, and 3x5 mins histoclear). Coverslips (P35G-0-14-C, MatTek Corporation) were mounted (permount mounting media; sp15-500, Thermo Fisher) and left to dry for 24 hours prior to analysis using NIS elements software. The

proportion of positive staining relative to placental area was determined using a threshold for DAB-positive staining.

2.7 Statistical analysis

All data were analyzed either by a Student's t test (male data as a result of high fat diet, mating data, pregnancy outcomes, and E18.5 Casp-3 IHC due to limited sample size where placentae could not be separated by sex) or by two-way ANOVA where paternal diet and placental sex were factors. Bonferroni's post-hoc analysis was used where appropriate. nCounter nanostring data were analyzed using a log-linear model in R, with Tukey's HSD post-hoc analysis used where appropriate. A repeated measures ANOVA was used for measures conducted over time (weight gain, glucose clearance, adiposity), all data are presented as mean +/- standard error of the mean (SEM) unless otherwise stated. In all cases, significance (*) was set at $p < 0.05$. All data were analyzed in GraphPad Prism version 6.0 (GraphPad Prism 6.0 © GraphPad Software Inc. 1994-2013).

Chapter 3.0 Results

3.1 Paternal phenotype and pregnancy outcomes

The purpose of this study was to investigate the impacts of paternal obesity on placental development, thus we verified our model by performing measures of adiposity and metabolic indices of diet-induced obesity. High fat fed male mice were heavier than controls after 3 weeks of diet (Figure 3.1.1A) and consumed more energy per body weight per day until week 5, where food intake was normalized (Figure 3.1.1B). Glucose clearance was similar between groups at week 0 (Figure 3.1.1C), however, by week 5 high fat fed males showed impaired glucose clearance (Figure 3.1.1D) and this was maintained to week 7 (Figure 3.1.1E). There was no difference in adiposity at week 0, but high fat fed males had significantly higher relative fat mass compared to controls by week 5 and this was maintained throughout the rest of the dietary intervention (Figure 3.1.1F). This suggests our mouse model induces an obese phenotype, characterized by impaired glucose clearance and increased adiposity [247].

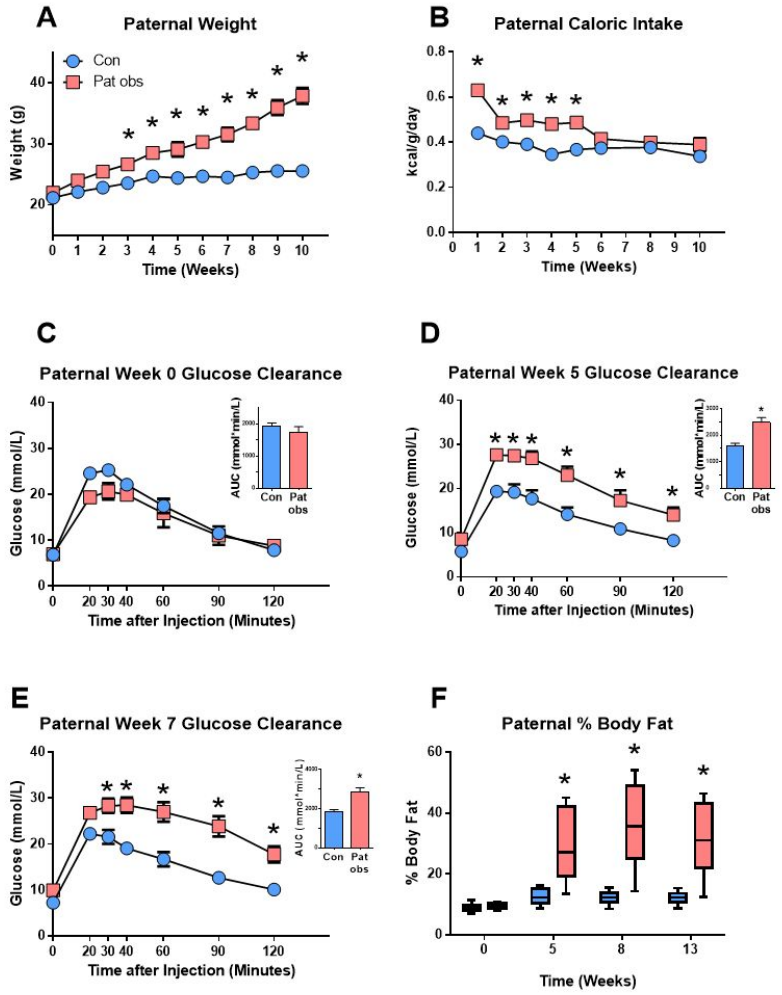

Figure 3.1.1: High fat diet alters metabolic indices in male mice. Male weight over 10 weeks of either control or high fat diet (A), and energy consumption (kcal/gram of body weight/day; B). Glucose clearance at week 0 (C), 5 (D), and 7 (E) was measured using an intraperitoneal glucose tolerance test (IPGTT). Adiposity was measured using an echoMRI at week 0, 5, 8, and 13 (F). Data are presented as mean +/- SEM (A-E), or median +/- upper and lower quartiles (F). * denotes $p<0.05$, after repeated measures ANOVA. Control-fed males (Con, n=15; 17% kcal/fat, blue), HF-fed males (Pat obs, n=15; 60% kcal/fat, pink).

After 13 weeks of dietary intervention, high fat fed males had increased gonadal fat weight (Figure 3.1.2A), mesenteric fat weight (Figure 3.1.2B), liver weight (Figure 3.1.2C), and epididymal weight (Figure 3.1.2D), without changes in testicular (Figure 3.1.2E) or seminal

vesicle weights (Figure 3.1.2F) compared to controls. This is expected as a high fat diet increases overall body weight, and has been previously shown to be associated with increased liver weight [248]. High fat fed males had significantly elevated fasting blood glucose and insulin levels compared to controls (Figure 3.1.2G). The homeostatic model assessment of insulin resistance (HOMA-IR) was calculated by the formula: HOMA-IR = glucose (mmol/L) * insulin (mU/L)/22.5 [249,250] (Figure 3.1.2H). High fat fed males had a significantly higher HOMA-IR index, indicating insulin resistance. This supports the glucose clearance data collected at weeks 5 and 7 as impaired glucose clearance is associated with insulin resistance [3].

We used several metrics to characterize mating efficacy (Table 3.1.1) and embryo viability (Table 3.1.2). There was no difference between groups in the number of overnight pairings required for the first pregnancy, or in the number of plug-producing pairings required for the first pregnancy (Table 3.1.1). Maternal weight gain across gestation, maternal fasting glucose levels, fetal sex ratio, fetal weight, and placental weight were not different between groups (Table 3.1.2).

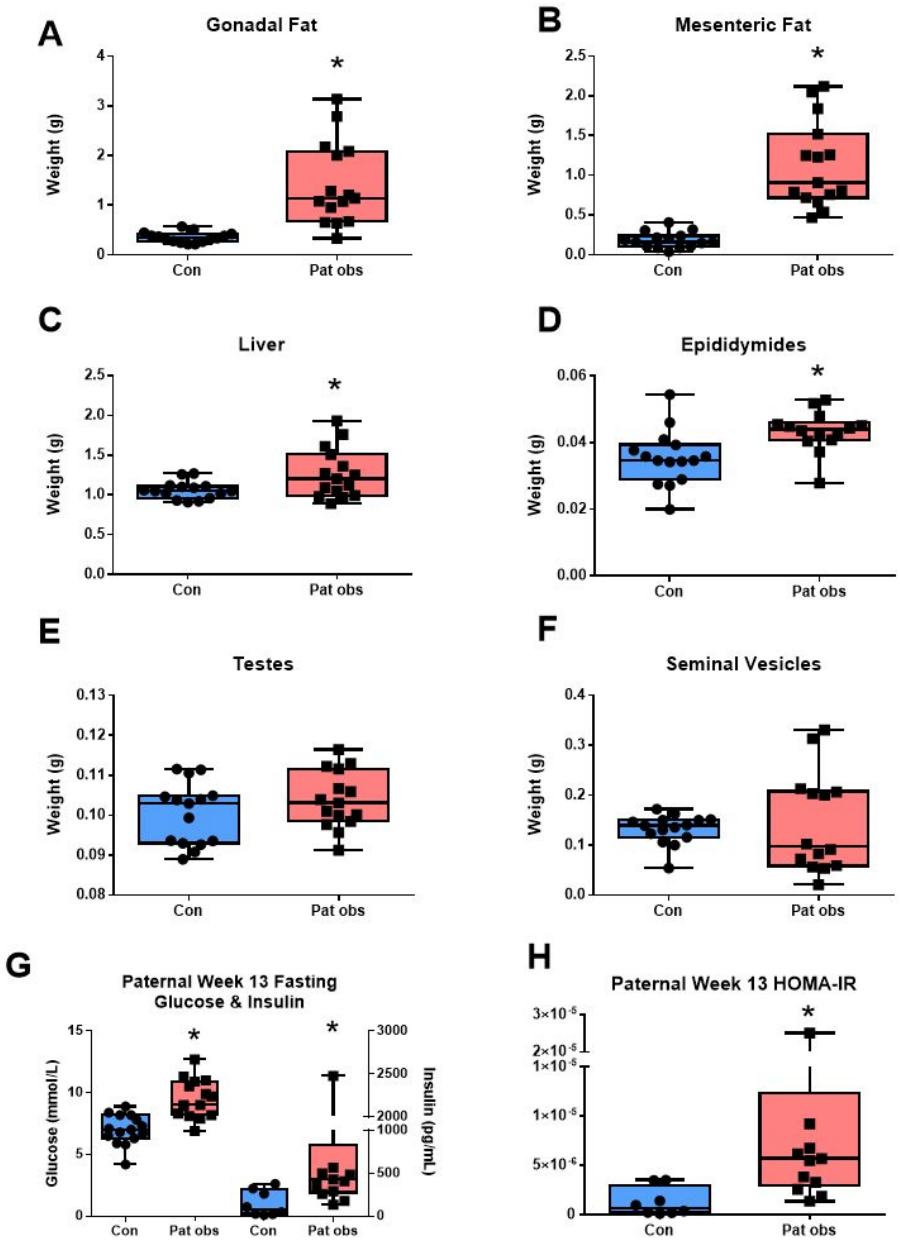

Figure 3.1.2: High fat diet results in obesity, impaired glucose control, and insulin resistance. Following 13 weeks of diet, male mice gonadal fat (A), mesenteric fat (B), liver (C), epididymides (D), testes (E), and seminal vesicles (F) were weighed. Fasting blood glucose and insulin levels were measured (G), and HOMA-IR (H) calculated [249, 250]. Data are presented as median +/- upper and lower quartiles. * denotes $p<0.05$, after Student's t-test. Control-fed males (Con, n=15, blue), HF-fed males (Pat obs, n=15, pink).

Table 3.1.1: Mating efficacy. Data are presented as mean +/- standard error of the mean. * denotes $p<0.05$, after Student's t-test for number of pairings required for first pregnancy; Mantel-Cox log-rank survival test used for the number of plug-producing pairings required for first pregnancy.

Mating efficacy parameter	Control fed (mean ± SEM) n = 15	High fat fed (mean ± SEM) n = 15	P value
Number of male and female pairings required for first pregnancy	3 ± 0.6	4 ± 1.4	0.4746
Number of plug-producing pairings required for first pregnancy	2 ± 0.3	3 ± 0.3	0.1047

Table 3.1.2: Pregnancy outcomes. Data are presented as mean +/- standard error of the mean. * denotes p<0.05, after Student's t-test for maternal data and fetal sex ratios, 2-way ANOVA used for fetal data with paternal diet and fetal sex as main factors.

Pregnancy parameter	Control fed (mean ± SEM) n = 9		High fat fed (mean ± SEM) n = 6-8		P value(s)		
E14.5 pregnancies							
Pregnancy weight gain (g)	5.2 ± 0.23		5.4 ± 0.29		0.7032		
Maternal fasting glucose (mmol/L)	5.6 ± 0.40		5.8 ± 0.26		0.7575		
Fetal sex ratio (male to female)	0.439 ± 0.069		0.414 ± 0.078		0.8199		
Number of resorptions	1 ± 0.3		1 ± 0.3		0.7513		
Litter size	8 ± 0.4		8 ± 0.3		> 0.9999		
	♂	♀	♂	♀	Main effect of diet	Main effect of sex	Interaction (diet, sex)
Fetal weight (g)	0.25 ± 0.004	0.23 ± 0.008	0.24 ± 0.006	0.23 ± 0.005	0.8126	*0.0382	0.6012
Placental weight (g)	0.01 ± 0.002	0.09 ± 0.003	0.09 ± 0.002	0.09 ± 0.003	0.9846	*0.0310	0.5264
Fetal glucose (mmol/L)	2.0 ± 0.18	2.2 ± 0.14	2.0 ± 0.13	1.8 ± 0.10	0.2242	0.8292	0.1771
E18.5 pregnancies							
Pregnancy weight gain (g)	14.2 ± 0.86		14.1 ± 0.67		0.9419		
Maternal fasting glucose (mmol/L)	6.7 ± 0.38		6.1 ± 0.33		0.2336		
Fetal sex ratio (male to female)	0.636 ± 0.064		0.484 ± 0.071		0.1392		
Litter size	8 ± 0.4		8 ± 0.5		> 0.9999		
	♂	♀	♂	♀	Main effect of diet	Main effect of sex	Interaction (diet, sex)
Fetal weight (g)	1.14 ± 0.034	1.09 ± 0.016	1.12 ± 0.033	1.12 ± 0.023	0.9009	0.3938	0.3747

3.2 Angiogenesis and hypoxia

The placenta is a highly vascularized organ and angiogenesis plays a key role in placental development [46,75]. We used carbonic anhydrase IX (CAIX) as a hypoxia marker, and found increased CAIX immunostaining in E14.5 Pat obs placentae (Figure 3.2.1A, C) and E18.5 Pat obs placentae compared to controls (Figure 3.2.1B, D), suggesting that paternal obesity is associated with placental hypoxia. This is consistent with the fact that hypoxia-inducible factor 1 alpha (HIF1α) protein levels were elevated in E14.5 Pat obs male placentae (Figure 3.2.1E, F), despite no difference in *Hif1α* transcript levels at E14.5 (Figure 3.2.1G) and E18.5 (Figure 3.2.1H). Since hypoxia promotes angiogenesis [190], we measured transcript levels of vascular endothelial growth factor (*Vegf*) and its pro-angiogenic receptor (*Vegfr2*). Female Pat obs E14.5 placentae had reduced transcript levels of *Vegf* compared to controls (Figure 3.2.2A), yet there was no difference between groups at E18.5 (Figure 3.2.2B). There was no difference between groups in *Vegfr2* transcripts at both time points (Figure 3.2.2C, D). Immunopositive VEGF was increased in male and female E14.5 Pat obs placental tissue (Figure 3.2.3A, C) and increased in female but not male Pat obs E18.5 placental tissue (Figure 3.2.3B, D), consistent with this, VEGFR2 positive staining was increased in both male and female E14.5 Pat obs placental tissue compared to controls (Figure 3.2.3E, G), and in female but not male E18.5 Pat obs placental tissue (Figure 3.2.3F, H). Similarly, there was an interaction between diet and sex in immunopositive CD31 staining where female E18.5 Pat obs placentae showed increased immunopositive staining compared to controls (Figure 3.2.4A, B).

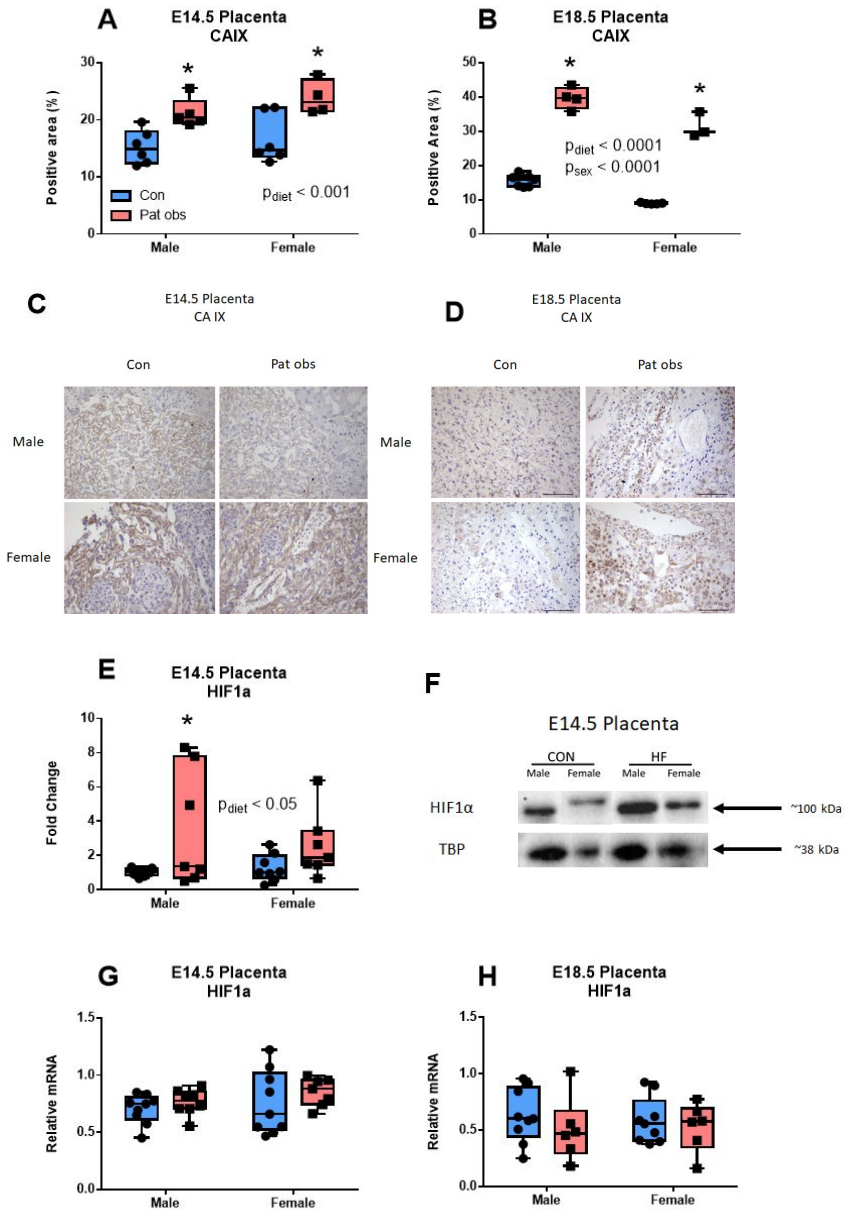

Figure 3.2.1: Paternal obesity is associated with increased hypoxia markers in placentae. E14.5 and E18.5 placentae were immunostained with hypoxia marker carbonic anhydrase IX (CAIX; A, B). Hypoxia-inducible factor 1 alpha (HIF1α) protein levels were measured using immunoblotting at E14.5 (E). HIF1α transcript levels were measured with RT-qPCR in E14.5 (G) and E18.5 placentae (H). Representative immunohistochemical images shown (C, D), scale bar represents 100 µm. Representative immunoblot bands shown (F), TBP used as an internal control. All mRNA levels are relative to the geometric mean of housekeeping genes. Data are presented as median +/- upper and lower quartiles. * denotes $p<0.05$, after 2-way ANOVA was used to compare data between groups. Control-fed males (Con, n=5-9, blue), HF-fed males (Pat obs, n=3-8, pink).

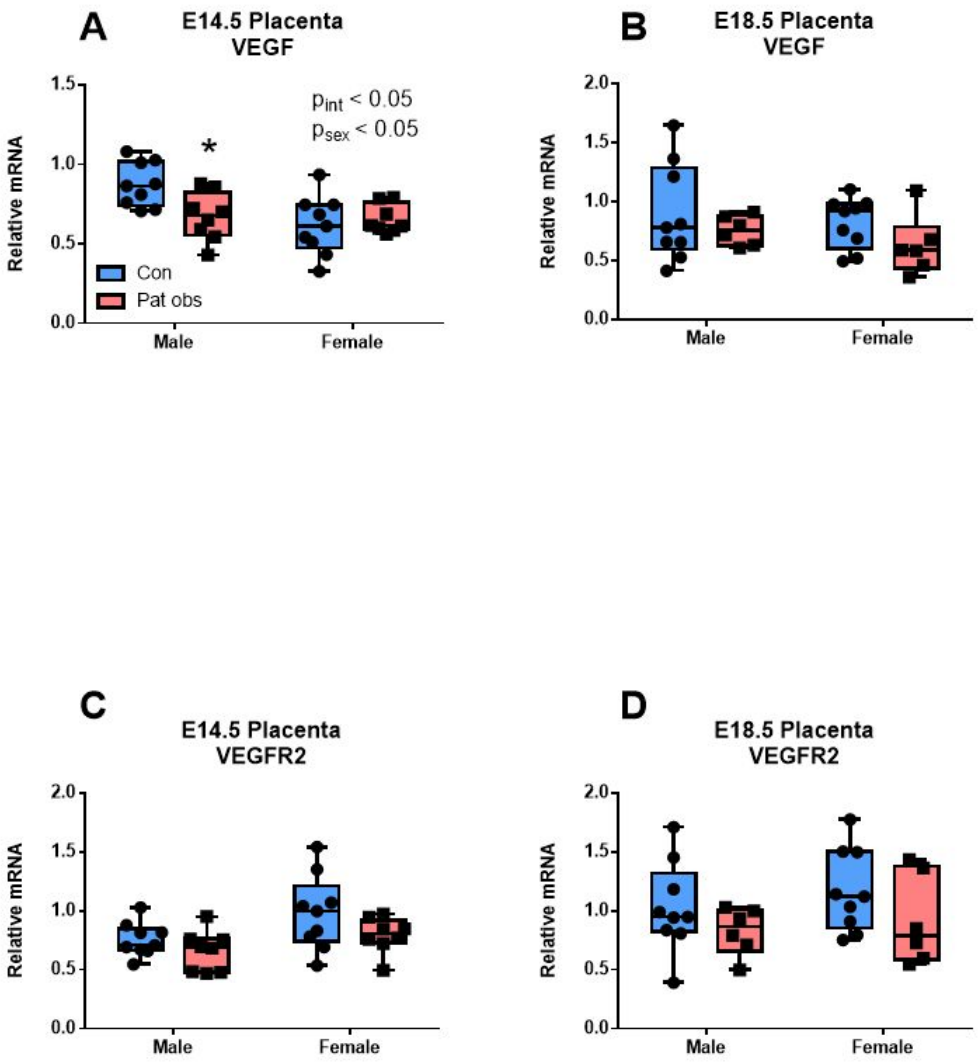

Figure 3.2.2: Paternal obesity is associated with reduced VEGF transcript levels in E14.5 placentae. Transcript levels of *VEGF* and its pro-angiogenic receptor, *VEGFR2* were measured in E14.5 (A, B) and E18.5 (C, D) placentae. All mRNA levels are relative to the geometric mean of housekeeping genes. Data are presented as median +/- upper and lower quartiles. * denotes $p<0.05$, after 2-way ANOVA was used to compare data between groups. Control-fed males (Con, n=9, blue), HF-fed males (Pat obs, n=6-8, pink).

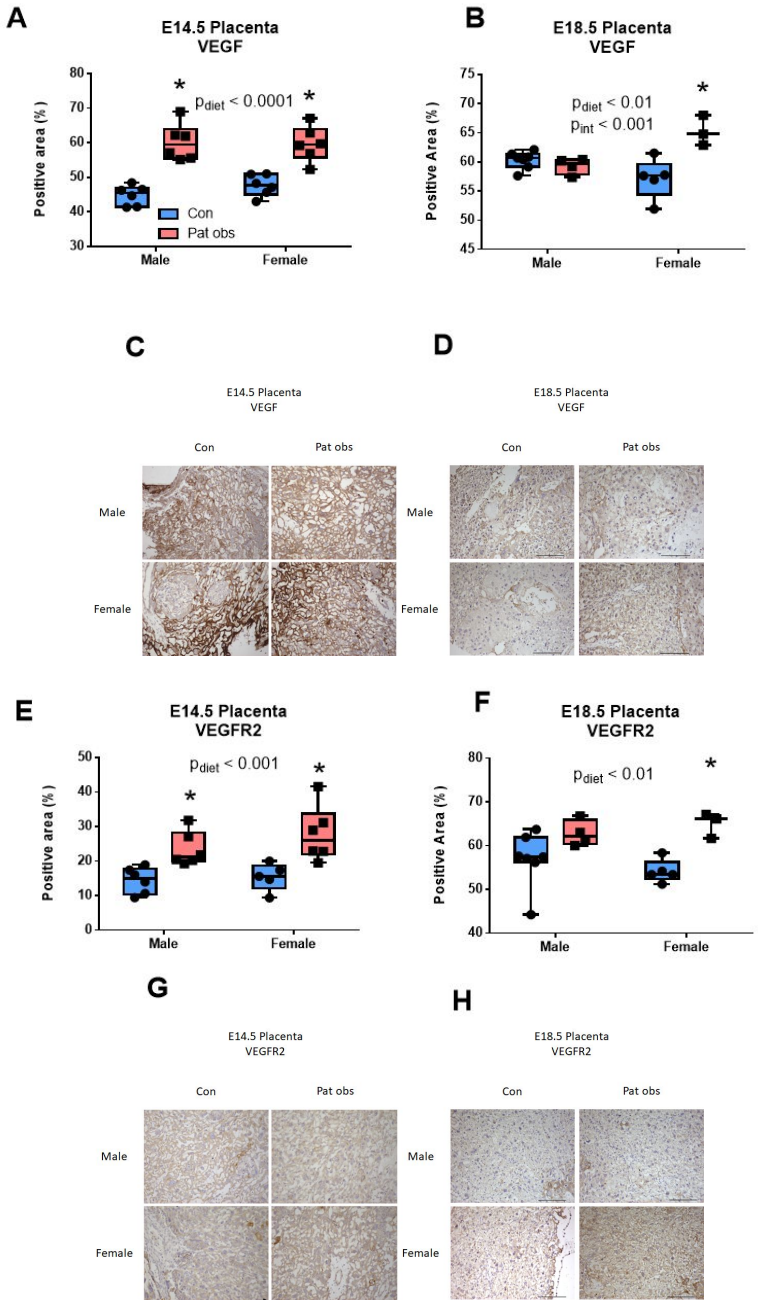

Figure 3.2.3: Paternal obesity is associated with increased angiogenesis factors in male and female E14.5 placentae, but only in females in E18.5 placentae. E14.5 and E18.5 placentae were immunostained with angiogenesis marker vascular endothelial growth factor (VEGF; A, B), and its pro-angiogenic receptor, VEGFR2 (E, F). Representative immunohistochemical images shown (C, D, G, H), scale bar represents 100 µm. Data are presented as median +/- upper and lower quartiles. * denotes $p<0.05$, after 2-way ANOVA was used to compare data between groups. Control-fed males (Con, n=5-7, blue), HF-fed males (Pat obs, n=3-6, pink).

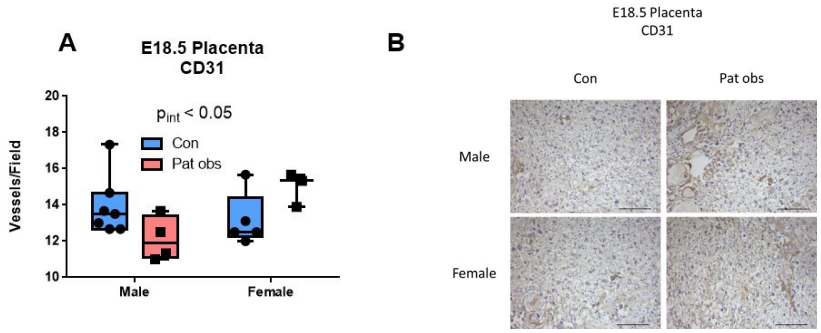

Figure 3.2.4: Paternal obesity is associated with an interaction between diet and sex in endothelial cell marker CD31 immunopositive staining. E18.5 placentae were immunostained with the endothelial cell marker CD31 (A). Representative immunohistochemical images shown (B), scale bar represents 100 µm. Data are presented as median +/- upper and lower quartiles. * denotes p<0.05, after 2-way ANOVA was used to compare data between groups. Control-fed males (Con, n=5-7, blue), HF-fed males (Pat obs, n=3-4, pink).

The notion that paternal obesity induces changes in placental vascular development is supported by lower levels of heme oxygenase 1 (*Hmox1*) transcript levels in E14.5 Pat obs placentae compared to controls (Figure 3.2.5A), with no difference between groups at E18.5 (Figure 3.2.5B). *Hmox1* mediates matrix metalloproteinase 2 (*Mmp2*), and *Mmp14* to facilitate blood vessel widening and maturation [251,252]. While there was no difference in *Mmp2* transcript levels at E14.5 (Figure 3.2.5C), or E18.5 (Figure 3.2.5D), *Mmp14* transcript levels were lower in E14.5 female Pat obs placental tissue compared to controls (Figure 3.2.5E). This was not maintained until E18.5 (Figure 3.2.5F), but, *Mmp1* and *Mmp9* transcript levels were lower in E18.5 Pat obs placentae compared to controls (Figure 3.2.6A, B). Consistent with these data, we show increased transcript levels of hypoxia-regulated *Snail1* in E18.5 Pat obs placentae compared to controls (Figure 3.2.6C), a transcription factor which regulates trophoblast

differentiation during placental vascular development [253]. There were hypoxia-regulated decreases in transcript levels of *Wnt1* [254,255], and *Wnt10b* [256] in E18.5 Pat obs placentae compared to controls (Figure 3.2.6D, E), which may indicate poor trophoblast invasion [254].

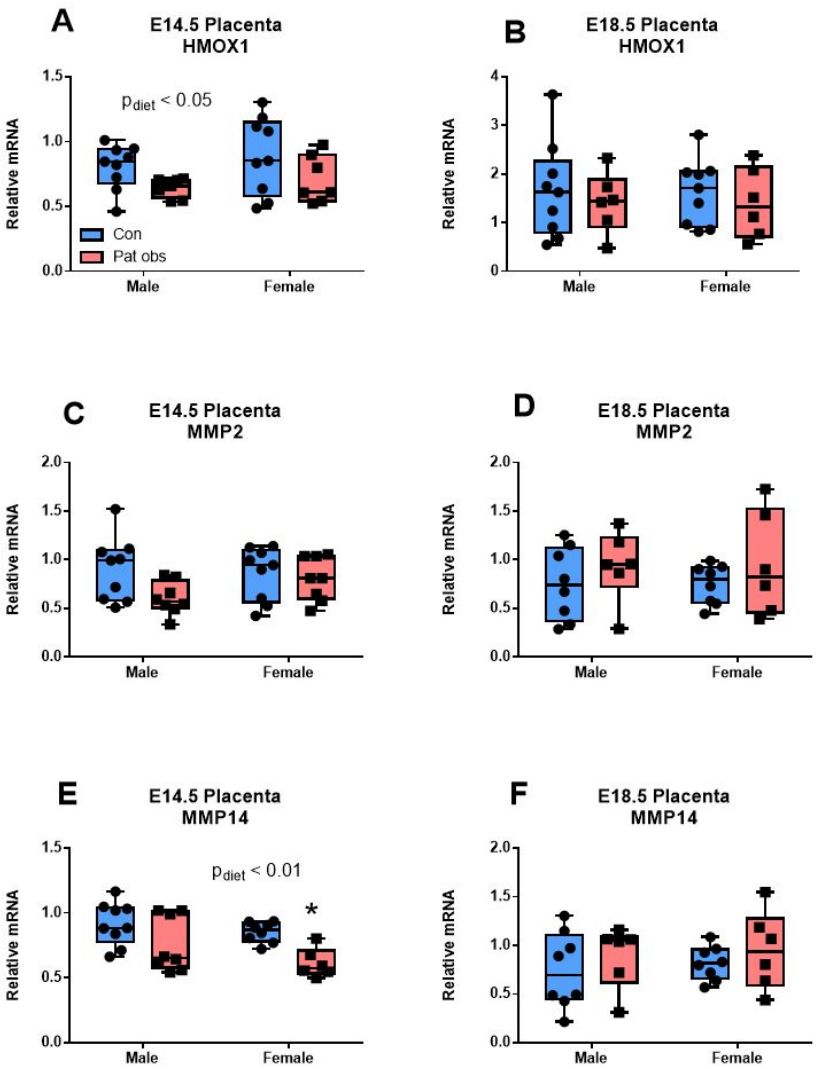

Figure 3.2.5: Paternal obesity is associated with lower transcription levels of blood vessel development factors in E14.5 placentae. Transcript levels of *HMOX1* were measured with RT-qPCR in E14.5 (A) and E18.5 placentae (B). Its downstream targets, *MMP2* and *MMP14*, were measured at E14.5 (C, E) and E18.5 (D, F). All mRNA levels are relative to the geometric mean of housekeeping genes. Data are presented as median +/- upper and lower quartiles. * denotes $p<0.05$, after 2-way ANOVA was used to compare data between groups. Control-fed males (Con, n=9, blue), HF-fed males (Pat obs, n=6-8, pink).

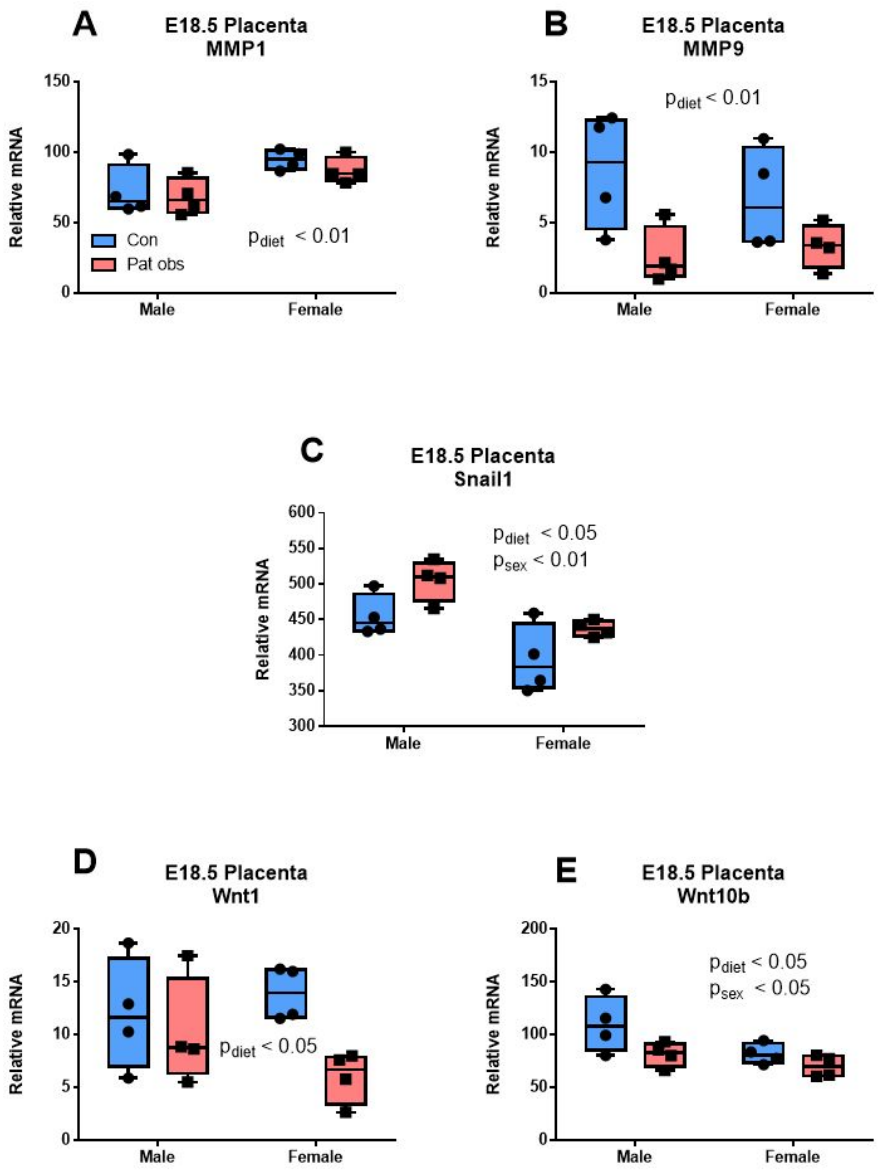

Figure 3.2.6: Paternal obesity is associated with altered hypoxia-mediated transcription levels of vascular development factors in E18.5 placentae. Transcript levels of *MMP1* (A), *MMP14* (B), *Snail1* (C), *Wnt1* (D), and *Wnt10b* (E) were measured using the Nanostring nCounter gene expression system. All mRNA levels are relative to the geometric mean of housekeeping genes. Data are presented as median +/- upper and lower quartiles. * denotes $p<0.05$, after 2-way ANOVA was used to compare data between groups. Control-fed males (Con, n=4, blue), HF-fed males (Pat obs, n=4, pink).

3.3 UPR and ER stress

Hypoxia and angiogenesis are strongly associated with ER stress in other models of poor placental development including preeclampsia [162] and maternal obesity [257,258], thus we investigated the role of ER stress in mediating paternal obesity induced hypoxia in the placenta. There are three branches of ER stress: protein kinase R-like ER protein kinase (PERK), inositol-requiring enzyme 1 alpha (IRE1α), and activating transcription factor 6 (ATF6). Each branch is activated by the binding of glucose-regulated protein 78 (GRP78) to the respective protein [168,170]. GRP78 protein levels were higher in male Pat obs placentae compared to controls at both E14.5 (Figure 3.3.1A, I) and E18.5 (Figure 3.3.1B, J). Protein levels of phosphorylated (phospho-)PERK to total PERK were higher in male but not female placentae at E14.5 (Figure 3.3.1C, I) and at E18.5 were higher in both male and female Pat obs placentae but differences were statistically significant only in females (Figure 3.3.1D, J). Protein levels of phospho-IRE1α to total IRE1α were higher in female but not male Pat obs placentae at E14.5 (Figure 3.3.1E, I), and at E18.5 levels were similar between groups (Figure 3.3.1F, J). There was no difference between groups in relative *Atf6* mRNA levels at both E14.5 (Figure 3.3.1G) and E18.5 (Figure 3.3.1H). This is consistent with the fact that transcript levels of the downstream ATF6 targets, *Gadd34* and *Edem1* were unaltered (Table 3.3.1). Protein disulfide isomerase (*Pdi*) transcript levels however, another downstream ATF6 target, were lower at E14.5 but not at E18.5 in female Pat obs placentae compared to controls (Table 3.3.1). PDI can act as a chaperone for misfolded proteins to promote their degradation to restore homeostasis [169].

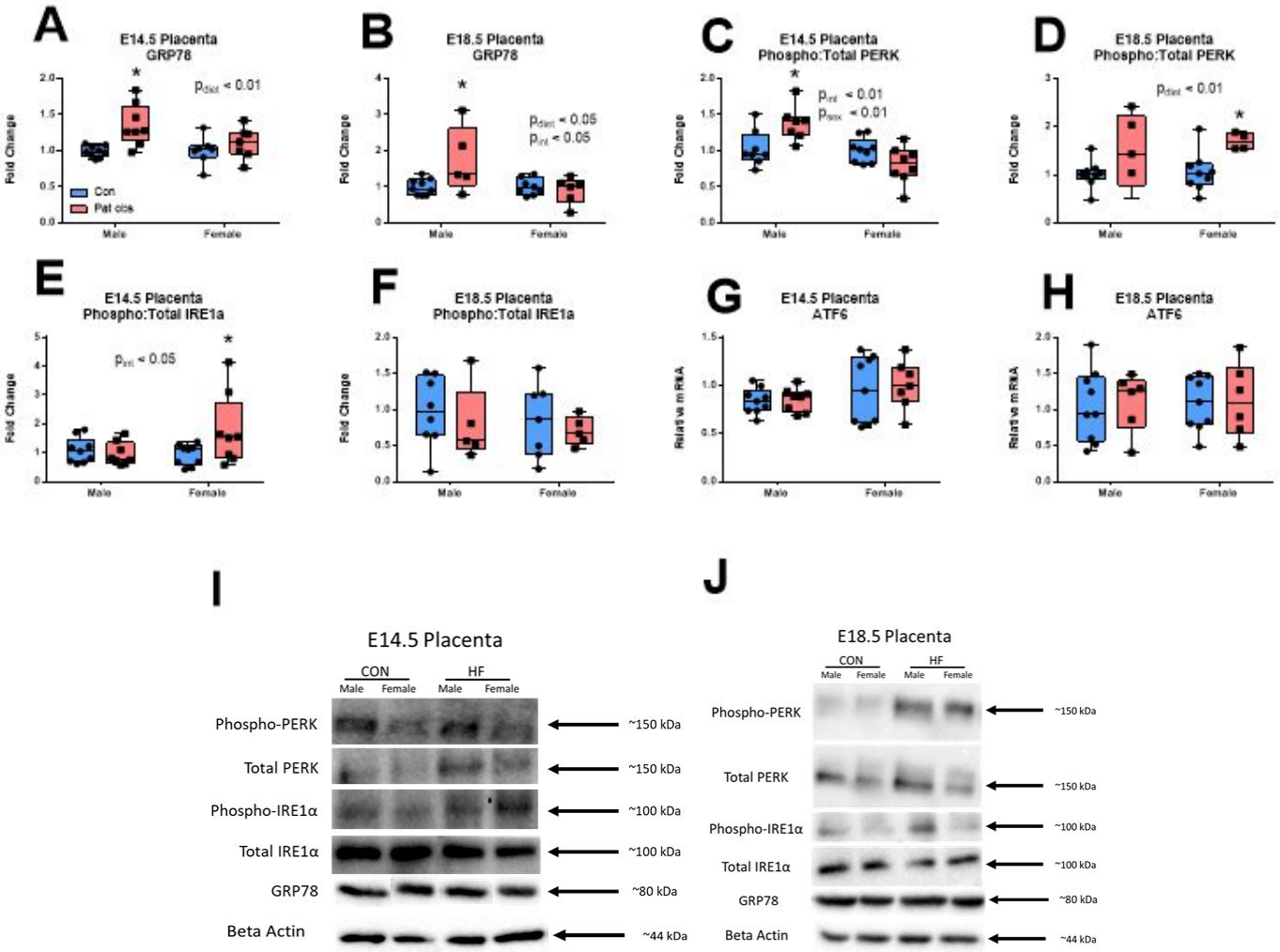

Figure 3.3.1: Paternal obesity is associated with placental UPR activation. GRP78 protein levels were measured at E14.5 (A) and E18.5 (B) with immunoblotting, as was PERK phosphorylation (C, D), and IRE1α phosphorylation (E, F). Transcript levels of *ATF6* were measured with RT-qPCR in E14.5 (G) and E18.5 (H) placentae. Representative immunoblot bands shown (I, J), β actin used as an internal control. *ATF6* mRNA levels are relative to the geometric mean of housekeeping genes. Data are presented as median +/- upper and lower quartiles. * denotes $p<0.05$, after 2-way ANOVA was used to compare data between groups. Control-fed males (Con, n=9, blue), HF-fed males (Pat obs, n=6-8, pink).

Table 3.3.1: Placental ATF6 signaling. Data are presented as mean +/- standard error of the mean. * denotes p<0.05, after 2-way ANOVA was used to compare data between groups.

Gene	Control fed (mean ± SEM) n = 9		High fat fed (mean ± SEM) n = 6-8		P values		
	♂	♀	♂	♀	Main effect of diet	Main effect of sex	Interaction (diet, sex)
E14.5 Placentae							
Relative mRNA transcription levels							
Gadd34	1.007 ± 0.102	1.160 ± 0.082	0.956 ± 0.013	0.844 ± 0.214	0.1694	0.8742	0.3186
Edem1	0.782 ± 0.051	0.815 ± 0.057	0.752 ± 0.070	0.715 ± 0.023	0.2645	0.9722	0.5516
Pdi	0.810 ± 0.077	1.023 ± 0.060	0.843 ± 0.103	*0.561 ± 0.075	*0.0139	0.6739	*0.0051
E18.5 Placentae							
Relative mRNA transcription levels							
Gadd34	2.070 ± 0.366	2.402 ± 0.323	2.075 ± 0.253	1.792 ± 0.408	0.4064	0.9461	0.3993
Edem1	0.756 ± 0.093	0.854 ± 0.093	0.866 ± 0.125	0.939 ± 0.149	0.3978	0.4599	0.9151
Pdi	1.219 ± 0.228	1.249 ± 0.147	0.996 ± 0.092	0.838 ± 0.128	0.0894	0.7252	0.6057

Our data suggest there may be an ER-stress mediated accumulation of misfolded proteins as evidenced by increased protein levels of UPR-associated proteins. To further explore this, we measured the downstream activity of PERK which promotes apoptosis through phosphorylation of eukaryotic initiation factor 2 alpha (eIF2α), and the subsequent transcriptional activation of pro-apoptotic genes [158]. Protein levels of phospho-eIF2α to total eIF2α were similar between

groups at both time points (Table 3.3.2), consistently, *Atf4* and *Chop* transcription levels were unchanged (Table 3.3.2). The Bcl2 family consists of pro- and anti-apoptotic factors that work antagonistically to regulate mitochondrial-induced apoptosis [259], which is promoted through ER stress [158]. *Bcl2* is anti-apoptotic, while *Bad, Bid, Bim,* and *Bax*, are pro-apoptotic. *Bcl2* and *Bax* are antagonistic and their overall activity can be estimated by measuring the ratio between their transcripts [260]. The transcript levels of *Bax* were similar between groups at both time points (Figure 3.3.2A, B). *Bcl2* mRNA levels were not different between groups at E14.5 (Figure 3.3.2C), but, transcript levels were increased in female Pat obs placentae compared to controls at E18.5 (Figure 3.3.2D). The ratio of *Bax*:*Bcl2* transcript levels was not different between groups at E14.5 (Figure 3.3.2E), but was decreased in female Pat obs placentae at E18.5 (Figure 3.3.2F). This is consistent with the transcript levels of *Bad, Bid,* and *Bim,* which were similar between groups in E14.5 placentae (Figure 3.3.2G, I, K) and lower in E18.5 Pat obs placentae, with the effects predominantly in females (Figure 3.3.2H, J, L). Caspase-3 (casp-3) cleavage is a key last step in apoptosis [172,261,262], protein levels of cleaved casp-3 were similar between groups at both time points as measured by immunoblotting (Figure 3.3.3A-D) and immunostaining (Figure 3.3.3E-H). This suggests that ER stress-mediated apoptosis is not occuring as a result of paternal obesity.

Table 3.3.2: Placental PERK signaling. Data are presented as mean +/- standard error of the mean. * denotes p<0.05, after 2-way ANOVA was used to compare data between groups.

Target	Control fed (mean ± SEM) n = 9		High fat fed (mean ± SEM) n = 6-8		P values		
	♂	♀	♂	♀	Main effect of diet	Main effect of sex	Interaction (diet, sex)
E14.5 Placentae							
Protein levels (fold change relative to controls)							
Phospho to total eIF2α	1.024 ± 0.116	1.023 ± 0.086	1.204 ± 0.097	1.104 ± 0.189	0.3195	0.7009	0.7032
Relative mRNA transcription levels							
Atf4	1.001 ± 0.072	1.157 ± 0.088	1.115 ± 0.112	1.347 ± 0.235	0.2754	0.1655	0.7824
Chop	0.916 ± 0.050	0.997 ± 0.087	0.861 ± 0.076	0.869 ± 0.085	0.2346	0.5586	0.6365
E18.5 Placentae							
Protein levels (fold change relative to controls)							
Phospho to total eIF2α	1.100 ± 0.176	1.1045 ± 0.148	1.295 ± 0.432	0.892 ± 0.327	0.9360	0.3863	0.5085
Relative mRNA transcription levels							
Atf4	1.019 ± 0.090	1.079 ± 0.140	1.120 ± 0.107	1.188 ± 0.193	0.4456	0.6391	0.9779
Chop	1.213 ± 0.210	1.085 ± 0.175	0.940 ± 0.069	0.983 ± 0.167	0.3186	0.8189	0.6468

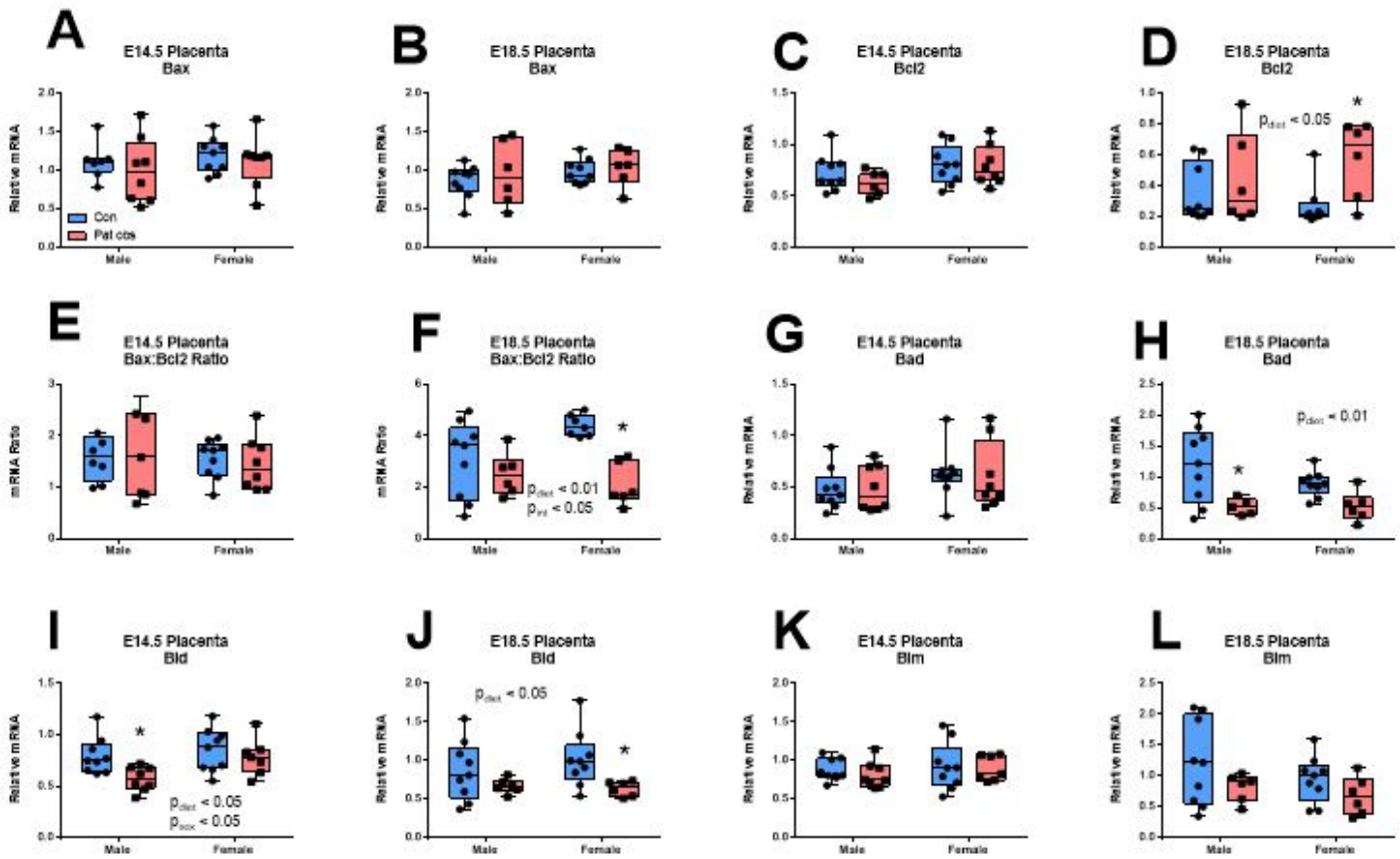

Figure 3.3.2: Paternal obesity is associated with a shift to anti-apoptotic signaling in placental tissue from E14.5 to E18.5. Pro-apoptotic *Bax* transcript levels were measured in E14.5 (A) and E18.5 (B) placentae using RT-qPCR. Anti-apoptotic *Bcl2* transcript levels were measured in E14.5 (C) and E18.5 (D) placentae using RT-qPCR. The ratio of these transcript levels was calculated in E14.5 (E) and E18.5 (F) placental tissues. Pro-apoptotic *Bad*, *Bid*, and *Bim* were measured at E14.5 (G, I, K) and E18.5 (H, J, L). All mRNA levels are relative to the geometric mean of housekeeping genes. Data are presented as median +/- upper and lower quartiles. * denotes $p<0.05$, after 2-way ANOVA was used to compare data between groups. Control-fed males (Con, n=9, blue), HF-fed males (Pat obs, n=6-8, pink).

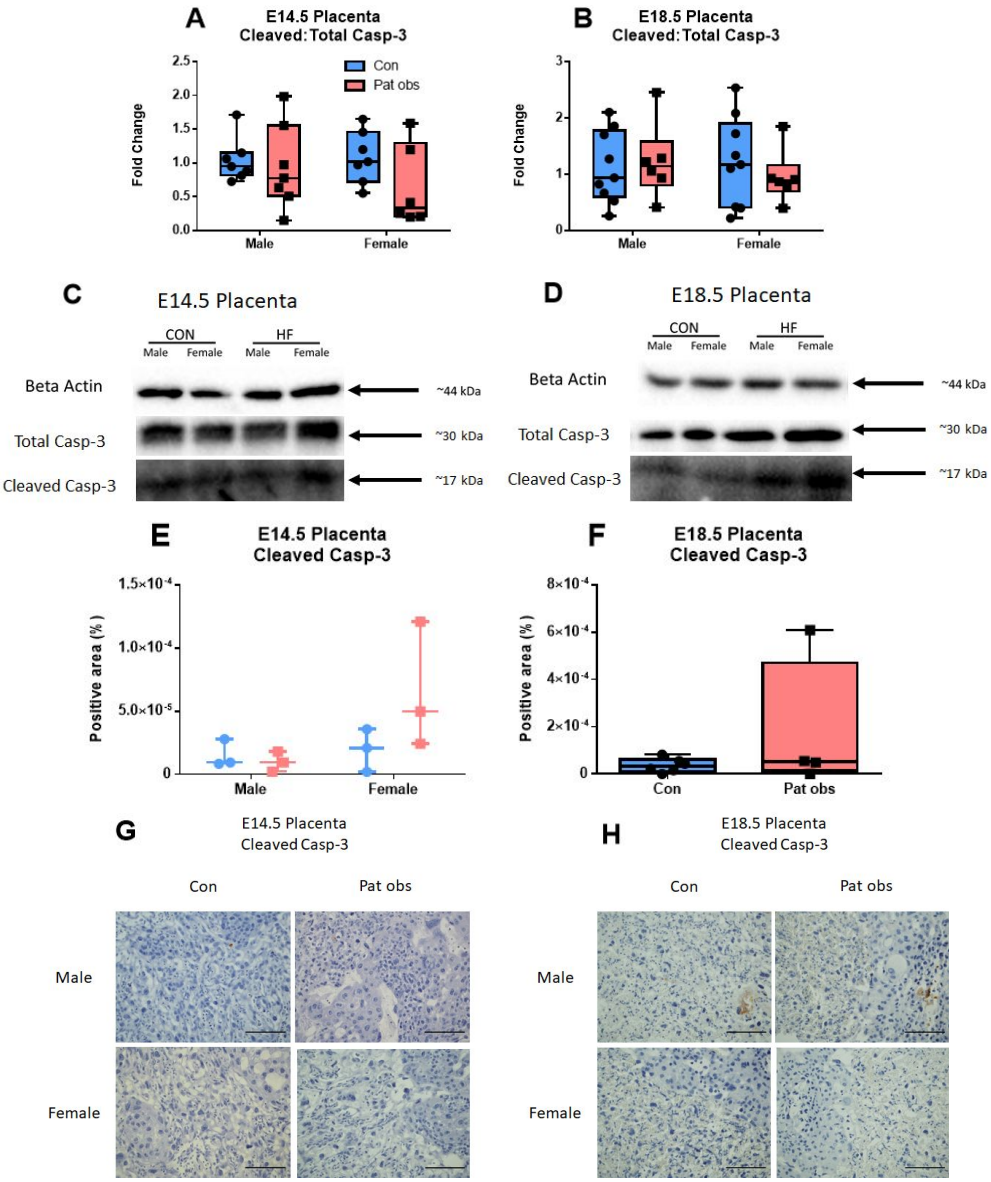

Figure 3.3.3: Paternal obesity does not impact placental cleaved caspase-3 protein levels. Placental caspase-3 (casp-3) protein levels were measured using immunoblotting at E14.5 (A) and E18.5 (B) and using immunostaining at E14.5 (E) and E18.5 (F). Representative immunoblot bands shown (C, D), β actin used as an internal control. Representative immunostaining images shown (G, H), scale bar represents 100 µm. Data are presented as median +/- upper and lower quartiles. * denotes $p<0.05$, after 2-way ANOVA was used to compare data between groups (A, B, E); Student's t test used for E18.5 casp-3 immunostaining (F). Control-fed males (Con, n=5-9, blue), HF-fed males (Pat obs, n=3-8, pink).

Since we observed elevated levels of phospho-IRE1α to total IRE1α in E14.5 placental tissue (Figure 3.3.1E, I), we expected that downstream transcriptional targets would be higher at E14.5 and similar between groups at E18.5. At both E14.5 and E18.5, NF-κB activity was similar between groups (Table 3.3.3). Consistent with this, transcript levels of inflammatory cytokines regulated by NF-κB, including *Traf6, Tnf, Il6,* and *Il1β* were similar between groups at both time points (Table 3.3.3). Similarly, there was no difference in the spliced or total *Xbp1* mRNA levels at both time points, and no difference in the ratio of these transcripts at both time points (Table 3.3.3).

Table 3.3.3: Placental IRE1α signaling. Data are presented as mean +/- standard error of the mean. * denotes p<0.05, after 2-way ANOVA was used to compare data between groups.

Target	Control fed (mean ± SEM) n=9		High fat fed (mean ± SEM) n=6-8		P values		
	♂	♀	♂	♀	Main effect of diet	Main effect of sex	Interaction (diet, sex)
E14.5 Placentae							
Protein levels (arbitrary units)							
NF-κB	0.169±0.002	0.173±0.003	0.173±0.002	0.171±0.017	0.7462	0.8483	0.4041
Relative mRNA transcription levels							
Traf6	0.888±0.037	0.920±0.079	0.830±0.070	1.007±0.020	0.8149	0.1067	0.2584
Tnf	0.868±0.089	1.309±0.197	0.950±0.117	0.981±0.164	0.4129	0.1231	0.1774
Il6	0.882±0.082	0.925±0.143	1.023±0.109	0.906±0.085	0.5857	0.7438	0.4755
Il1β	1.128±0.093	1.470±0.142	0.868±0.079	1.614±0.192	0.6708	*0.0004	0.1493
Spliced *Xbp1*	0.906±0.065	1.083±0.070	0.960±0.089	1.097±0.175	0.7467	0.1444	0.8495
Total *Xbp1*	0.922±0.046	0.992±0.083	0.848±0.064	0.989±0.125	0.6443	0.2133	0.6714
mRNA ratio							
Spliced to total *Xbp1*	1.041±0.053	0.922±0.056	0.895±0.032	0.943±0.056	0.2310	0.4915	0.1121
E18.5 Placentae							
Protein levels (arbitrary units)							
NF-κB	0.140±0.016	0.207±0.017	0.159±0.023	0.184±0.036	0.9366	*0.0492	0.3440
Relative mRNA transcription levels							
Traf6	0.595±0.059	0.622±0.074	0.576±0.039	0.725±0.070	0.5543	0.2182	0.3869
Tnf	1.394±0.291	1.386±0.191	1.121±0.112	0.850±0.107	0.0833	0.5398	0.5623
Il6	0.731±0.080	0.635±0.088	0.939±0.206	*1.989±0.845	*0.0431	0.2049	0.1309
Il1β	0.692±0.134	1.033±0.162	0.976±0.217	1.037±0.185	0.4179	0.2602	0.4296
Spliced *Xbp1*	1.062±0.260	0.983±0.163	0.907±0.097	0.687±0.120	0.2709	0.4620	0.7267
Total *Xbp1*	0.721±0.091	0.773±0.074	0.763±0.065	0.802±0.094	0.6756	0.5933	0.9396
mRNA ratio							
Spliced to total *Xbp1*	1.158±0.105	1.225±0.123	1.208±0.129	0.835±0.073	0.1556	0.1989	0.0696

3.4 Placental nutrient transport

One key function of the placenta is to transport nutrients from the mother to the fetus [121]. We found no difference between groups in either glucose transporter 1 (*Glut1*) transcript levels, or protein levels in placentae at both time points (Table 3.4.1). Correspondingly, we observed no change in *Glut3,* or fatty acid binding protein 4 (*Fabp4*) transcript levels with paternal obesity at both time points (Table 3.4.1). Transcript levels of sodium-coupled neutral amino acid transporter 2 (*Snat2*), a neutral amino acid transporter [263], were not different between groups at E14.5 (Table 3.4.1), but we observed an interaction between diet and sex at E18.5 where transcript levels in female Pat obs placentae, but not males, were higher compared to controls (Table 3.4.1).

Table 3.4.1: Placental macronutrient transporters. Data are presented as mean +/- standard error of the mean. * denotes p<0.05, after 2-way ANOVA was used to compare data between groups.

Target	Control fed (mean ± SEM) n = 9		High fat fed (mean ± SEM) n = 6-8		P values		
	♂	♀	♂	♀	Main effect of diet	Main effect of sex	Interaction (diet, sex)
E14.5 Placentae							
Protein levels (fold change relative to controls)							
GLUT1	1.159 ± 0.291	1.020 ± 0.146	1.262 ± 0.241	0.945 ± 0.160	0.9469	0.2960	0.6801
Relative mRNA transcription levels							
Glut1	1.618 ± 0.097	1.353 ± 0.068	1.442 ± 0.080	1.476 ± 0.121	0.7770	0.2216	0.1168
Glut3	1.025 ± 0.064	1.015 ± 0.055	0.895 ± 0.081	1.124 ± 0.056	0.8671	0.0990	0.0723
Fabp4	1.271 ± 0.101	1.514 ± 0.180	1.258 ± 0.077	1.348 ± 0.094	0.4922	0.2083	0.5587
Snat2	1.155 ± 0.033	1.414 ± 0.126	1.234 ± 0.111	1.361 ± 0.107	0.9026	0.0715	0.5259
E18.5 Placentae							
Protein levels (fold change relative to controls)							
GLUT1	1.058 ± 0.129	1.057 ± 0.142	1.171 ± 0.231	1.379 ± 0.245	0.2436	0.5739	0.5697
Relative mRNA transcription levels							
Glut1	0.762 ± 0.030	0.804 ± 0.065	0.738 ± 0.110	0.830 ± 0.033	0.9849	0.3222	0.7030
Glut3	0.748 ± 0.026	1.060 ± 0.089	0.873 ± 0.109	0.904 ± 0.137	0.8685	0.0775	0.1438
Fabp4	0.580 ± 0.066	0.727 ± 0.082	0.756 ± 0.050	0.848 ± 0.175	0.1413	0.2315	0.7795
Snat2	0.725 ± 0.027	0.658 ± 0.051	0.700 ± 0.067	*0.860 ± 0.028	0.0837	0.3475	*0.0282

3.5 Placental growth factors

The placenta secretes a number of endocrine factors throughout gestation. One such factor is placental lactogen (in the mouse two placental lactogens exist), PLI and PLII during the first and second half pregnancy, encoded by the *Csh1* and *Csh2* genes respectively [264]. Paternal obesity did not alter the transcript levels of *Csh1* or *Csh2* at E14.5 (Figure 3.5.1A, C) or E18.5 (Figure 3.5.1B, D).

Insulin-like growth factors and insulin signaling directly regulate placental growth [71,265]. Transcript levels of paternally regulated insulin-like growth factor 2 (*Igf2*) [132], were increased in female but not male Pat obs placentae at E14.5 (Figure 3.5.1E) but similar between groups at E18.5 (Figure 3.5.1F), however, we observed similar transcript levels of *Igfbp3* between groups at both time points (Figure 3.5.1G, H). IGF2 binds to downstream targets insulin receptor substrate (IRS) 1 and 2, promoting cell proliferation and placental development [31]. At E14.5 *Irs1* transcript levels were higher in Pat obs placentae compared controls (Figure 3.5.1I), with no difference between groups at E18.5 (Figure 3.5.1J). There was no difference between groups in *Irs2* transcript levels at E14.5 (Figure 3.5.1K), however, we observed an interaction between diet and sex at E18.5 (Figure 3.5.1L), with an increase in female Pat obs transcript levels compared to controls.

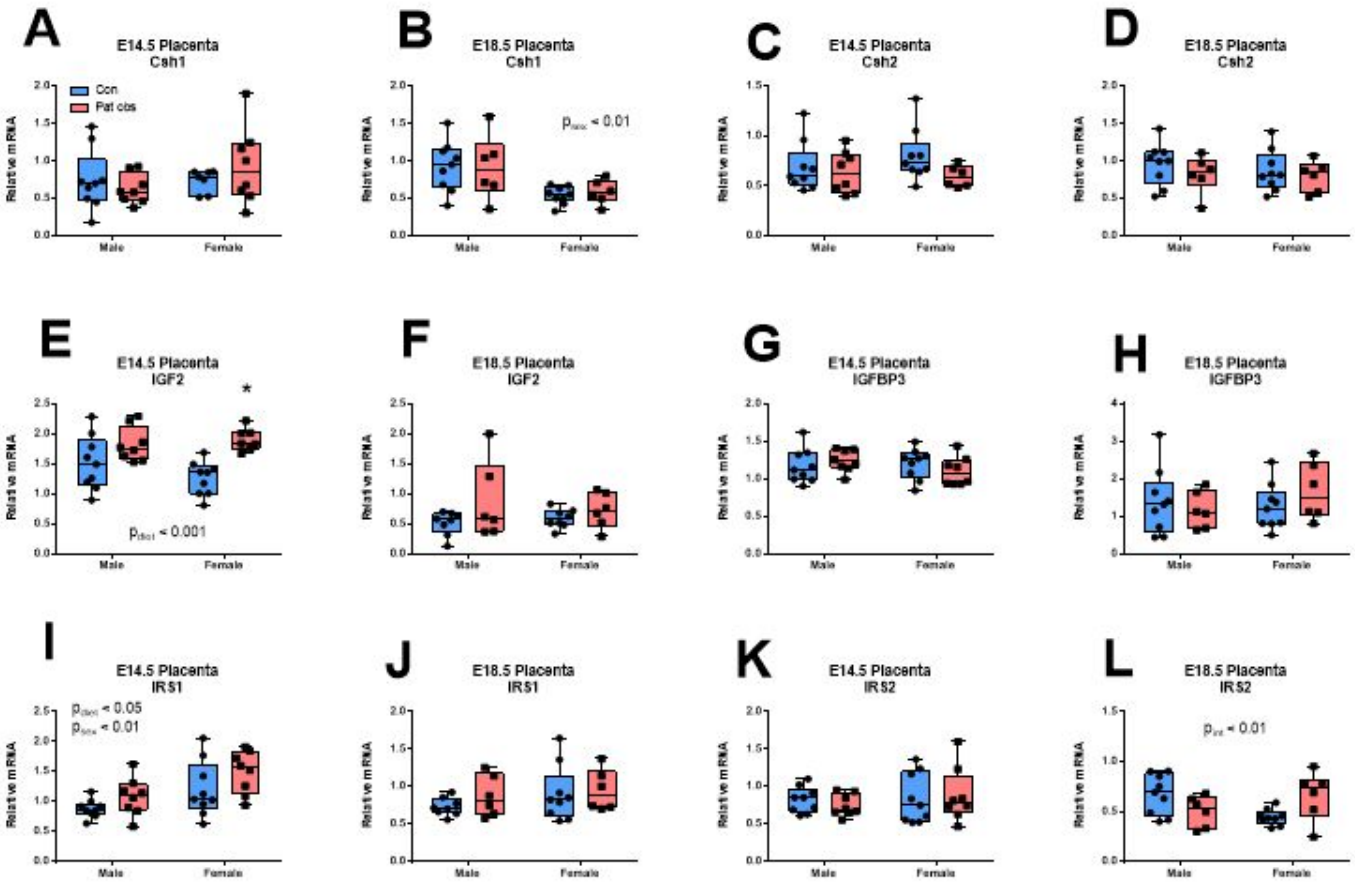

Figure 3.5.1: Paternal obesity is associated with increased placental IGF2 and downstream IRS transcription levels. Transcript levels of *Csh1* and *Csh2* were measured in E14.5 (A, C) and E18.5 (B, D) placentae using RT-qPCR. *IGF2* and *IGFBP3* transcript levels were measured at E14.5 (E, G) and E18.5 (F, H). *IRS1* and *IRS2* transcript levels were measured at E14.5 (I, K) and E18.5 (J, L). All mRNA levels are relative to the geometric mean of housekeeping genes. Data are presented as median +/- upper and lower quartiles. * denotes $p<0.05$, after 2-way ANOVA was used to compare data between groups. Control-fed males (Con, n=9, blue), HF-fed males (Pat obs, n=6-8, pink).

Chapter 4.0 Discussion

In this study, we show that paternal obesity is associated with placental hypoxia, leading to increased vasculogenesis and blood vessel development, and that these changes are sex- and gestational age-dependent. At E14.5, hypoxia-inducible factor 1 alpha (HIF1α) and carbonic anhydrase IX (CAIX) protein levels were higher in placentae from obese fathers, suggesting placental hypoxia [266]. This is maintained to E18.5, where CAIX protein levels remain higher in placentae from obese fathers. Placental hypoxia was associated with increased angiogenesis marker, vascular endothelial growth factor (VEGF), and its pro-angiogenic receptor, VEGFR2 in E14.5 placentae, however, this was only maintained in female but not male E18.5 placentae. Consistent with this, CD31, an endothelial cell marker was increased in E18.5 female but not male placentae. These were associated with reduced transcript levels of blood vessel maturity factors *Hmox1*, *Mmp1*, *9*, and *14*. Despite the cellular stress typically associated with hypoxia-mediated angiogenesis [55,56], these changes appear to be largely independent of the unfolded protein response (UPR) and endoplasmic reticulum (ER) stress.

4.1 Paternal obesity does not change pregnancy outcomes

Our findings are consistent with previous studies that showed a HF diet results in: increased body weight/caloric intake [267], increased adiposity [268], and impaired glucose clearance and metabolism [269]. Since this obese phenotype has been associated with reduced male fertility [270], semen quality [271], and spermatozoa health [272], we investigated the impacts of paternal obesity on mating efficacy. We found no differences in mating efficacy as measured by the number of male and female pairings required for the first pregnancy, number plug-producing pairings

required for the first pregnancy, resorptions per litter, fetal sex ratio, or litter size. These results contradict previous findings [32,34,200,273], however, previous reports have used superovulation in determining embryo number [32,34,200,273], which in itself has adverse outcomes [274–276]. Superovulation has been shown to impair ova quality [274], result in poor offspring outcomes [275], and alter the epigenome [276]. Thus, our results may differ due to influences of superovulation methods. Furthermore, we show no differences in the fetal sex ratio, with data from all groups showing a slight female bias, similar to previous reports [277]. The role of paternal obesity on altered pregnancy outcomes and spermatozoa parameters in humans is inconsistent, some studies show poor outcomes due to paternal diet [209,216], while others show it has no effect [217,218]. A large confounding variable these studies have in common is that men are typically recruited from fertility clinics, introducing inherent biases. Since our study did not explicitly investigate spermatozoa parameters, it is difficult to make any conclusions at this time. While we show no evidence of paternal obesity influencing pregnancy outcomes, our data indicates high fat-fed male mice require more pairings that do not produce a pregnancy compared to controls to produce equal numbers of viable pregnancies (Appendix Figure 9.1.1), possibly suggesting some evidence of fertility impairment due to paternal high fat diet.

4.2 Paternal obesity induces placental hypoxia and impaired vascularization and angiogenesis

We show that paternal obesity results in placental hypoxia as early as E14.5 and that this condition persists to E18.5, and we show that placental hypoxia is associated with impairments in key factors that mediate vascular development. Although previous studies have investigated

the role of paternal obesity on placental function and embryo development [32,34], placental vascular development was not investigated. Others investigating placental outcomes in the context of maternal obesity find impaired vascularization [178], and increased ER stress and inflammation [25].

Placental vascular development is critical as it is the primary site of oxygen and macronutrient transport between the mother and fetus [32–35]. Disruptions to fetal blood supply such as pregnancies complicated by preeclampsia, are associated with placental hypoxia and result in developmental abnormalities including growth retardation, and reduced embryo viability [195]. In our study, paternal obesity increased VEGF and its pro-angiogenic receptor, VEGFR2 in E14.5 placentae, consistent with observations made in preeclamptic hypoxic placentae [278]. Interestingly, this hypoxia-mediated pro-angiogenic signaling is only maintained to E18.5 in female but not male placentae, suggesting sex-specific placental adaptations to the hypoxic environment. Consistent with this, CD31, an endothelial cell marker, is increased in female E18.5 placentae, suggesting increased hypoxia-mediated endothelial cell proliferation in female but not male placentae. Hypoxia promotes the dissociation of hydroxyl groups from HIF1α prolyl residues [266], freeing up HIF1α to bind to target genes, including *Vegf*, to promote transcriptional activation in response to the hypoxic environment [279]. VEGF promotes endothelial cell differentiation and proliferation via cyclin dependent kinase (CDK) [47,280], and this expansion of endothelial cells increases CD31 protein levels, as CD31 is a key endothelial cell adhesion protein necessary for endothelial cell proliferation [281]. Our data suggest that paternal obesity-induced hypoxia and its downstream impacts are sex-specific, since CD31, VEGF, and VEGFR2 changes were found in female but not male E18.5 placentae. Others have suggested sex-specific changes in pregnancies

complicated by pregnancy-induced hypertension and preeclampsia [282,283] where females may be more vulnerable. Despite this, others suggest that males may be more vulnerable [284]. These associations also appear to be modulated by gestational age, where the female (but not male) sex is associated with very early preterm preeclampsia [284,285]. These observations are not dissimilar to our findings that changes in key regulators of vascular development are sex and gestational age dependent.

Transcript levels of heme oxygenase 1 (*Hmox1*) in males, and matrix metalloproteinase 14 (*Mmp14*) in females were lower in E14.5 placenta from obese fathers. At E18.5, *Mmp2*, and *7* (which play a role in blood vessel development [286,287]) were decreased in males but not females. HMOX1, MMP2, MMP7, and MMP14 promote the breakdown of the extracellular matrix between endothelial cells to promote blood vessel widening during proper vascular development [286]. These key vascular modulators are regulated by hypoxia and lower transcript levels have been associated with preeclampsia [288]. The increased angiogenesis and possible reduced blood vessel maturity, as seen with preeclampsia [288], are precursors to placental ER stress [289].

4.3 Paternal obesity is associated with placental UPR activation

The upstream drivers of hypoxia-mediated induction of placental angiogenesis (potentially as a compensation method to maintain transport to the fetus in spite of an oxygen deficiency [290]) are unknown. Hypoxia and ER stress are known to independently promote VEGF expression [55,291] and ER stress enhances the phosphorylation of HIF1α and potentiates HIF1α activity to induce VEGF expression (at least in cultured neuronal cells) [159]. Increased protein demand is often followed by the UPR and subsequent ER stress [292], and it has been suggested

that the placenta is in a state of mild chronic ER stress [56]. In our study, GRP78 is increased at both E14.5 and E18.5, albeit in male placentae only. This may be due to sex differences in placental adaptations to an adverse environment [35,156], where female placentae make more compensatory adaptations (such as increased angiogenesis) while male placentae induce UPR activation. GRP78 regulates all three arms (PERK, IRE1α, and ATF6) of the UPR [293], which is consistent with our observation that phospho-PERK is increased at these time points. Although induction of the PERK arm of the UPR typically induces caspase-3 (casp-3) mediated apoptotic signaling via CHOP [158], we did not find any changes in apoptotic signaling in placentae from obese fathers. We observed increased transcripts of anti-apoptotic Bcl2 which inhibits casp-3 activation [158,294].

Conventional PERK signaling promotes casp-3 mediated apoptosis [158,294], however, a report investigating placental development found PERK is also associated with vascular development via unconventional signaling [55]. Using PERK knockout mice, Ghosh et al. (2010) found that PERK and placental ER stress mediate VEGF activity through ATF4, a downstream transcription factor. A report investigated placental development in IRE1α knockout mice, and similarly, found IRE1α plays a role in placental ER stress. They go on to show that IRE1α mediates VEGF expression through unconventional pathways via its RNase activity and cleavage of X-box binding protein (XBP1) [56]. They found mutant mice showed no changes in placental apoptosis [56], this is further supported by findings showing anti-apoptotic Bcl2 activity is associated with HIF1α and VEGF to facilitate maintained angiogenesis in carcinoma cell lines [295,296], which is partially mediated by the PERK branch of the UPR [158].

We show signs of increased phospho-PERK in male and female Pat obs placentae, at E14.5 and E18.5 respectively. Consistent with the suggestions by Iwawaki et al. and Ghosh et al. that the placenta appears to be under a baseline state of ER stress [55,56]. The source of this ER stress, however, and how it regulates placental development is unclear. In these studies using PERK and IRE1α knockout mice, it was shown that both are separately necessary for placental labyrinth VEGF expression and placental angiogenesis [55,56]. In the present study, we do observe an increase in phospho-IRE1α in female E14.5 placentae, but whether this increase directly participates in VEGF induction is unknown.

Assuming conventional UPR signaling pathways are operating in the placenta, since we show increased levels of phospho-PERK and phospho-IRE1α, we would expect increased levels of pro-inflammatory cytokines induced by IRE1α [174] and hypoxia [288]. Instead, we found little evidence of inflammation or changes in pro-inflammatory cytokine expression in placentae from obese fathers. This could be due to the fact that while the placentae are hypoxic, there is no robust ER stress occurring and as a result, no changes in inflammatory and apoptotic signaling. An explanation for this could be that maternal and placental adaptations to hypoxia (such as increased angiogenesis and increased perfusion) are sufficient in maintaining protein homeostasis and preventing ER stress.

4.4 Paternal obesity has modest effects on placental nutrient transport

A primary function of the placenta is to transport nutrients from the mother to the fetus, including glucose, fatty acids, and amino acids [121]. Previous studies have reported that disruptions in placental development, disrupt nutrient transport and lead to intrauterine growth

restriction [32,74]. We do not show any change in the expression of glucose transporter 1 (GLUT1, mRNA and protein), *Glut3*, or fatty acid binding protein 4 (*Fabp4*) transcript levels at both E14.5 and E18.5 with paternal obesity. However, sodium-coupled neutral amino acid transporter 2 (*Snat2*) transcript levels were increased in female E18.5 placentae from obese fathers. SNAT2 is a key amino acid transporter which transports neutral amino acids including alanine and glutamine [79], which are particularly important as they are glucogenic amino acids [81]. It is possible that paternal obesity may increase fetal gluconeogenesis, in females, but gluconeogenesis was not measured. This notion however, is consistent with offspring studies showing increased expression of gluconeogenic markers in female F_1 and F_2 progeny of obese fathers [160].

IGF2 is is a key growth factor which promotes fetal growth through increased transplacental nutrient diffusion [110]. We show increased *Igf2* transcript levels at E14.5 in placentae from obese fathers, without associated changes in insulin-like growth factor binding protein 3 (*Igfbp3*), which shuttles and transports IGF2 to its receptors [112]. *Igf2* expression is regulated by a number of factors, but most notably its expression is regulated by DNA methylation during development [297]. *Igf2* is paternally inherited [132] where the *Igf2* maternal allele is methylated, gene expression is paternally inherited [139]. This imprinting is the result of an interaction between *Igf2* and *H19*, which is expressed only from the maternal allele [133] and is maintained by epigenetic mechanisms, primarily DNA methylation. One study has shown that paternal obesity alters paternal allelic activity and is associated with *Igf2* hypomethylation in sperm [219]. This sperm hypomethylation is transferred to the developing placenta, and is associated with hypomethylation in placental tissues [298]. Similarly, hypomethylation of *Igf2* in placental

tissues is associated with increased risk of macrosomia and placental overgrowth [221], similar to other reports showing increased IGF2 activity [299].

It has been suggested, in other tissue types, that oxidative stress may impose a loss of imprinting of the *Igf2* gene [300] resulting in increased *Igf2* expression. Whether this has occurred in placental tissue from obese fathers is unknown, but it is consistent with the notion that paternal obesity results in placental hypoxia and provides another explanation for paternal obesity-regulated increased *Igf2* expression. This increase in *Igf2* transcription levels is consistent with increased E14.5 *Irs1* and E18.5 *Irs2* levels (in females) in Pat obs placentae compared to controls. IRS1 primarily promotes cell growth and proliferation through phosphoinositide-3-kinase (PI3K) and mitogen-activated protein kinase (MAPK) [301] and IRS2 promotes anti-apoptotic signaling and mediates macronutrient homeostasis through extracellular signal-related kinase (ERK) signaling [302]. These changes in IGF2-IRS signaling could be reflective of hypoxia-mediated angiogenesis occuring at E14.5 and then at E18.5, a shift to anti-apoptotic signaling. HIF1α-mediated IRS2 has been shown to promote *Bcl2* transcription through IGF2 signaling pathways [303,304], to protect cells against apoptosis in rapidly proliferating environments, such as during hypoxia-mediated angiogenesis [303,305]. This would be cohesive with our data showing a shift to anti-apoptotic Bcl2 signaling from E14.5 to E18.5 placentae, as IRS2 has been previously shown to be increased in hypoxic environments [306] and mediate anti-apoptotic signaling through Bcl2 [304]. This would suggest that IGF2-IRS2 signaling may in part, mediate some of the anti-apoptotic transcriptional changes observed in E18.5 placentae from obese fathers.

4.5 Data summary

Our data suggest that paternal obesity is associated with placental hypoxia, possibly mediated by obesity-induced changes in the spermatozoa, such as micro RNA (miRNA) [225] and/or DNA methylation inheritance [219] (Figure 4.5.1). This hypoxia is associated with increased HIF1α and CAIX protein levels in Pat obs placentae at E14.5 and E18.5, which is associated with increased angiogenesis as evidenced by elevated VEGF and VEGFR2 immunopositive staining (Figure 4.5.1, Figure 4.5.2). While E14.5 male and female Pat obs placentae have increased VEGF and VEGFR2, this only persists to E18.5 in female, but not male placentae suggesting sex-specific interactions with the obesity-induced hypoxic environment (Figure 4.5.1, Figure 4.5.2). Placental hypoxia is typically associated with ER stress and subsequent UPR activation in response to the adverse environment [55,56,159].

We show increased GRP78 protein levels at E14.5 and E18.5 in male placentae (Figure 4.5.1, Figure 4.5.2), suggesting that there may be an accumulation of misfolded proteins (and ER stress, possibly due to hypoxia) [159]. Despite this, we show no evidence of conventional downstream PERK-mediated apoptosis, IRE1α-mediated inflammation, or ATF6-mediated pro-survival responses in Pat obs placentae (Figure 4.5.1, Figure 4.5.2). Furthermore, there is increased phospho-PERK and phospho-IRE1α protein levels in Pat obs E14.5 male and female placenta respectively (Figure 4.5.1, Figure 4.5.2), despite no conventional downstream signal transduction. This may suggest unconventional PERK and IRE1α placental signaling, which promotes VEGF activity through ATF4 and XBP1 respectively [55,56] (Figure 4.5.1). VEGF and VEGFR2 are pro-angiogenic proteins which promote placental angiogenesis and vascular development [46,55,56].

Placental hypoxia-mediated angiogenesis involves rapid endothelial cell proliferation via VEGF, which promotes CDK-mediated mitogenic signaling [47], this process is very demanding on the ER and is associated with ER stress [55,56] (Figure 4.5.1). We show evidence of an interaction between diet and sex in CD31 immunopositive staining in E18.5 placentae, with females showing elevated CD31 levels. Furthermore, we show a reduction in *Hmox1* and *Mmp14* in E14.5 Pat obs male placentae, and *Mmp1* and *Mmp9* in E18.5 Pat obs male placentae (Figure 4.5.1). HMOX1 regulates MMP activity, and these are involved in blood vessel maturation via breakdown of the ECM [53] to facilitate blood vessel widening [50,52]. This poor vascular development, combined with placental hypoxia may indicate poor placental perfusion to the fetus [50,52,204,253]. In response to inadequate placental perfusion, a key placental growth factor, IGF2 is activated to increase placental growth [299] and macronutrient transport [115,307,308].

We show increased *Igf2* transcript levels in E14.5 female placentae (Figure 4.5.1, Figure 4.5.2), this promotes activation of the downstream targets, IRS1 and IRS2 [31,307]. We show a main effect of diet, with increased *Irs1* transcript levels in E14.5 placentae and increased *Irs2* transcript levels in E18.5 placentae (Figure 4.5.1, Figure 4.5.2). This shows gestational age-specific differences in downstream *Igf2* signaling. IRS1 primarily promotes proliferation via CDK-mediated mitogenic signaling [301], which in turn is associated with ER stress [47]. Alternatively, IRS2 promotes antiapoptotic signaling through mTOR-mediated inhibition of pro-apoptotic Bcl2 family members [304]. Consistent with this, we show no difference between groups in Bcl2 family members at E14.5, however, there is a significant reduction in *Bad* and *Bid*, two pro-apoptotic factors in Pat obs E18.5 placentae (Figure 4.5.1, Figure 4.5.2). mTOR regulates placental macronutrient transport by mediating glucose transporter translocation [115],

fatty acid synthesis and availability for fatty acid transport [308], and protein synthesis and amino acid availability for transport [307,308]. Despite this, we show no difference between groups in *Glut1* and *Glut3*, or *Fabp4* at both time points for glucose and fatty acid transport respectively (Figure 4.5.1, Figure 4.5.2). However, we have evidence of increased *Snat2* transcript levels in female E18.5 Pat obs placentae compared to controls (Figure 4.5.1, Figure 4.5.2). SNAT2 transports glucogenic amino acids to the fetus [81], suggesting that perhaps female but not male fetuses are more impacted by placental hypoxia, and require increased amino acid transport.

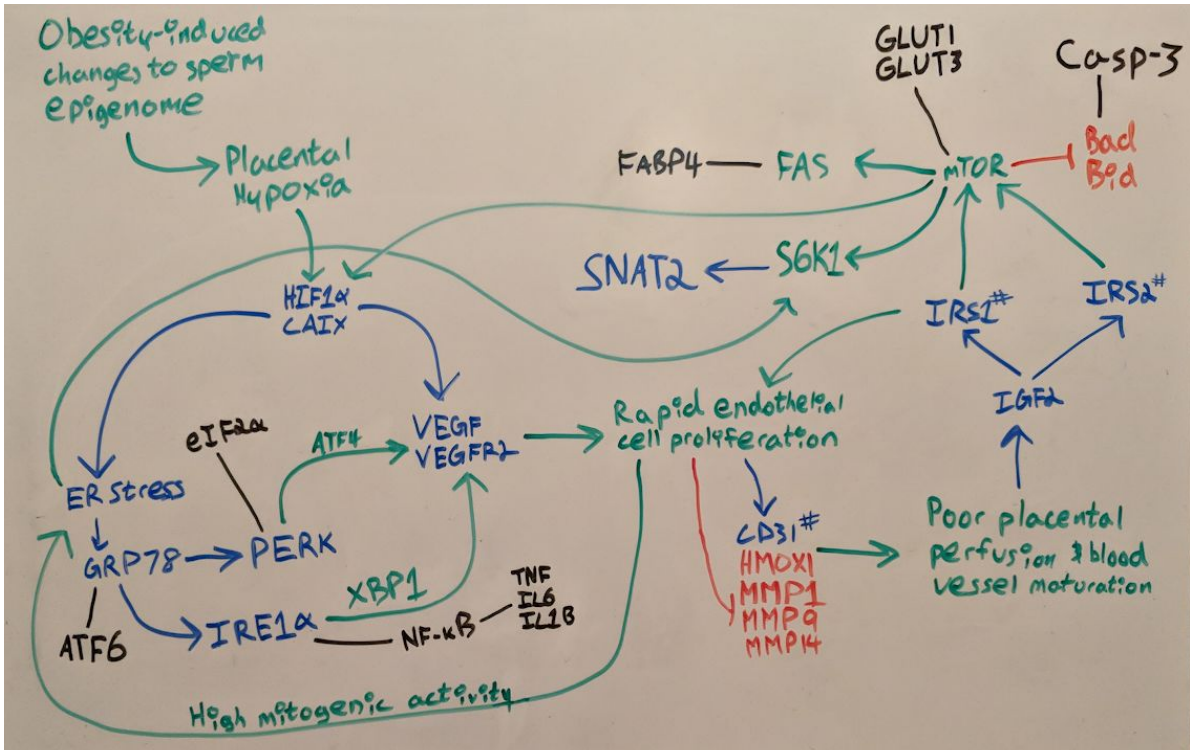

Figure 4.5.1: Graphical representation of investigated signaling pathways. Shown here is a graphical overview of the various pathways investigated in this study. Green arrows represent an inferred association based on previous studies, blue arrows represent a measured increase in protein and/or transcript levels in placentae from obese fathers, black lines represent a measured similarity between groups, and red capped lines represent a measured decrease in transcription levels in placentae from obese fathers. # denotes an increase that was only significant at the main effect level, but not in post-hoc analysis.

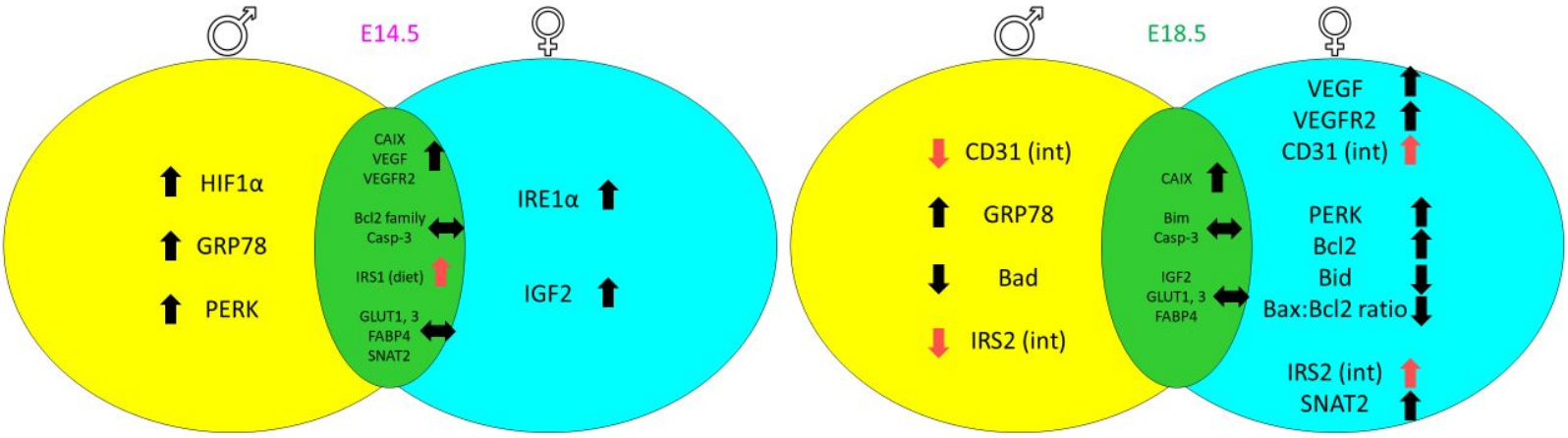

Figure 4.5.2: Data summary separated by gestational age and placental sex. Here is a pictorial representation of the primary findings from this study separated by placental sex (male, yellow; female, cyan) and gestational age (E14.5, left; E18.5 right), with differences in both males and females shown in green. Increases in protein and/or transcription levels are represented by up black arrows, with decreases by down black arrows. Differences that were only significant at the main effect level, but not in post-hoc analysis are represented by red up and down arrows for increases and decreases respectively, with the statistically significant main effect shown.

Chapter 5.0 Limitations

There were a few limitations in this study due to study design and feasibility. The control and high fat diets are not manufacturer-matched, and as such have differences in the micronutrient and vitamin content [238,239]. One key difference between the diets is that the high fat diet contains no phytoestrogens, while the control diet contains 350-650 mg/kg isoflavones (the predominant phytoestrogen of this diet) [238]. Phytoestrogens have been shown to improve steatosis and reduce adipose and triglyceride accumulation associated with a high fat diet [309]. Phytoestrogens have also been associated with reduced male and female fertility [310], possibly explaining the observed lack of difference in fertility due to paternal diet. However, complete loss of phytoestrogens has been demonstrated to be associated with increased weight gain, impaired glucose clearance, and insulin resistance [311]. As such, it is unclear if our results are due to the high fat diet alone, or if they are due to the conjunction of increased dietary fat and complete ablation of dietary phytoestrogens.

The males used for E14.5 pregnancies and E18.5 pregnancies were different and this could produce cohort-specific biases. This could be improved by using one group of males to produce pregnancies at both time points, to minimize variability between groups.

The majority of the data collected at both time points represents data collected from reverse transcriptase quantitative polymerase chain reaction (RT-qPCR) and immunoblotting. As such, our data reflect overall changes in transcription and translation respectively. Changes at the transcriptional level do not necessarily reflect changes in protein levels, as evidenced by some our of data. Finally, the placenta is a heterogenous organ and contains two primary zones: the junctional and labyrinth zones [98]. As such, our RT-qPCR and immunoblotting data do not reflect

zone-specific changes. This could have been improved by using immunohistochemical analysis for all proteins of interest in the placentae at both time points.

Chapter 6.0 Future directions

We have begun to characterize the impacts of paternal obesity on placental vascular development, hypoxic status, and macronutrient transport across gestation. While this is important, the primary concern is offspring outcomes and overall health. The placenta is a key organ responsible for adequate fetal growth and development, and hypoxia may alter fetal growth and result in changes in offspring risk of metabolic compromise. In order to fully understand the impacts of paternal obesity, it would be ideal to investigate fetal tissue development and offspring metabolic outcomes. Our preliminary evidence suggests that there may be impaired fetal hepatic development, hepatic ER stress, and increased hepatic apoptosis. This could explain how disruptions in placental development from paternal obesity influence offspring metabolic outcomes. Lastly, characterizing metabolic changes that occur in the offspring would give further insight into what developmental pathways may be influenced by paternal obesity.

Chapter 7.0 Conclusions

We conclude that paternal obesity is associated with placental hypoxia and angiogenesis. This hypoxic environment was not associated with ER stress-mediated apoptosis or inflammation as we hypothesized, but did increase PERK and IRE1α levels which could be associated with HIF1α-mediated hypoxia, and ER stress-mediated activation of VEGF via unconventional signaling pathways [55,56]. While we have some evidence of increased amino acid transporter levels in female E18.5 placentae, overall, paternal obesity does not appear to have any significant impacts on placental glucose or fatty acid transporter levels. Placental hypoxia is a strong predictor of fetal hypoxia and while our data do not suggest significant impacts on placental growth, there may be implications for fetal growth and development.

Chapter 8.0 References

(1) Vieira, M. C.; Poston, L.; Fyfe, E.; Gillett, A.; Kenny, L. C.; Roberts, C. T.; Baker, P. N.; Myers, J. E.; Walker, J. J.; McCowan, L. M.; et al. Clinical and Biochemical Factors Associated with Preeclampsia in Women with Obesity. *Obesity* **2016**.

(2) Kang, Y.-R.; Lee, H.-Y.; Kim, J.-H.; Moon, D.-I.; Seo, M.-Y.; Park, S.-H.; Choi, K.-H.; Kim, C.-R.; Kim, S.-H.; Oh, J.-H.; et al. Anti-Obesity and Anti-Diabetic Effects of Yerba Mate (Ilex Paraguariensis) in C57BL/6J Mice Fed a High-Fat Diet. *Lab. Anim. Res.* **2012**, *28* (1), 23–29.

(3) Mitrou, P.; Raptis, S. A.; Dimitriadis, G. Insulin Action in Morbid Obesity: A Focus on Muscle and Adipose Tissue. *Hormones* **2013**, *12* (2), 201–213.

(4) Liu, J.; Wu, Y.-Y.; Huang, X.-M.; Yang, M.; Zha, B.-B.; Wang, F.; Zha, Y.; Sheng, L.; Chen, Z.-P. G.; Gu, Y. Ageing and Type 2 Diabetes in an Elderly Chinese Population: The Role of Insulin Resistance and Beta Cell Dysfunction. *Eur. Rev. Med. Pharmacol. Sci.* **2014**, *18* (12), 1790–1797.

(5) Mathijs, I.; Da Cunha, D. A.; Himpe, E.; Ladriere, L.; Chellan, N.; Roux, C. R.; Joubert, E.; Muller, C.; Cnop, M.; Louw, J.; et al. Phenylpropenoic Acid Glucoside Augments Pancreatic Beta Cell Mass in High-Fat Diet-Fed Mice and Protects Beta Cells from ER Stress-Induced Apoptosis. *Mol. Nutr. Food Res.* **2014**, *58* (10), 1980–1990.

(6) Noguchi, R.; Kubota, H.; Yugi, K.; Toyoshima, Y.; Komori, Y.; Soga, T.; Kuroda, S. The Selective Control of Glycolysis, Gluconeogenesis and Glycogenesis by Temporal Insulin Patterns. *Mol. Syst. Biol.* **2013**, *9*, 664.

(7) Bonen, A.; Jain, S. S.; Snook, L. A.; Han, X.-X.; Yoshida, Y.; Buddo, K. H.; Lally, J. S.; Pask, E. D.; Paglialunga, S.; Beaudoin, M.-S.; et al. Extremely Rapid Increase in Fatty Acid Transport and Intramyocellular Lipid Accumulation but Markedly Delayed Insulin Resistance after High Fat Feeding in Rats. *Diabetologia* **2015**, *58* (10), 2381–2391.

(8) De Koster, J.; Nelli, R. K.; Strieder-Barboza, C.; de Souza, J.; Lock, A. L.; Contreras, G. A. The Contribution of Hormone Sensitive Lipase to Adipose Tissue Lipolysis and Its Regulation by Insulin in Periparturient Dairy Cows. *Sci. Rep.* **2018**, *8* (1), 13378.

(9) Wanless, I. R.; Shiota, K. The Pathogenesis of Nonalcoholic Steatohepatitis and Other Fatty Liver Diseases: A Four-Step Model Including the Role of Lipid Release and Hepatic Venular Obstruction in the Progression to Cirrhosis. *Semin. Liver Dis.* **2004**, *24* (1), 99–106.

(10) Lee, Y. J.; Ko, E. H.; Kim, J. E.; Kim, E.; Lee, H.; Choi, H.; Yu, J. H.; Kim, H. J.; Seong, J.-K.; Kim, K.-S.; et al. Nuclear Receptor PPARγ-Regulated Monoacylglycerol O-Acyltransferase 1 (MGAT1) Expression Is Responsible for the Lipid Accumulation in Diet-Induced Hepatic Steatosis. *Proc. Natl. Acad. Sci. U. S. A.* **2012**, *109* (34), 13656–13661.

(11) Yu, J.; Shen, J.; Sun, T. T.; Zhang, X.; Wong, N. Obesity, Insulin Resistance, NASH and Hepatocellular Carcinoma. *Semin. Cancer Biol.* **2013**, *23* (6 Pt B), 483–491.

(12) Manna, P.; Jain, S. K. Obesity, Oxidative Stress, Adipose Tissue Dysfunction, and the Associated Health Risks: Causes and Therapeutic Strategies. *Metab. Syndr. Relat. Disord.* **2015**, *13* (10), 423–444.

(13) Ryan, E. A.; Enns, L. Role of Gestational Hormones in the Induction of Insulin Resistance. *J. Clin. Endocrinol. Metab.* **1988**, *67* (2), 341–347.

(14) Palm, M.; Axelsson, O.; Wernroth, L.; Larsson, A.; Basu, S. Involvement of Inflammation

in Normal Pregnancy. *Acta Obstet. Gynecol. Scand.* **2013**, *92* (5), 601–605.

(15) Howie, G. J.; Sloboda, D. M.; Kamal, T.; Vickers, M. H. Maternal Nutritional History Predicts Obesity in Adult Offspring Independent of Postnatal Diet. *J. Physiol.* **2009**, *587* (Pt 4), 905–915.

(16) Barker, D. J. P. Developmental Origins of Adult Health and Disease. *J. Epidemiol. Community Health* **2004**, *58* (2), 114–115.

(17) Barker, D. J.; Gluckman, P. D.; Godfrey, K. M.; Harding, J. E.; Owens, J. A.; Robinson, J. S. Fetal Nutrition and Cardiovascular Disease in Adult Life. *Lancet* **1993**, *341* (8850), 938–941.

(18) Barker, D. J.; Osmond, C. Infant Mortality, Childhood Nutrition, and Ischaemic Heart Disease in England and Wales. *Lancet* **1986**, *1* (8489), 1077–1081.

(19) Barker, D. J.; Winter, P. D.; Osmond, C.; Margetts, B.; Simmonds, S. J. Weight in Infancy and Death from Ischaemic Heart Disease. *Lancet* **1989**, *2* (8663), 577–580.

(20) McCarthy, K.; Ye, Y.-L.; Yuan, S.; He, Q.-Q. Parental Weight Status and Offspring Cardiovascular Disease Risks: A Cross-Sectional Study of Chinese Children. *Prev. Chronic Dis.* **2015**, *12*, E01.

(21) Sebire, N. J.; Jolly, M.; Harris, J. P.; Wadsworth, J.; Joffe, M.; Beard, R. W.; Regan, L.; Robinson, S. Maternal Obesity and Pregnancy Outcome: A Study of 287,213 Pregnancies in London. *Int. J. Obes. Relat. Metab. Disord.* **2001**, *25* (8), 1175–1182.

(22) Rosario, F. J.; Kanai, Y.; Powell, T. L.; Jansson, T. Increased Placental Nutrient Transport in a Novel Mouse Model of Maternal Obesity with Fetal Overgrowth. *Obesity* **2015**, *23* (8), 1663–1670.

(23) Young, S. M.; Gryder, L. K.; David, W. B.; Teng, Y.; Gerstenberger, S.; Benyshek, D. C. Human Placenta Processed for Encapsulation Contains Modest Concentrations of 14 Trace Minerals and Elements. *Nutr. Res.* **2016**, *36* (8), 872–878.

(24) Sakamoto, M.; Yasutake, A.; Domingo, J. L.; Chan, H. M.; Kubota, M.; Murata, K. Relationships between Trace Element Concentrations in Chorionic Tissue of Placenta and Umbilical Cord Tissue: Potential Use as Indicators for Prenatal Exposure. *Environ. Int.* **2013**, *60*, 106–111.

(25) Westermeier, F.; Sáez, P. J.; Villalobos-Labra, R.; Sobrevia, L.; Farías-Jofré, M. Programming of Fetal Insulin Resistance in Pregnancies with Maternal Obesity by ER Stress and Inflammation. *Biomed Res. Int.* **2014**, *2014*, 917672.

(26) Gluckman, P. D.; Lillycrop, K. A.; Vickers, M. H.; Pleasants, A. B.; Phillips, E. S.; Beedle, A. S.; Burdge, G. C.; Hanson, M. A. Metabolic Plasticity during Mammalian Development Is Directionally Dependent on Early Nutritional Status. *Proc. Natl. Acad. Sci. U. S. A.* **2007**, *104* (31), 12796–12800.

(27) Bateson, P.; Barker, D.; Clutton-Brock, T.; Deb, D.; D'Udine, B.; Foley, R. A.; Gluckman, P.; Godfrey, K.; Kirkwood, T.; Lahr, M. M.; et al. Developmental Plasticity and Human Health. *Nature* **2004**, *430* (6998), 419–421.

(28) Ravelli, G. P.; Stein, Z. A.; Susser, M. W. Obesity in Young Men after Famine Exposure in Utero and Early Infancy. *N. Engl. J. Med.* **1976**, *295* (7), 349–353.

(29) Clayton, Z. E.; Vickers, M. H.; Bernal, A.; Yap, C.; Sloboda, D. M. Early Life Exposure to Fructose Alters Maternal, Fetal and Neonatal Hepatic Gene Expression and Leads to Sex-Dependent Changes in Lipid Metabolism in Rat Offspring. *PLoS One* **2015**, *10* (11), e0141962.

(30) Rosario, F. J.; Nathanielsz, P. W.; Powell, T. L.; Jansson, T. Maternal Folate Deficiency Causes Inhibition of mTOR Signaling, down-Regulation of Placental Amino Acid Transporters and Fetal Growth Restriction in Mice. *Sci. Rep.* **2017**, *7* (1), 3982.
(31) Street, M. E.; Viani, I.; Ziveri, M. A.; Volta, C.; Smerieri, A.; Bernasconi, S. Impairment of Insulin Receptor Signal Transduction in Placentas of Intra-Uterine Growth-Restricted Newborns and Its Relationship with Fetal Growth. *Eur. J. Endocrinol.* **2011**, *164* (1), 45–52.
(32) McPherson, N. O.; Bell, V. G.; Zander-Fox, D. L.; Fullston, T.; Wu, L. L.; Robker, R. L.; Lane, M. When Two Obese Parents Are Worse than One! Impacts on Embryo and Fetal Development. *Am. J. Physiol. Endocrinol. Metab.* **2015**, *309* (6), E568–E581.
(33) Gohir, W.; Whelan, F. J.; Surette, M. G.; Moore, C.; Schertzer, J. D.; Sloboda, D. M. Pregnancy-Related Changes in the Maternal Gut Microbiota Are Dependent upon the Mother's Periconceptional Diet. *Gut Microbes* **2015**, *6* (5), 310–320.
(34) Binder, N. K.; Beard, S. A.; Kaitu'u-Lino, T. J.; Tong, S.; Hannan, N. J.; Gardner, D. K. Paternal Obesity in a Rodent Model Affects Placental Gene Expression in a Sex-Specific Manner. *Reproduction* **2015**, *149* (5), 435–444.
(35) Kim, D. W.; Young, S. L.; Grattan, D. R.; Jasoni, C. L. Obesity during Pregnancy Disrupts Placental Morphology, Cell Proliferation, and Inflammation in a Sex-Specific Manner across Gestation in the Mouse. *Biol. Reprod.* **2014**, *90* (6), 130.
(36) Murthi, P.; Abumaree, M.; Kalionis, B. Analysis of Homeobox Gene Action May Reveal Novel Angiogenic Pathways in Normal Placental Vasculature and in Clinical Pregnancy Disorders Associated with Abnormal Placental Angiogenesis. *Front. Pharmacol.* **2014**, *5*, 133.
(37) Li, H.; Qu, D.; McDonald, A.; Isaac, S. M.; Whiteley, K. J.; Sung, H.-K.; Nagy, A.; Adamson, S. L. Trophoblast-Specific Reduction of VEGFA Alters Placental Gene Expression and Maternal Cardiovascular Function in Mice. *Biol. Reprod.* **2014**, *91* (4), 87.
(38) Reynolds, C. M.; Vickers, M. H.; Harrison, C. J.; Segovia, S. A.; Gray, C. Maternal High Fat And/or Salt Consumption Induces Sex-Specific Inflammatory and Nutrient Transport in the Rat Placenta. *Physiol Rep* **2015**, *3* (5).
(39) Isaac, S. M.; Langford, M. B.; Simmons, D. G.; Adamson, S. L. 4 - Anatomy of the Mouse Placenta Throughout Gestation. In *The Guide to Investigation of Mouse Pregnancy*; Croy, B. A., Yamada, A. T., DeMayo, F. J., Adamson, S. L., Eds.; Academic Press: Boston, 2014; pp 69–73.
(40) Furukawa, S.; Kuroda, Y.; Sugiyama, A. A Comparison of the Histological Structure of the Placenta in Experimental Animals. *J. Toxicol. Pathol.* **2014**, *27* (1), 11–18.
(41) Knipp, G. T.; Liu, B.; Audus, K. L.; Fujii, H.; Ono, T.; Soares, M. J. Fatty Acid Transport Regulatory Proteins in the Developing Rat Placenta and in Trophoblast Cell Culture Models. *Placenta* **2000**, *21* (4), 367–375.
(42) Hu, D.; Cross, J. C. Development and Function of Trophoblast Giant Cells in the Rodent Placenta. *Int. J. Dev. Biol.* **2010**, *54* (2-3), 341–354.
(43) Kröger, C.; Vijayaraj, P.; Reuter, U.; Windoffer, R.; Simmons, D.; Heukamp, L.; Leube, R.; Magin, T. M. Placental Vasculogenesis Is Regulated by Keratin-Mediated Hyperoxia in Murine Decidual Tissues. *Am. J. Pathol.* **2011**, *178* (4), 1578–1590.
(44) Bevilacqua, E. M.; Abrahamsohn, P. A. Trophoblast Invasion during Implantation of the Mouse Embryo. *Arch. Biol. Med. Exp.* **1989**, *22* (2), 107–118.

(45) Bany, B. M.; Cross, J. C. Post-Implantation Mouse Conceptuses Produce Paracrine Signals That Regulate the Uterine Endometrium Undergoing Decidualization. *Dev. Biol.* **2006**, *294* (2), 445–456.
(46) Sones, J. L.; Merriam, A. A.; Seffens, A.; Brown-Grant, D.-A.; Butler, S. D.; Zhao, A. M.; Xu, X.; Shawber, C. J.; Grenier, J. K.; Douglas, N. C. Angiogenic Factor Imbalance Precedes Complement Deposition in Placentae of the BPH/5 Model of Preeclampsia. *FASEB J.* **2018**, fj201701008R.
(47) Yu, Y.; Sato, J. D. MAP Kinases, Phosphatidylinositol 3-Kinase, and p70 S6 Kinase Mediate the Mitogenic Response of Human Endothelial Cells to Vascular Endothelial Growth Factor. *J. Cell. Physiol.* **1999**, *178* (2), 235–246.
(48) Ashton, S. V.; Whitley, G. S. J.; Dash, P. R.; Wareing, M.; Crocker, I. P.; Baker, P. N.; Cartwright, J. E. Uterine Spiral Artery Remodeling Involves Endothelial Apoptosis Induced by Extravillous Trophoblasts through Fas/FasL Interactions. *Arterioscler. Thromb. Vasc. Biol.* **2005**, *25* (1), 102–108.
(49) Gasperowicz, M.; Surmann-Schmitt, C.; Hamada, Y.; Otto, F.; Cross, J. C. The Transcriptional Co-Repressor TLE3 Regulates Development of Trophoblast Giant Cells Lining Maternal Blood Spaces in the Mouse Placenta. *Dev. Biol.* **2013**, *382* (1), 1–14.
(50) Robson, A.; Harris, L. K.; Innes, B. A.; Lash, G. E.; Aljunaidy, M. M.; Aplin, J. D.; Baker, P. N.; Robson, S. C.; Bulmer, J. N. Uterine Natural Killer Cells Initiate Spiral Artery Remodeling in Human Pregnancy. *FASEB J.* **2012**, *26* (12), 4876–4885.
(51) Zhang, D.; Wang, L.; Qiao, C.; Yu, Y.; Fu, L.; Shang, T. The Role of the Reduction of Spiral Artery Remodeling and Heme Oxygenase 1 in Mediating AT1-AA-Induced Hypertension and Intrauterine Growth Restriction in Pregnant Rats. *Am. J. Perinatol.* **2014**, *31* (10), 883–890.
(52) Harris, L. K.; Smith, S. D.; Keogh, R. J.; Jones, R. L.; Baker, P. N.; Knöfler, M.; Cartwright, J. E.; Whitley, G. S. J.; Aplin, J. D. Trophoblast- and Vascular Smooth Muscle Cell-Derived MMP-12 Mediates Elastolysis during Uterine Spiral Artery Remodeling. *Am. J. Pathol.* **2010**, *177* (4), 2103–2115.
(53) Tsuji, N.; Matsuura, T.; Narama, I.; Yoshiki, A.; Ozaki, K. Macrophage-Associated Gelatinase Degrades Basement Membrane at the Optic Fissure Margins During Normal Ocular Development in Mice. *Invest. Ophthalmol. Vis. Sci.* **2018**, *59* (3), 1368–1373.
(54) Bevilacqua, E.; Lorenzon, A. R.; Bandeira, C. L.; Hoshida, M. S. 10 - Biology of the Ectoplacental Cone. In *The Guide to Investigation of Mouse Pregnancy*; Croy, B. A., Yamada, A. T., DeMayo, F. J., Adamson, S. L., Eds.; Academic Press: Boston, 2014; pp 113–124.
(55) Ghosh, R.; Lipson, K. L.; Sargent, K. E.; Mercurio, A. M.; Hunt, J. S.; Ron, D.; Urano, F. Transcriptional Regulation of VEGF-A by the Unfolded Protein Response Pathway. *PLoS One* **2010**, *5* (3), e9575.
(56) Iwawaki, T.; Akai, R.; Yamanaka, S.; Kohno, K. Function of IRE1 Alpha in the Placenta Is Essential for Placental Development and Embryonic Viability. *Proc. Natl. Acad. Sci. U. S. A.* **2009**, *106* (39), 16657–16662.
(57) Bax, B. E.; Bloxam, D. L. Energy Metabolism and Glycolysis in Human Placental Trophoblast Cells during Differentiation. *Biochim. Biophys. Acta* **1997**, *1319* (2-3), 283–292.
(58) Gabbe, S. G.; Demers, L. M.; Greep, R. O.; Villee, C. A. Placental Glycogen Metabolism in

Diabetes Mellitus. *Diabetes* **1972**, *21* (12), 1185–1191.
(59) Coan, P. M.; Conroy, N.; Burton, G. J.; Ferguson-Smith, A. C. Origin and Characteristics of Glycogen Cells in the Developing Murine Placenta. *Dev. Dyn.* **2006**, *235* (12), 3280–3294.
(60) Tunster, S. J.; Van de Pette, M.; John, R. M. Impact of Genetic Background on Placental Glycogen Storage in Mice. *Placenta* **2012**, *33* (2), 124–127.
(61) Kidima, W. B. Syncytiotrophoblast Functions and Fetal Growth Restriction during Placental Malaria: Updates and Implication for Future Interventions. *Biomed Res. Int.* **2015**, *2015*, 451735.
(62) Kitazawa, M.; Tamura, M.; Kaneko-Ishino, T.; Ishino, F. Severe Damage to the Placental Fetal Capillary Network Causes Mid- to Late Fetal Lethality and Reduction in Placental Size in Peg11/Rtl1 KO Mice. *Genes Cells* **2017**, *22* (2), 174–188.
(63) Jauniaux, E.; Watson, A. L.; Hempstock, J.; Bao, Y. P.; Skepper, J. N.; Burton, G. J. Onset of Maternal Arterial Blood Flow and Placental Oxidative Stress. A Possible Factor in Human Early Pregnancy Failure. *Am. J. Pathol.* **2000**, *157* (6), 2111–2122.
(64) Yalu, R.; Oyesiji, A. E.; Eisenberg, I.; Imbar, T.; Meidan, R. HIF1A-Dependent Increase in Endothelin 2 Levels in Granulosa Cells: Role of Hypoxia, LH/cAMP, and Reactive Oxygen Species. *Reproduction* **2015**, *149* (1), 11–20.
(65) Parer, J. T.; Del Lannoy, C. W.; Hoversland, A. S.; Metcalfe, J. Effect of Decreased Uterine Blood Flow on Uterine Oxygen Consumption in Pregnant Macaques. *Am. J. Obstet. Gynecol.* **1968**, *100* (6), 813–820.
(66) Marangoni, F.; Cetin, I.; Verduci, E.; Canzone, G.; Giovannini, M.; Scollo, P.; Corsello, G.; Poli, A. Maternal Diet and Nutrient Requirements in Pregnancy and Breastfeeding. An Italian Consensus Document. *Nutrients* **2016**, *8* (10).
(67) Ericsson, A.; Hamark, B.; Powell, T. L.; Jansson, T. Glucose Transporter Isoform 4 Is Expressed in the Syncytiotrophoblast of First Trimester Human Placenta. *Hum. Reprod.* **2005**, *20* (2), 521–530.
(68) Nagai, A.; Takebe, K.; Nio-Kobayashi, J.; Takahashi-Iwanaga, H.; Iwanaga, T. Cellular Expression of the Monocarboxylate Transporter (MCT) Family in the Placenta of Mice. *Placenta* **2010**, *31* (2), 126–133.
(69) Coan, P. M.; Angiolini, E.; Sandovici, I.; Burton, G. J.; Constância, M.; Fowden, A. L. Adaptations in Placental Nutrient Transfer Capacity to Meet Fetal Growth Demands Depend on Placental Size in Mice. *J. Physiol.* **2008**, *586* (18), 4567–4576.
(70) Garvey, W. T.; Huecksteadt, T. P.; Birnbaum, M. J. Pretranslational Suppression of an Insulin-Responsive Glucose Transporter in Rats with Diabetes Mellitus. *Science* **1989**, *245* (4913), 60–63.
(71) Sferruzzi-Perri, A. N.; Vaughan, O. R.; Coan, P. M.; Suciu, M. C.; Darbyshire, R.; Constancia, M.; Burton, G. J.; Fowden, A. L. Placental-Specific Igf2 Deficiency Alters Developmental Adaptations to Undernutrition in Mice. *Endocrinology* **2011**, *152* (8), 3202–3212.
(72) Harris, L. K.; Crocker, I. P.; Baker, P. N.; Aplin, J. D.; Westwood, M. IGF2 Actions on Trophoblast in Human Placenta Are Regulated by the Insulin-like Growth Factor 2 Receptor, Which Can Function as Both a Signaling and Clearance Receptor. *Biol. Reprod.* **2011**, *84* (3), 440–446.
(73) Jolley, R. L.; Cheldelin, V. H.; Newburgh, R. W. Glucose Catabolism in Fetal and Adult Heart. *J. Biol. Chem.* **1958**, *233* (6), 1289–1294.

(74) Hay, W. W., Jr. Placental-Fetal Glucose Exchange and Fetal Glucose Metabolism. *Trans. Am. Clin. Climatol. Assoc.* **2006**, *117*, 321–339; discussion 339–340.
(75) Gibbins, K. J.; Gibson-Corley, K. N.; Brown, A. S.; Wieben, M.; Law, R. C.; Fung, C. M. Effects of Excess Thromboxane A2 on Placental Development and Nutrient Transporters in a Mus Musculus Model of Fetal Growth Restriction. *Biol. Reprod.* **2018**.
(76) Desforges, M.; Mynett, K. J.; Jones, R. L.; Greenwood, S. L.; Westwood, M.; Sibley, C. P.; Glazier, J. D. The SNAT4 Isoform of the System A Amino Acid Transporter Is Functional in Human Placental Microvillous Plasma Membrane. *J. Physiol.* **2009**, *587* (1), 61–72.
(77) Kanai, Y.; Segawa, H.; Miyamoto, K. i.; Uchino, H.; Takeda, E.; Endou, H. Expression Cloning and Characterization of a Transporter for Large Neutral Amino Acids Activated by the Heavy Chain of 4F2 Antigen (CD98). *J. Biol. Chem.* **1998**, *273* (37), 23629–23632.
(78) Pineda, M.; Fernández, E.; Torrents, D.; Estévez, R.; López, C.; Camps, M.; Lloberas, J.; Zorzano, A.; Palacín, M. Identification of a Membrane Protein, LAT-2, That Co-Expresses with 4F2 Heavy Chain, an L-Type Amino Acid Transport Activity with Broad Specificity for Small and Large Zwitterionic Amino Acids. *J. Biol. Chem.* **1999**, *274* (28), 19738–19744.
(79) Zhang, Z.; Grewer, C. The Sodium-Coupled Neutral Amino Acid Transporter SNAT2 Mediates an Anion Leak Conductance That Is Differentially Inhibited by Transported Substrates. *Biophys. J.* **2007**, *92* (7), 2621–2632.
(80) Mackenzie, B.; Erickson, J. D. Sodium-Coupled Neutral Amino Acid (System N/A) Transporters of the SLC38 Gene Family. *Pflugers Arch.* **2004**, *447* (5), 784–795.
(81) Manta-Vogli, P. D.; Schulpis, K. H.; Dotsikas, Y.; Loukas, Y. L. The Significant Role of Amino Acids during Pregnancy: Nutritional Support. *J. Matern. Fetal. Neonatal Med.* **2018**, 1–181.
(82) Kim, S.-R.; Kubo, T.; Kuroda, Y.; Hojyo, M.; Matsuo, T.; Miyajima, A.; Usami, M.; Sekino, Y.; Matsushita, T.; Ishida, S. Comparative Metabolome Analysis of Cultured Fetal and Adult Hepatocytes in Humans. *J. Toxicol. Sci.* **2014**, *39* (5), 717–723.
(83) Holme, A. M.; Roland, M. C. P.; Lorentzen, B.; Michelsen, T. M.; Henriksen, T. Placental Glucose Transfer: A Human in Vivo Study. *PLoS One* **2015**, *10* (2), e0117084.
(84) Teng, C.; Battaglia, F. C.; Meschia, G.; Narkewicz, M. R.; Wilkening, R. B. Fetal Hepatic and Umbilical Uptakes of Glucogenic Substrates during a Glucagon-Somatostatin Infusion. *Am. J. Physiol. Endocrinol. Metab.* **2002**, *282* (3), E542–E550.
(85) Shennan, D. B.; Calvert, D. T.; Travers, M. T.; Kudo, Y.; Boyd, C. A. R. A Study of L-Leucine, L-Phenylalanine and L-Alanine Transport in the Perfused Rat Mammary Gland: Possible Involvement of LAT1 and LAT2. *Biochim. Biophys. Acta* **2002**, *1564* (1), 133–139.
(86) Boado, R. J.; Li, J. Y.; Nagaya, M.; Zhang, C.; Pardridge, W. M. Selective Expression of the Large Neutral Amino Acid Transporter at the Blood-Brain Barrier. *Proc. Natl. Acad. Sci. U. S. A.* **1999**, *96* (21), 12079–12084.
(87) Mitsuhashi, S. Current Topics in the Biotechnological Production of Essential Amino Acids, Functional Amino Acids, and Dipeptides. *Curr. Opin. Biotechnol.* **2014**, *26*, 38–44.
(88) Stremmel, W.; Strohmeyer, G.; Borchard, F.; Kochwa, S.; Berk, P. D. Isolation and Partial Characterization of a Fatty Acid Binding Protein in Rat Liver Plasma Membranes. *Proc. Natl. Acad. Sci. U. S. A.* **1985**, *82* (1), 4–8.
(89) Makkar, A.; Mishima, T.; Chang, G.; Scifres, C.; Sadovsky, Y. Fatty Acid Binding

Protein-4 Is Expressed in the Mouse Placental Labyrinth, yet Is Dispensable for Placental Triglyceride Accumulation and Fetal Growth. *Placenta* **2014**, *35* (10), 802–807.

(90) Abumrad, N. A.; el-Maghrabi, M. R.; Amri, E. Z.; Lopez, E.; Grimaldi, P. A. Cloning of a Rat Adipocyte Membrane Protein Implicated in Binding or Transport of Long-Chain Fatty Acids That Is Induced during Preadipocyte Differentiation. Homology with Human CD36. *J. Biol. Chem.* **1993**, *268* (24), 17665–17668.

(91) Hirsch, D.; Stahl, A.; Lodish, H. F. A Family of Fatty Acid Transporters Conserved from Mycobacterium to Man. *Proc. Natl. Acad. Sci. U. S. A.* **1998**, *95* (15), 8625–8629.

(92) Mishima, T.; Miner, J. H.; Morizane, M.; Stahl, A.; Sadovsky, Y. The Expression and Function of Fatty Acid Transport Protein-2 and -4 in the Murine Placenta. *PLoS One* **2011**, *6* (10), e25865.

(93) Hirschmugl, B.; Desoye, G.; Catalano, P.; Klymiuk, I.; Scharnagl, H.; Payr, S.; Kitzinger, E.; Schliefsteiner, C.; Lang, U.; Wadsack, C.; et al. Maternal Obesity Modulates Intracellular Lipid Turnover in the Human Term Placenta. *Int. J. Obes.* **2017**, *41* (2), 317–323.

(94) Barrett, H. L.; Kubala, M. H.; Scholz Romero, K.; Denny, K. J.; Woodruff, T. M.; McIntyre, H. D.; Callaway, L. K.; Nitert, M. D. Placental Lipases in Pregnancies Complicated by Gestational Diabetes Mellitus (GDM). *PLoS One* **2014**, *9* (8), e104826.

(95) Coleman, R. A.; Haynes, E. B. Synthesis and Release of Fatty Acids by Human Trophoblast Cells in Culture. *J. Lipid Res.* **1987**, *28* (11), 1335–1341.

(96) Campbell, F. M.; Bush, P. G.; Veerkamp, J. H.; Dutta-Roy, A. K. Detection and Cellular Localization of Plasma Membrane-Associated and Cytoplasmic Fatty Acid-Binding Proteins in Human Placenta. *Placenta* **1998**, *19* (5-6), 409–415.

(97) Heuckeroth, R. O.; Birkenmeier, E. H.; Levin, M. S.; Gordon, J. I. Analysis of the Tissue-Specific Expression, Developmental Regulation, and Linkage Relationships of a Rodent Gene Encoding Heart Fatty Acid Binding Protein. *J. Biol. Chem.* **1987**, *262* (20), 9709–9717.

(98) Rawn, S. M.; Huang, C.; Hughes, M.; Shaykhutdinov, R.; Vogel, H. J.; Cross, J. C. Pregnancy Hyperglycemia in Prolactin Receptor Mutant, but Not Prolactin Mutant, Mice and Feeding-Responsive Regulation of Placental Lactogen Genes Implies Placental Control of Maternal Glucose Homeostasis. *Biol. Reprod.* **2015**, *93* (3), 75.

(99) Magnusson-Olsson, A. L.; Lager, S.; Jacobsson, B.; Jansson, T.; Powell, T. L. Effect of Maternal Triglycerides and Free Fatty Acids on Placental LPL in Cultured Primary Trophoblast Cells and in a Case of Maternal LPL Deficiency. *Am. J. Physiol. Endocrinol. Metab.* **2007**, *293* (1), E24–E30.

(100) Newbern, D.; Freemark, M. Placental Hormones and the Control of Maternal Metabolism and Fetal Growth. *Curr. Opin. Endocrinol. Diabetes Obes.* **2011**, *18* (6), 409–416.

(101) Mitrou, P.; Boutati, E.; Lambadiari, V.; Maratou, E.; Papakonstantinou, A.; Komesidou, V.; Sidossis, L.; Tountas, N.; Katsilambros, N.; Economopoulos, T.; et al. Rates of Glucose Uptake in Adipose Tissue and Muscle in Vivo after a Mixed Meal in Women with Morbid Obesity. *J. Clin. Endocrinol. Metab.* **2009**, *94* (8), 2958–2961.

(102) Männik, J.; Vaas, P.; Rull, K.; Teesalu, P.; Laan, M. Differential Placental Expression Profile of Human Growth Hormone/Chorionic Somatomammotropin Genes in Pregnancies with Pre-Eclampsia and Gestational Diabetes Mellitus. *Mol. Cell. Endocrinol.* **2012**, *355* (1), 180–187.

(103) Karabulut, A. K.; Layfield, R.; Pratten, M. K. Growth Promoting Effects of Human Placental Lactogen during Early Organogenesis: A Link to Insulin-like Growth Factors. *J. Anat.* **2001**, *198* (Pt 6), 651–662.

(104) Lain, K. Y.; Catalano, P. M. Metabolic Changes in Pregnancy. *Clin. Obstet. Gynecol.* **2007**, *50* (4), 938–948.

(105) Catalano, P. M.; Shankar, K. Obesity and Pregnancy: Mechanisms of Short Term and Long Term Adverse Consequences for Mother and Child. *BMJ* **2017**, *356*, j1.

(106) Kniss, D. A.; Shubert, P. J.; Zimmerman, P. D.; Landon, M. B.; Gabbe, S. G. Insulinlike Growth Factors. Their Regulation of Glucose and Amino Acid Transport in Placental Trophoblasts Isolated from First-Trimester Chorionic Villi. *J. Reprod. Med.* **1994**, *39* (4), 249–256.

(107) Diderholm, B.; Stridsberg, M.; Ewald, U.; Lindeberg-Nordén, S.; Gustafsson, J. Increased Lipolysis in Non-Obese Pregnant Women Studied in the Third Trimester. *BJOG* **2005**, *112* (6), 713–718.

(108) Scholl, T. O.; Sowers, M.; Chen, X.; Lenders, C. Maternal Glucose Concentration Influences Fetal Growth, Gestation, and Pregnancy Complications. *Am. J. Epidemiol.* **2001**, *154* (6), 514–520.

(109) Roberts, C. T.; Kind, K. L.; Earl, R. A.; Grant, P. A.; Robinson, J. S.; Sohlstrom, A.; Owens, P. C.; Owens, J. A. Circulating Insulin-like Growth Factor (IGF)-I and IGF Binding Proteins -1 and -3 and Placental Development in the Guinea-Pig. *Placenta* **2002**, *23* (10), 763–770.

(110) Sibley, C. P.; Coan, P. M.; Ferguson-Smith, A. C.; Dean, W.; Hughes, J.; Smith, P.; Reik, W.; Burton, G. J.; Fowden, A. L.; Constância, M. Placental-Specific Insulin-like Growth Factor 2 (Igf2) Regulates the Diffusional Exchange Characteristics of the Mouse Placenta. *Proc. Natl. Acad. Sci. U. S. A.* **2004**, *101* (21), 8204–8208.

(111) Constância, M.; Angiolini, E.; Sandovici, I.; Smith, P.; Smith, R.; Kelsey, G.; Dean, W.; Ferguson-Smith, A.; Sibley, C. P.; Reik, W.; et al. Adaptation of Nutrient Supply to Fetal Demand in the Mouse Involves Interaction between the Igf2 Gene and Placental Transporter Systems. *Proc. Natl. Acad. Sci. U. S. A.* **2005**, *102* (52), 19219–19224.

(112) Beattie, J.; Allan, G. J.; Lochrie, J. D.; Flint, D. J. Insulin-like Growth Factor-Binding Protein-5 (IGFBP-5): A Critical Member of the IGF Axis. *Biochem. J* **2006**, *395* (1), 1–19.

(113) Hamilton, G. S.; Lysiak, J. J.; Han, V. K.; Lala, P. K. Autocrine-Paracrine Regulation of Human Trophoblast Invasiveness by Insulin-like Growth Factor (IGF)-II and IGF-Binding Protein (IGFBP)-1. *Exp. Cell Res.* **1998**, *244* (1), 147–156.

(114) Liang, L.; Guo, W. H.; Esquiliano, D. R.; Asai, M.; Rodriguez, S.; Giraud, J.; Kushner, J. A.; White, M. F.; Lopez, M. F. Insulin-like Growth Factor 2 and the Insulin Receptor, but Not Insulin, Regulate Fetal Hepatic Glycogen Synthesis. *Endocrinology* **2010**, *151* (2), 741–747.

(115) Zhou, Q. L.; Jiang, Z. Y.; Holik, J.; Chawla, A.; Hagan, G. N.; Leszyk, J.; Czech, M. P. Akt Substrate TBC1D1 Regulates GLUT1 Expression through the mTOR Pathway in 3T3-L1 Adipocytes. *Biochem. J* **2008**, *411* (3), 647–655.

(116) Wang, R.; Dillon, C. P.; Shi, L. Z.; Milasta, S.; Carter, R.; Finkelstein, D.; McCormick, L. L.; Fitzgerald, P.; Chi, H.; Munger, J.; et al. The Transcription Factor Myc Controls Metabolic Reprogramming upon T Lymphocyte Activation. *Immunity* **2011**, *35* (6), 871–882.

(117) Luiken, J. J. F. P.; Koonen, D. P. Y.; Willems, J.; Zorzano, A.; Becker, C.; Fischer, Y.; Tandon, N. N.; Van Der Vusse, G. J.; Bonen, A.; Glatz, J. F. C. Insulin Stimulates Long-Chain Fatty Acid Utilization by Rat Cardiac Myocytes through Cellular Redistribution of FAT/CD36. *Diabetes* **2002**, *51* (10), 3113–3119.

(118) Green, C. J.; Göransson, O.; Kular, G. S.; Leslie, N. R.; Gray, A.; Alessi, D. R.; Sakamoto, K.; Hundal, H. S. Use of Akt Inhibitor and a Drug-Resistant Mutant Validates a Critical Role for Protein Kinase B/Akt in the Insulin-Dependent Regulation of Glucose and System A Amino Acid Uptake. *J. Biol. Chem.* **2008**, *283* (41), 27653–27667.

(119) Ding, Y.; Shan, L.; Nai, W.; Lin, X.; Zhou, L.; Dong, X.; Wu, H.; Xiao, M.; Zhou, X.; Wang, L.; et al. DEPTOR Deficiency-Mediated mTORc1 Hyperactivation in Vascular Endothelial Cells Promotes Angiogenesis. *Cell. Physiol. Biochem.* **2018**, *46* (2), 520–531.

(120) Kent, L. N.; Ohboshi, S.; Soares, M. J. Akt1 and Insulin-like Growth Factor 2 (Igf2) Regulate Placentation and Fetal/postnatal Development. *Int. J. Dev. Biol.* **2012**, *56* (4), 255–261.

(121) Bell, A. W.; Ehrhardt, R. A. Regulation of Placental Nutrient Transport and Implications for Fetal Growth. *Nutr. Res. Rev.* **2002**, *15* (2), 211–230.

(122) Rossant, J.; Cross, J. C. Placental Development: Lessons from Mouse Mutants. *Nat. Rev. Genet.* **2001**, *2* (7), 538–548.

(123) Arora, R.; Papaioannou, V. E. The Murine Allantois: A Model System for the Study of Blood Vessel Formation. *Blood* **2012**, *120* (13), 2562–2572.

(124) Chen, D.-B.; Zheng, J. Regulation of Placental Angiogenesis. *Microcirculation* **2014**, *21* (1), 15–25.

(125) Xu, W.; Zhou, W.; Cheng, M.; Wang, J.; Liu, Z.; He, S.; Luo, X.; Huang, W.; Chen, T.; Yan, W.; et al. Hypoxia Activates Wnt/β-Catenin Signaling by Regulating the Expression of BCL9 in Human Hepatocellular Carcinoma. *Sci. Rep.* **2017**, *7*, 40446.

(126) Easwaran, V.; Lee, S. H.; Inge, L.; Guo, L.; Goldbeck, C.; Garrett, E.; Wiesmann, M.; Garcia, P. D.; Fuller, J. H.; Chan, V.; et al. Beta-Catenin Regulates Vascular Endothelial Growth Factor Expression in Colon Cancer. *Cancer Res.* **2003**, *63* (12), 3145–3153.

(127) Wang, Y.; Zhao, S. *Vasculogenesis and Angiogenesis of Human Placenta*; Morgan & Claypool Life Sciences, 2010.

(128) Yuan, X.-H.; Yang, J.; Wang, X.-Y.; Zhang, X.-L.; Qin, T.-T.; Li, K. Association between EGFR/KRAS Mutation and Expression of VEGFA, VEGFR and VEGFR2 in Lung Adenocarcinoma. *Oncol. Lett.* **2018**, *16* (2), 2105–2112.

(129) Kendall, R. L.; Thomas, K. A. Inhibition of Vascular Endothelial Cell Growth Factor Activity by an Endogenously Encoded Soluble Receptor. *Proc. Natl. Acad. Sci. U. S. A.* **1993**, *90* (22), 10705–10709.

(130) Lee, S.; Chen, T. T.; Barber, C. L.; Jordan, M. C.; Murdock, J.; Desai, S.; Ferrara, N.; Nagy, A.; Roos, K. P.; Iruela-Arispe, M. L. Autocrine VEGF Signaling Is Required for Vascular Homeostasis. *Cell* **2007**, *130* (4), 691–703.

(131) Taricco, E.; Radaelli, T.; Rossi, G.; Nobile de Santis, M. S.; Bulfamante, G. P.; Avagliano, L.; Cetin, I. Effects of Gestational Diabetes on Fetal Oxygen and Glucose Levels in Vivo. *BJOG* **2009**, *116* (13), 1729–1735.

(132) Moore, G. E.; Ishida, M.; Demetriou, C.; Al-Olabi, L.; Leon, L. J.; Thomas, A. C.; Abu-Amero, S.; Frost, J. M.; Stafford, J. L.; Chaoqun, Y.; et al. The Role and Interaction of Imprinted Genes in Human Fetal Growth. *Philos. Trans. R. Soc. Lond. B Biol. Sci.* **2015**,

370 (1663), 20140074.

(133) Ratajczak, M. Z. Igf2-H19, an Imprinted Tandem Gene, Is an Important Regulator of Embryonic Development, a Guardian of Proliferation of Adult Pluripotent Stem Cells, a Regulator of Longevity, and a "Passkey" to Cancerogenesis. *Folia Histochem. Cytobiol.* **2012**, *50* (2), 171–179.

(134) Yu, H.; Diao, H.; Wang, C.; Lin, Y.; Yu, F.; Lu, H.; Xu, W.; Li, Z.; Shi, H.; Zhao, S.; et al. Acetylproteomic Analysis Reveals Functional Implications of Lysine Acetylation in Human Spermatozoa (sperm). *Mol. Cell. Proteomics* **2015**, *14* (4), 1009–1023.

(135) Kageyama, S.-I.; Liu, H.; Kaneko, N.; Ooga, M.; Nagata, M.; Aoki, F. Alterations in Epigenetic Modifications during Oocyte Growth in Mice. *Reproduction* **2007**, *133* (1), 85–94.

(136) Youngson, N. A.; Lecomte, V.; Maloney, C. A.; Leung, P.; Liu, J.; Hesson, L. B.; Luciani, F.; Krause, L.; Morris, M. J. Obesity-Induced Sperm DNA Methylation Changes at Satellite Repeats Are Reprogrammed in Rat Offspring. *Asian J. Androl.* **2016**, *18* (6), 930–936.

(137) Brickner, D. G.; Cajigas, I.; Fondufe-Mittendorf, Y.; Ahmed, S.; Lee, P.-C.; Widom, J.; Brickner, J. H. H2A.Z-Mediated Localization of Genes at the Nuclear Periphery Confers Epigenetic Memory of Previous Transcriptional State. *PLoS Biol.* **2007**, *5* (4), e81.

(138) Kantake, M.; Yoshitake, H.; Ishikawa, H.; Araki, Y.; Shimizu, T. Postnatal Epigenetic Modification of Glucocorticoid Receptor Gene in Preterm Infants: A Prospective Cohort Study. *BMJ Open* **2014**, *4* (7), e005318.

(139) Brouwer-Visser, J.; Huang, G. S. IGF2 Signaling and Regulation in Cancer. *Cytokine Growth Factor Rev.* **2015**, *26* (3), 371–377.

(140) Mayer, W.; Hemberger, M.; Frank, H. G.; Grümmer, R.; Winterhager, E.; Kaufmann, P.; Fundele, R. Expression of the Imprinted Genes MEST/Mest in Human and Murine Placenta Suggests a Role in Angiogenesis. *Dev. Dyn.* **2000**, *217* (1), 1–10.

(141) McMinn, J.; Wei, M.; Sadovsky, Y.; Thaker, H. M.; Tycko, B. Imprinting of PEG1/MEST Isoform 2 in Human Placenta. *Placenta* **2006**, *27* (2-3), 119–126.

(142) Miozzo, M.; Grati, F. R.; Bulfamante, G.; Rossella, F.; Cribiù, M.; Radaelli, T.; Cassani, B.; Persico, T.; Cetin, I.; Pardi, G.; et al. Post-Zygotic Origin of Complete Maternal Chromosome 7 Isodisomy and Consequent Loss of Placental PEG1/MEST Expression. *Placenta* **2001**, *22* (10), 813–821.

(143) Sakian, S.; Louie, K.; Wong, E. C.; Havelock, J.; Kashyap, S.; Rowe, T.; Taylor, B.; Ma, S. Altered Gene Expression of H19 and IGF2 in Placentas from ART Pregnancies. *Placenta* **2015**, *36* (10), 1100–1105.

(144) Gao, W.-L.; Liu, M.; Yang, Y.; Yang, H.; Liao, Q.; Bai, Y.; Li, Y.-X.; Li, D.; Peng, C.; Wang, Y.-L. The Imprinted H19 Gene Regulates Human Placental Trophoblast Cell Proliferation via Encoding miR-675 That Targets Nodal Modulator 1 (NOMO1). *RNA Biol.* **2012**, *9* (7), 1002–1010.

(145) Tunster, S. J.; Creeth, H. D. J.; John, R. M. The Imprinted Phlda2 Gene Modulates a Major Endocrine Compartment of the Placenta to Regulate Placental Demands for Maternal Resources. *Dev. Biol.* **2016**, *409* (1), 251–260.

(146) Gabory, A.; Ripoche, M.-A.; Le Digarcher, A.; Watrin, F.; Ziyyat, A.; Forné, T.; Jammes, H.; Ainscough, J. F. X.; Surani, M. A.; Journot, L.; et al. H19 Acts as a Trans Regulator of the Imprinted Gene Network Controlling Growth in Mice. *Development* **2009**,

136 (20), 3413–3421.

(147) Ha, M.; Kim, V. N. Regulation of microRNA Biogenesis. *Nat. Rev. Mol. Cell Biol.* **2014**, *15* (8), 509–524.

(148) Murchison, E. P.; Hannon, G. J. miRNAs on the Move: miRNA Biogenesis and the RNAi Machinery. *Curr. Opin. Cell Biol.* **2004**, *16* (3), 223–229.

(149) Lund, E.; Dahlberg, J. E. Substrate Selectivity of Exportin 5 and Dicer in the Biogenesis of microRNAs. *Cold Spring Harb. Symp. Quant. Biol.* **2006**, *71*, 59–66.

(150) Bakos, H. W.; Henshaw, R. C.; Mitchell, M.; Lane, M. Paternal Body Mass Index Is Associated with Decreased Blastocyst Development and Reduced Live Birth Rates Following Assisted Reproductive Technology. *Fertil. Steril.* **2011**, *95* (5), 1700–1704.

(151) Yuan, S.; Schuster, A.; Tang, C.; Yu, T.; Ortogero, N.; Bao, J.; Zheng, H.; Yan, W. Sperm-Borne miRNAs and Endo-siRNAs Are Important for Fertilization and Preimplantation Embryonic Development. *Development* **2016**, *143* (4), 635–647.

(152) Hromadnikova, I.; Kotlabova, K.; Ondrackova, M.; Pirkova, P.; Kestlerova, A.; Novotna, V.; Hympanova, L.; Krofta, L. Expression Profile of C19MC microRNAs in Placental Tissue in Pregnancy-Related Complications. *DNA Cell Biol.* **2015**, *34* (6), 437–457.

(153) Noguer-Dance, M.; Abu-Amero, S.; Al-Khtib, M.; Lefèvre, A.; Coullin, P.; Moore, G. E.; Cavaillé, J. The Primate-Specific microRNA Gene Cluster (C19MC) Is Imprinted in the Placenta. *Hum. Mol. Genet.* **2010**, *19* (18), 3566–3582.

(154) Ye, W.; Lv, Q.; Wong, C.-K. A.; Hu, S.; Fu, C.; Hua, Z.; Cai, G.; Li, G.; Yang, B. B.; Zhang, Y. The Effect of Central Loops in miRNA:MRE Duplexes on the Efficiency of miRNA-Mediated Gene Regulation. *PLoS One* **2008**, *3* (3), e1719.

(155) Neel, J. V. Diabetes Mellitus: A "Thrifty" Genotype Rendered Detrimental by "Progress"? *Am. J. Hum. Genet.* **1962**, *14*, 353–362.

(156) van Abeelen, A. F. M.; de Rooij, S. R.; Osmond, C.; Painter, R. C.; Veenendaal, M. V. E.; Bossuyt, P. M. M.; Elias, S. G.; Grobbee, D. E.; van der Schouw, Y. T.; Barker, D. J. P.; et al. The Sex-Specific Effects of Famine on the Association between Placental Size and Later Hypertension. *Placenta* **2011**, *32* (9), 694–698.

(157) Davis, E. F.; Lazdam, M.; Lewandowski, A. J.; Worton, S. A.; Kelly, B.; Kenworthy, Y.; Adwani, S.; Wilkinson, A. R.; McCormick, K.; Sargent, I.; et al. Cardiovascular Risk Factors in Children and Young Adults Born to Preeclamptic Pregnancies: A Systematic Review. *Pediatrics* **2012**, *129* (6), e1552–e1561.

(158) Tsai, T.-C.; Lai, K.-H.; Su, J.-H.; Wu, Y.-J.; Sheu, J.-H. 7-Acetylsinumaximol B Induces Apoptosis and Autophagy in Human Gastric Carcinoma Cells through Mitochondria Dysfunction and Activation of the PERK/eIF2α/ATF4/CHOP Signaling Pathway. *Mar. Drugs* **2018**, *16* (4).

(159) Pereira, E. R.; Frudd, K.; Awad, W.; Hendershot, L. M. Endoplasmic Reticulum (ER) Stress and Hypoxia Response Pathways Interact to Potentiate Hypoxia-Inducible Factor 1 (HIF-1) Transcriptional Activity on Targets like Vascular Endothelial Growth Factor (VEGF). *J. Biol. Chem.* **2014**, *289* (6), 3352–3364.

(160) Park, J. H.; Yoo, Y.; Cho, M.; Lim, J.; Lindroth, A. M.; Park, Y. J. Diet-Induced Obesity Leads to Metabolic Dysregulation in Offspring via Endoplasmic Reticulum Stress in a Sex-Specific Manner. *Int. J. Obes.* **2018**, *42* (2), 244–251.

(161) Kandala, P. K.; Srivastava, S. K. Regulation of Macroautophagy in Ovarian Cancer Cells in Vitro and in Vivo by Controlling Glucose Regulatory Protein 78 and AMPK. *Oncotarget*

2012, *3* (4), 435–449.

(162) Jain, A.; Olovsson, M.; Burton, G. J.; Yung, H.-W. Endothelin-1 Induces Endoplasmic Reticulum Stress by Activating the PLC-IP(3) Pathway: Implications for Placental Pathophysiology in Preeclampsia. *Am. J. Pathol.* **2012**, *180* (6), 2309–2320.

(163) Szegezdi, E.; Logue, S. E.; Gorman, A. M.; Samali, A. Mediators of Endoplasmic Reticulum Stress-Induced Apoptosis. *EMBO Rep.* **2006**, *7* (9), 880–885.

(164) Deegan, S.; Koryga, I.; Glynn, S. A.; Gupta, S.; Gorman, A. M.; Samali, A. A Close Connection between the PERK and IRE Arms of the UPR and the Transcriptional Regulation of Autophagy. *Biochem. Biophys. Res. Commun.* **2015**, *456* (1), 305–311.

(165) Oslowski, C. M.; Urano, F. Measuring ER Stress and the Unfolded Protein Response Using Mammalian Tissue Culture System. *Methods Enzymol.* **2011**, *490*, 71–92.

(166) Oslowski, C. M.; Urano, F. The Binary Switch between Life and Death of Endoplasmic Reticulum-Stressed Beta Cells. *Curr. Opin. Endocrinol. Diabetes Obes.* **2010**, *17* (2), 107–112.

(167) Snowden, C. J.; Leborgne-Castel, N.; Wootton, L. J.; Hadlington, J. L.; Denecke, J. In Vivo Analysis of the Lumenal Binding Protein (BiP) Reveals Multiple Functions of Its ATPase Domain. *Plant J.* **2007**, *52* (6), 987–1000.

(168) Shen, J.; Chen, X.; Hendershot, L.; Prywes, R. ER Stress Regulation of ATF6 Localization by Dissociation of BiP/GRP78 Binding and Unmasking of Golgi Localization Signals. *Dev. Cell* **2002**, *3* (1), 99–111.

(169) Soares Moretti, A. I.; Martins Laurindo, F. R. Protein Disulfide Isomerases: Redox Connections in and out of the Endoplasmic Reticulum. *Arch. Biochem. Biophys.* **2017**, *617*, 106–119.

(170) Harding, H. P.; Novoa, I.; Zhang, Y.; Zeng, H.; Wek, R.; Schapira, M.; Ron, D. Regulated Translation Initiation Controls Stress-Induced Gene Expression in Mammalian Cells. *Mol. Cell* **2000**, *6* (5), 1099–1108.

(171) Ishioka, S.-I.; Ezaka, Y.; Umemura, K.; Hayashi, T.; Endo, T.; Saito, T. Proteomic Analysis of Mechanisms of Hypoxia-Induced Apoptosis in Trophoblastic Cells. *Int. J. Med. Sci.* **2006**, *4* (1), 36–44.

(172) Cui, W.; Ma, J.; Wang, X.; Yang, W.; Zhang, J.; Ji, Q. Free Fatty Acid Induces Endoplasmic Reticulum Stress and Apoptosis of β-Cells by Ca2+/calpain-2 Pathways. *PLoS One* **2013**, *8* (3), e59921.

(173) Walsh, J. G.; Cullen, S. P.; Sheridan, C.; Lüthi, A. U.; Gerner, C.; Martin, S. J. Executioner Caspase-3 and Caspase-7 Are Functionally Distinct Proteases. *Proc. Natl. Acad. Sci. U. S. A.* **2008**, *105* (35), 12815–12819.

(174) Tam, A. B.; Mercado, E. L.; Hoffmann, A.; Niwa, M. ER Stress Activates NF-κB by Integrating Functions of Basal IKK Activity, IRE1 and PERK. *PLoS One* **2012**, *7* (10), e45078.

(175) Yoshida, H.; Matsui, T.; Yamamoto, A.; Okada, T.; Mori, K. XBP1 mRNA Is Induced by ATF6 and Spliced by IRE1 in Response to ER Stress to Produce a Highly Active Transcription Factor. *Cell* **2001**, *107* (7), 881–891.

(176) Lee, A.-H.; Iwakoshi, N. N.; Glimcher, L. H. XBP-1 Regulates a Subset of Endoplasmic Reticulum Resident Chaperone Genes in the Unfolded Protein Response. *Mol. Cell. Biol.* **2003**, *23* (21), 7448–7459.

(177) Reiss, K.; Breckenkamp, J.; Borde, T.; Brenne, S.; Henrich, W.; David, M.; Razum, O.

The Association of Pre-Pregnancy Overweight and Obesity with Delivery Outcomes: A Comparison of Immigrant and Non-Immigrant Women in Berlin, Germany. *Int. J. Public Health* **2016**, *61* (4), 455–463.

(178) Bar, J.; Kovo, M.; Schraiber, L.; Shargorodsky, M. Placental Maternal and Fetal Vascular Circulation in Healthy Non-Obese and Metabolically Healthy Obese Pregnant Women. *Atherosclerosis* **2017**, *260*, 63–66.

(179) Colomiere, M.; Permezel, M.; Riley, C.; Desoye, G.; Lappas, M. Defective Insulin Signaling in Placenta from Pregnancies Complicated by Gestational Diabetes Mellitus. *Eur. J. Endocrinol.* **2009**, *160* (4), 567–578.

(180) Zalbahar, N.; Najman, J.; McIntrye, H. D.; Mamun, A. Parental Pre-Pregnancy BMI Influences on Offspring BMI and Waist Circumference at 21 Years. *Aust. N. Z. J. Public Health* **2016**, *40* (6), 572–578.

(181) Liu, P.; Xu, L.; Wang, Y.; Zhang, Y.; Du, Y.; Sun, Y.; Wang, Z. Association between Perinatal Outcomes and Maternal Pre-Pregnancy Body Mass Index. *Obes. Rev.* **2016**, *17* (11), 1091–1102.

(182) Ma, R. C. W.; Chan, J. C. N.; Tam, W. H.; Hanson, M. A.; Gluckman, P. D. Gestational Diabetes, Maternal Obesity, and the NCD Burden. *Clin. Obstet. Gynecol.* **2013**, *56* (3), 633–641.

(183) Gaillard, R. Maternal Obesity during Pregnancy and Cardiovascular Development and Disease in the Offspring. *Eur. J. Epidemiol.* **2015**, *30* (11), 1141–1152.

(184) Madan, J. C.; Davis, J. M.; Craig, W. Y.; Collins, M.; Allan, W.; Quinn, R.; Dammann, O. Maternal Obesity and Markers of Inflammation in Pregnancy. *Cytokine* **2009**, *47* (1), 61–64.

(185) Spellacy, W. N.; Buhi, W. C.; Birk, S. A. Human Placental Lactogen and Intrauterine Growth Retardation. *Obstet. Gynecol.* **1976**, *47* (4), 446–448.

(186) Obiekwe, B. C.; Sturdee, D.; Cockrill, B. L.; Chard, T. Human Placental Lactogen in Pre-Eclampsia. *Br. J. Obstet. Gynaecol.* **1984**, *91* (11), 1077–1080.

(187) Huang, L.; Liu, J.; Feng, L.; Chen, Y.; Zhang, J.; Wang, W. Maternal Prepregnancy Obesity Is Associated with Higher Risk of Placental Pathological Lesions. *Placenta* **2014**, *35* (8), 563–569.

(188) Kovo, M.; Schreiber, L.; Ben-Haroush, A.; Wand, S.; Golan, A.; Bar, J. Placental Vascular Lesion Differences in Pregnancy-Induced Hypertension and Normotensive Fetal Growth Restriction. *Am. J. Obstet. Gynecol.* **2010**, *202* (6), 561.e1–e5.

(189) Richardson, B. S.; Ruttinger, S.; Brown, H. K.; Regnault, T. R. H.; de Vrijer, B. Maternal Body Mass Index Impacts Fetal-Placental Size at Birth and Umbilical Cord Oxygen Values with Implications for Regulatory Mechanisms. *Early Hum. Dev.* **2017**, *112*, 42–47.

(190) Rahimi, N. The Ubiquitin-Proteasome System Meets Angiogenesis. *Mol. Cancer Ther.* **2012**, *11* (3), 538–548.

(191) Sohlberg, S.; Mulic-Lutvica, A.; Olovsson, M.; Weis, J.; Axelsson, O.; Wikström, J.; Wikström, A.-K. Magnetic Resonance Imaging-Estimated Placental Perfusion in Fetal Growth Assessment. *Ultrasound Obstet. Gynecol.* **2015**, *46* (6), 700–705.

(192) Ferrazzi, E.; Rigano, S.; Bozzo, M.; Bellotti, M.; Giovannini, N.; Galan, H.; Battaglia, F. C. Umbilical Vein Blood Flow in Growth-Restricted Fetuses. *Ultrasound Obstet. Gynecol.* **2000**, *16* (5), 432–438.

(193) Aljunaidy, M. M.; Morton, J. S.; Cooke, C.-L. M.; Davidge, S. T. Prenatal Hypoxia and

Placental Oxidative Stress: Linkages to Developmental Origins of Cardiovascular Disease. *Am. J. Physiol. Regul. Integr. Comp. Physiol.* **2017**, *313* (4), R395–R399.

(194) Männik, J.; Vaas, P.; Rull, K.; Teesalu, P.; Rebane, T.; Laan, M. Differential Expression Profile of Growth Hormone/chorionic Somatomammotropin Genes in Placenta of Small- and Large-for-Gestational-Age Newborns. *J. Clin. Endocrinol. Metab.* **2010**, *95* (5), 2433–2442.

(195) Rueda-Clausen, C. F.; Stanley, J. L.; Thambiraj, D. F.; Poudel, R.; Davidge, S. T.; Baker, P. N. Effect of Prenatal Hypoxia in Transgenic Mouse Models of Preeclampsia and Fetal Growth Restriction. *Reprod. Sci.* **2014**, *21* (4), 492–502.

(196) Basso, O.; Rasmussen, S.; Weinberg, C. R.; Wilcox, A. J.; Irgens, L. M.; Skjaerven, R. Trends in Fetal and Infant Survival Following Preeclampsia. *JAMA* **2006**, *296* (11), 1357–1362.

(197) Kajantie, E.; Eriksson, J. G.; Osmond, C.; Thornburg, K.; Barker, D. J. P. Pre-Eclampsia Is Associated with Increased Risk of Stroke in the Adult Offspring: The Helsinki Birth Cohort Study. *Stroke* **2009**, *40* (4), 1176–1180.

(198) Farley, D. M.; Choi, J.; Dudley, D. J.; Li, C.; Jenkins, S. L.; Myatt, L.; Nathanielsz, P. W. Placental Amino Acid Transport and Placental Leptin Resistance in Pregnancies Complicated by Maternal Obesity. *Placenta* **2010**, *31* (8), 718–724.

(199) Gallo, L. A.; Barrett, H. L.; Dekker Nitert, M. Review: Placental Transport and Metabolism of Energy Substrates in Maternal Obesity and Diabetes. *Placenta* **2017**, *54*, 59–67.

(200) Finger, B. J.; Harvey, A. J.; Green, M. P.; Gardner, D. K. Combined Parental Obesity Negatively Impacts Preimplantation Mouse Embryo Development, Kinetics, Morphology and Metabolism. *Hum. Reprod.* **2015**, *30* (9), 2084–2096.

(201) Redmer, D. A.; Aitken, R. P.; Milne, J. S.; Reynolds, L. P.; Wallace, J. M. Influence of Maternal Nutrition on Messenger RNA Expression of Placental Angiogenic Factors and Their Receptors at Midgestation in Adolescent Sheep. *Biol. Reprod.* **2005**, *72* (4), 1004–1009.

(202) Ravishankar, S.; Bourjeily, G.; Lambert-Messerlian, G.; He, M.; De Paepe, M. E.; Gündoğan, F. Evidence of Placental Hypoxia in Maternal Sleep Disordered Breathing. *Pediatr. Dev. Pathol.* **2015**, *18* (5), 380–386.

(203) Li, H.-P.; Chen, X.; Li, M.-Q. Gestational Diabetes Induces Chronic Hypoxia Stress and Excessive Inflammatory Response in Murine Placenta. *Int. J. Clin. Exp. Pathol.* **2013**, *6* (4), 650–659.

(204) Roberts, V. H. J.; Lo, J. O.; Lewandowski, K. S.; Blundell, P.; Grove, K. L.; Kroenke, C. D.; Sullivan, E. L.; Roberts, C. T., Jr; Frias, A. E. Adverse Placental Perfusion and Pregnancy Outcomes in a New Nonhuman Primate Model of Gestational Protein Restriction. *Reprod. Sci.* **2018**, *25* (1), 110–119.

(205) Cuffe, J. S. M.; Walton, S. L.; Singh, R. R.; Spiers, J. G.; Bielefeldt-Ohmann, H.; Wilkinson, L.; Little, M. H.; Moritz, K. M. Mid- to Late Term Hypoxia in the Mouse Alters Placental Morphology, Glucocorticoid Regulatory Pathways and Nutrient Transporters in a Sex-Specific Manner. *J. Physiol.* **2014**, *592* (14), 3127–3141.

(206) Kleppa, M.-J.; Erlenwein, S.-V.; Darashchonak, N.; von Kaisenberg, C. S.; von Versen-Höynck, F. Hypoxia and the Anticoagulants Dalteparin and Acetylsalicylic Acid Affect Human Placental Amino Acid Transport. *PLoS One* **2014**, *9* (6), e99217.

(207) Nguyen, R. H. N.; Wilcox, A. J.; Skjaerven, R.; Baird, D. D. Men's Body Mass Index and Infertility. *Hum. Reprod.* **2007**, *22* (9), 2488–2493.
(208) Petersen, G. L.; Schmidt, L.; Pinborg, A.; Kamper-Jørgensen, M. The Influence of Female and Male Body Mass Index on Live Births after Assisted Reproductive Technology Treatment: A Nationwide Register-Based Cohort Study. *Fertil. Steril.* **2013**, *99* (6), 1654–1662.
(209) Hammoud, A. O.; Wilde, N.; Gibson, M.; Parks, A.; Carrell, D. T.; Meikle, A. W. Male Obesity and Alteration in Sperm Parameters. *Fertil. Steril.* **2008**, *90* (6), 2222–2225.
(210) Giagulli, V. A.; Kaufman, J. M.; Vermeulen, A. Pathogenesis of the Decreased Androgen Levels in Obese Men. *J. Clin. Endocrinol. Metab.* **1994**, *79* (4), 997–1000.
(211) Tsai, E. C.; Matsumoto, A. M.; Fujimoto, W. Y.; Boyko, E. J. Association of Bioavailable, Free, and Total Testosterone with Insulin Resistance: Influence of Sex Hormone-Binding Globulin and Body Fat. *Diabetes Care* **2004**, *27* (4), 861–868.
(212) Peiris, A. N.; Sothmann, M. S.; Aiman, E. J.; Kissebah, A. H. The Relationship of Insulin to Sex Hormone-Binding Globulin: Role of Adiposity. *Fertil. Steril.* **1989**, *52* (1), 69–72.
(213) Yarrow, J. F.; Wronski, T. J.; Borst, S. E. Testosterone and Adult Male Bone: Actions Independent of 5α-Reductase and Aromatase. *Exerc. Sport Sci. Rev.* **2015**, *43* (4), 222–230.
(214) Nistal, M.; Gonzalez-Peramato, P.; De Miguel, M. P. Sertoli Cell Dedifferentiation in Human Cryptorchidism and Gender Reassignment Shows Similarities between Fetal Environmental and Adult Medical Treatment Estrogen and Antiandrogen Exposure. *Reprod. Toxicol.* **2013**, *42*, 172–179.
(215) Kodama, H.; Yamaguchi, R.; Fukuda, J.; Kasai, H.; Tanaka, T. Increased Oxidative Deoxyribonucleic Acid Damage in the Spermatozoa of Infertile Male Patients. *Fertil. Steril.* **1997**, *68* (3), 519–524.
(216) Campbell, J. M.; Lane, M.; Owens, J. A.; Bakos, H. W. Paternal Obesity Negatively Affects Male Fertility and Assisted Reproduction Outcomes: A Systematic Review and Meta-Analysis. *Reprod. Biomed. Online* **2015**, *31* (5), 593–604.
(217) Chavarro, J. E.; Toth, T. L.; Wright, D. L.; Meeker, J. D.; Hauser, R. Body Mass Index in Relation to Semen Quality, Sperm DNA Integrity, and Serum Reproductive Hormone Levels among Men Attending an Infertility Clinic. *Fertil. Steril.* **2010**, *93* (7), 2222–2231.
(218) MacDonald, A. A.; Herbison, G. P.; Showell, M.; Farquhar, C. M. The Impact of Body Mass Index on Semen Parameters and Reproductive Hormones in Human Males: A Systematic Review with Meta-Analysis. *Hum. Reprod. Update* **2010**, *16* (3), 293–311.
(219) Soubry, A.; Guo, L.; Huang, Z.; Hoyo, C.; Romanus, S.; Price, T.; Murphy, S. K. Obesity-Related DNA Methylation at Imprinted Genes in Human Sperm: Results from the TIEGER Study. *Clin. Epigenetics* **2016**, *8*, 51.
(220) López, P.; Castro, A.; Flórez, M.; Miranda, K.; Aranda, P.; Sánchez-González, C.; Llopis, J.; Arredondo, M. miR-155 and miR-122 Expression of Spermatozoa in Obese Subjects. *Front. Genet.* **2018**, *9*, 175.
(221) St-Pierre, J.; Hivert, M.-F.; Perron, P.; Poirier, P.; Guay, S.-P.; Brisson, D.; Bouchard, L. IGF2 DNA Methylation Is a Modulator of Newborn's Fetal Growth and Development. *Epigenetics* **2012**, *7* (10), 1125–1132.
(222) Cai, X.; Yin, Y.; Li, N.; Zhu, D.; Zhang, J.; Zhang, C.-Y.; Zen, K. Re-Polarization of Tumor-Associated Macrophages to pro-Inflammatory M1 Macrophages by microRNA-155. *J. Mol. Cell Biol.* **2012**, *4* (5), 341–343.

(223) Castoldi, M.; Vujic Spasic, M.; Altamura, S.; Elmén, J.; Lindow, M.; Kiss, J.; Stolte, J.; Sparla, R.; D'Alessandro, L. A.; Klingmüller, U.; et al. The Liver-Specific microRNA miR-122 Controls Systemic Iron Homeostasis in Mice. *J. Clin. Invest.* **2011**, *121* (4), 1386–1396.

(224) Bakos, H. W.; Mitchell, M.; Setchell, B. P.; Lane, M. The Effect of Paternal Diet-Induced Obesity on Sperm Function and Fertilization in a Mouse Model. *Int. J. Androl.* **2011**, *34* (5 Pt 1), 402–410.

(225) de Castro Barbosa, T.; Ingerslev, L. R.; Alm, P. S.; Versteyhe, S.; Massart, J.; Rasmussen, M.; Donkin, I.; Sjögren, R.; Mudry, J. M.; Vetterli, L.; et al. High-Fat Diet Reprograms the Epigenome of Rat Spermatozoa and Transgenerationally Affects Metabolism of the Offspring. *Mol Metab* **2016**, *5* (3), 184–197.

(226) Nowicka-Bauer, K.; Lepczynski, A.; Ozgo, M.; Kamieniczna, M.; Fraczek, M.; Stanski, L.; Olszewska, M.; Malcher, A.; Skrzypczak, W.; Kurpisz, M. K. Sperm Mitochondrial Dysfunction and Oxidative Stress as Possible Reasons for Isolated Asthenozoospermia. *J. Physiol. Pharmacol.* **2018**, *69* (3).

(227) Noguchi, T.; Koizumi, M.; Hayashi, S. Sustained Elongation of Sperm Tail Promoted by Local Remodeling of Giant Mitochondria in Drosophila. *Curr. Biol.* **2011**, *21* (10), 805–814.

(228) Penumathsa, S. V.; Thirunavukkarasu, M.; Koneru, S.; Juhasz, B.; Zhan, L.; Pant, R.; Menon, V. P.; Otani, H.; Maulik, N. Statin and Resveratrol in Combination Induces Cardioprotection against Myocardial Infarction in Hypercholesterolemic Rat. *J. Mol. Cell. Cardiol.* **2007**, *42* (3), 508–516.

(229) de Oliveira, F. A.; Costa, W. S.; B Sampaio, F. J.; Gregorio, B. M. Resveratrol Attenuates Metabolic, Sperm, and Testicular Changes in Adult Wistar Rats Fed a Diet Rich in Lipids and Simple Carbohydrates. *Asian J. Androl.* **2018**.

(230) Sawa, K.; Uematsu, T.; Korenaga, Y.; Hirasawa, R.; Kikuchi, M.; Murata, K.; Zhang, J.; Gai, X.; Sakamoto, K.; Koyama, T.; et al. Krebs Cycle Intermediates Protective against Oxidative Stress by Modulating the Level of Reactive Oxygen Species in Neuronal HT22 Cells. *Antioxidants (Basel)* **2017**, *6* (1).

(231) McPherson, N. O.; Fullston, T.; Aitken, R. J.; Lane, M. Paternal Obesity, Interventions, and Mechanistic Pathways to Impaired Health in Offspring. *Ann. Nutr. Metab.* **2014**, *64* (3-4), 231–238.

(232) Fullston, T.; Ohlsson Teague, E. M. C.; Palmer, N. O.; DeBlasio, M. J.; Mitchell, M.; Corbett, M.; Print, C. G.; Owens, J. A.; Lane, M. Paternal Obesity Initiates Metabolic Disturbances in Two Generations of Mice with Incomplete Penetrance to the F2 Generation and Alters the Transcriptional Profile of Testis and Sperm microRNA Content. *FASEB J.* **2013**, *27* (10), 4226–4243.

(233) Ornellas, F.; Carapeto, P. V.; Mandarim-de-Lacerda, C. A.; Aguila, M. B. Obese Fathers Lead to an Altered Metabolism and Obesity in Their Children in Adulthood: Review of Experimental and Human Studies. *J. Pediatr.* **2017**, *93* (6), 551–559.

(234) Frost, R. J. A.; Olson, E. N. Control of Glucose Homeostasis and Insulin Sensitivity by the Let-7 Family of microRNAs. *Proc. Natl. Acad. Sci. U. S. A.* **2011**, *108* (52), 21075–21080.

(235) Morris, A. J.; Smyth, S. S. Lipid Phosphate Phosphatases: More than One Way to Put the Brakes on LPA Signaling? *J. Lipid Res.* **2014**, *55* (11), 2195–2197.

(236) Lambrot, R.; Xu, C.; Saint-Phar, S.; Chountalos, G.; Cohen, T.; Paquet, M.; Suderman, M.; Hallett, M.; Kimmins, S. Low Paternal Dietary Folate Alters the Mouse Sperm Epigenome and Is Associated with Negative Pregnancy Outcomes. *Nat. Commun.* **2013**, *4*, 2889.

(237) Khera, A.; Vanderlelie, J. J.; Holland, O.; Perkins, A. V. Overexpression of Endogenous Anti-Oxidants with Selenium Supplementation Protects Trophoblast Cells from Reactive Oxygen Species-Induced Apoptosis in a Bcl-2-Dependent Manner. *Biol. Trace Elem. Res.* **2016**.

(238) Traditional rodent diets | Envigo https://www.envigo.com/products-services/teklad/laboratory-animal-diets/natural-ingredient/rodent/traditional-diets.aspx (accessed Sep 20, 2018).

(239) D12492 Formula - OpenSource Diets - Search Formulas - Research Diets, Inc https://researchdiets.com/formulas/d12492 (accessed Sep 20, 2018).

(240) Ayala, J. E.; Samuel, V. T.; Morton, G. J.; Obici, S.; Croniger, C. M.; Shulman, G. I.; Wasserman, D. H.; McGuinness, O. P.; NIH Mouse Metabolic Phenotyping Center Consortium. Standard Operating Procedures for Describing and Performing Metabolic Tests of Glucose Homeostasis in Mice. *Dis. Model. Mech.* **2010**, *3* (9-10), 525–534.

(241) Primer designing tool https://www.ncbi.nlm.nih.gov/tools/primer-blast/ (accessed Jul 7, 2018).

(242) PREMIER Biosoft. *Financial Times*.

(243) Nucleotide BLAST: Search nucleotide databases using a nucleotide query https://blast.ncbi.nlm.nih.gov/Blast.cgi?PROGRAM=blastn&PAGE_TYPE=BlastSearch&LINK_LOC=blasthome (accessed Jul 7, 2018).

(244) Gene Quantification on the LightCycler 480 System https://lifescience.roche.com/en_ca/articles/gene-quantification-on-the-lightcycler-480-system.html (accessed Aug 15, 2018).

(245) Melting Point Analysis with the LightCycler® Carousel-Based System https://lifescience.roche.com/en_ca/articles/melting-point-analysis-with-the-lightcycler-carousel-based-system.html (accessed Aug 15, 2018).

(246) Nuclear Protein Extraction Without the Use of Detergent Protocol https://www.sigmaaldrich.com/technical-documents/protocols/biology/nuclear-protein-extraction.html (accessed Jul 4, 2018).

(247) Samson, S. L.; Garber, A. J. Metabolic Syndrome. *Endocrinol. Metab. Clin. North Am.* **2014**, *43* (1), 1–23.

(248) Lombardo, G. E.; Lepore, S. M.; Morittu, V. M.; Arcidiacono, B.; Colica, C.; Procopio, A.; Maggisano, V.; Bulotta, S.; Costa, N.; Mignogna, C.; et al. Effects of Oleacein on High-Fat Diet-Dependent Steatosis, Weight Gain, and Insulin Resistance in Mice. *Front. Endocrinol.* **2018**, *9*, 116.

(249) Matthews, D. R.; Hosker, J. P.; Rudenski, A. S.; Naylor, B. A.; Treacher, D. F.; Turner, R. C. Homeostasis Model Assessment: Insulin Resistance and Beta-Cell Function from Fasting Plasma Glucose and Insulin Concentrations in Man. *Diabetologia* **1985**, *28* (7), 412–419.

(250) Wallace, T. M.; Levy, J. C.; Matthews, D. R. Use and Abuse of HOMA Modeling. *Diabetes Care* **2004**, *27* (6), 1487–1495.

(251) Hu, X.; Li, J.; Zhang, Q.; Zheng, L.; Wang, G.; Zhang, X.; Zhang, J.; Gu, Q.; Ye, Y.;

Guo, S.-W.; et al. Phosphoinositide 3-Kinase (PI3K) Subunit p110δ Is Essential for Trophoblast Cell Differentiation and Placental Development in Mouse. *Sci. Rep.* **2016**, *6*, 28201.

(252) Fraccaroli, L.; Grasso, E.; Hauk, V.; Paparini, D.; Soczewski, E.; Mor, G.; Pérez Leirós, C.; Ramhorst, R. VIP Boosts Regulatory T Cell Induction by Trophoblast Cells in an in Vitro Model of Trophoblast-Maternal Leukocyte Interaction. *J. Leukoc. Biol.* **2015**, *98* (1), 49–58.

(253) Fedorova, L.; Gatto-Weis, C.; Smaili, S.; Khurshid, N.; Shapiro, J. I.; Malhotra, D.; Horrigan, T. Down-Regulation of the Transcription Factor Snail in the Placentas of Patients with Preeclampsia and in a Rat Model of Preeclampsia. *Reprod. Biol. Endocrinol.* **2012**, *10*, 15.

(254) Wang, X.; Zhang, Z.; Zeng, X.; Wang, J.; Zhang, L.; Song, W.; Shi, Y. Wnt/β-Catenin Signaling Pathway in Severe Preeclampsia. *J. Mol. Histol.* **2018**, *49* (3), 317–327.

(255) Shi, Z.-Y.; Deng, J.-X.; Fu, S.; Wang, L.; Wang, Q.; Liu, B.; Li, Y.-Q.; Deng, J.-B. Protective Effect of Autophagy in Neural Ischemia and Hypoxia: Negative Regulation of the Wnt/β-Catenin Pathway. *Int. J. Mol. Med.* **2017**, *40* (6), 1699–1708.

(256) Park, Y.-K.; Park, B.; Lee, S.; Choi, K.; Moon, Y.; Park, H. Hypoxia-Inducible Factor-2α-Dependent Hypoxic Induction of Wnt10b Expression in Adipogenic Cells. *J. Biol. Chem.* **2013**, *288* (36), 26311–26322.

(257) Saben, J.; Lindsey, F.; Zhong, Y.; Thakali, K.; Badger, T. M.; Andres, A.; Gomez-Acevedo, H.; Shankar, K. Maternal Obesity Is Associated with a Lipotoxic Placental Environment. *Placenta* **2014**, *35* (3), 171–177.

(258) Villalobos-Labra, R.; Sáez, P. J.; Subiabre, M.; Silva, L.; Toledo, F.; Westermeier, F.; Pardo, F.; Farías, M.; Sobrevia, L. Pre-Pregnancy Maternal Obesity Associates with Endoplasmic Reticulum Stress in Human Umbilical Vein Endothelium. *Biochim. Biophys. Acta* **2018**.

(259) Leibowitz, B.; Yu, J. Mitochondrial Signaling in Cell Death via the Bcl-2 Family. *Cancer Biol. Ther.* **2010**, *9* (6), 417–422.

(260) Hosny, G.; Ismail, W.; Makboul, R.; Badary, F. A. M.; Sotouhy, T. M. M. Increased Glomerular Bax/Bcl2 Ratio Is Positively Correlated with Glomerular Sclerosis in Lupus Nephritis. *Pathophysiology* **2018**.

(261) McIlwain, D. R.; Berger, T.; Mak, T. W. Caspase Functions in Cell Death and Disease. *Cold Spring Harb. Perspect. Biol.* **2013**, *5* (4), a008656.

(262) Westerberg, C. M.; Hägglund, H.; Nilsson, G. Proteasome Inhibition Upregulates Bim and Induces Caspase-3-Dependent Apoptosis in Human Mast Cells Expressing the Kit D816V Mutation. *Cell Death Dis.* **2012**, *3*, e417.

(263) Mandò, C.; Tabano, S.; Pileri, P.; Colapietro, P.; Marino, M. A.; Avagliano, L.; Doi, P.; Bulfamante, G.; Miozzo, M.; Cetin, I. SNAT2 Expression and Regulation in Human Growth-Restricted Placentas. *Pediatr. Res.* **2013**, *74* (2), 104–110.

(264) Handwerger, S.; Freemark, M. The Roles of Placental Growth Hormone and Placental Lactogen in the Regulation of Human Fetal Growth and Development. *J. Pediatr. Endocrinol. Metab.* **2000**, *13* (4), 343–356.

(265) Roberts, C. T.; Owens, J. A.; Sferruzzi-Perri, A. N. Distinct Actions of Insulin-like Growth Factors (IGFs) on Placental Development and Fetal Growth: Lessons from Mice and Guinea Pigs. *Placenta* **2008**, *29 Suppl A*, S42–S47.

(266) Schofield, C. J.; Ratcliffe, P. J. Oxygen Sensing by HIF Hydroxylases. *Nat. Rev. Mol. Cell Biol.* **2004**, *5* (5), 343–354.
(267) Fonken, L. K.; Lieberman, R. A.; Weil, Z. M.; Nelson, R. J. Dim Light at Night Exaggerates Weight Gain and Inflammation Associated with a High-Fat Diet in Male Mice. *Endocrinology* **2013**, *154* (10), 3817–3825.
(268) Sun, Q.; Xiao, X.; Kim, Y.; Kim, D.; Yoon, K. S.; Clark, J. M.; Park, Y. Imidacloprid Promotes High Fat Diet-Induced Adiposity and Insulin Resistance in Male C57BL/6J Mice. *J. Agric. Food Chem.* **2016**, *64* (49), 9293–9306.
(269) Howell, G. E.; Mulligan, C.; Meek, E.; Chambers, J. E. Effect of Chronic P,p′-Dichlorodiphenyldichloroethylene (DDE) Exposure on High Fat Diet-Induced Alterations in Glucose and Lipid Metabolism in Male C57BL/6H Mice. *Toxicology* **2015**, *328*, 112–122.
(270) Sallmén, M.; Sandler, D. P.; Hoppin, J. A.; Blair, A.; Baird, D. D. Reduced Fertility among Overweight and Obese Men. *Epidemiology* **2006**, *17* (5), 520–523.
(271) Jensen, T. K.; Andersson, A.-M.; Jørgensen, N.; Andersen, A.-G.; Carlsen, E.; Petersen, J. H.; Skakkebaek, N. E. Body Mass Index in Relation to Semen Quality and Reproductive Hormones among 1,558 Danish Men. *Fertil. Steril.* **2004**, *82* (4), 863–870.
(272) Bieniek, J. M.; Kashanian, J. A.; Deibert, C. M.; Grober, E. D.; Lo, K. C.; Brannigan, R. E.; Sandlow, J. I.; Jarvi, K. A. Influence of Increasing Body Mass Index on Semen and Reproductive Hormonal Parameters in a Multi-Institutional Cohort of Subfertile Men. *Fertil. Steril.* **2016**, *106* (5), 1070–1075.
(273) Mitchell, M.; Bakos, H. W.; Lane, M. Paternal Diet-Induced Obesity Impairs Embryo Development and Implantation in the Mouse. *Fertil. Steril.* **2011**, *95* (4), 1349–1353.
(274) Fabian, D.; Babeľová, J.; Čikoš, Š.; Šefčíková, Z. Overweight Negatively Affects Outcome of Superovulation Treatment in Female Mice. *Zygote* **2017**, *25* (6), 751–759.
(275) Weinerman, R.; Ord, T.; Bartolomei, M. S.; Coutifaris, C.; Mainigi, M. The Superovulated Environment, Independent of Embryo Vitrification, Results in Low Birthweight in a Mouse Model. *Biol. Reprod.* **2017**, *97* (1), 133–142.
(276) Huffman, S. R.; Pak, Y.; Rivera, R. M. Superovulation Induces Alterations in the Epigenome of Zygotes, and Results in Differences in Gene Expression at the Blastocyst Stage in Mice. *Mol. Reprod. Dev.* **2015**, *82* (3), 207–217.
(277) Krackow, S.; Gruber, F. Sex Ratio and Litter Size in Relation to Parity and Mode of Conception in Three Inbred Strains of Mice. *Lab. Anim.* **1990**, *24* (4), 345–352.
(278) Ali, L. E.; Salih, M. M.; Elhassan, E. M.; Mohmmed, A. A.; Adam, I. Placental Growth Factor, Vascular Endothelial Growth Factor, and Hypoxia-Inducible Factor-1α in the Placentas of Women with Pre-Eclampsia. *J. Matern. Fetal. Neonatal Med.* **2018**, 1–5.
(279) Rathmell, W. K.; Chen, S. VHL Inactivation in Renal Cell Carcinoma: Implications for Diagnosis, Prognosis and Treatment. *Expert Rev. Anticancer Ther.* **2008**, *8* (1), 63–73.
(280) Ferrara, N.; Gerber, H.-P.; LeCouter, J. The Biology of VEGF and Its Receptors. *Nat. Med.* **2003**, *9* (6), 669–676.
(281) Kasprzak, A.; Surdacka, A.; Tomczak, M.; Przybyszewska, W.; Seraszek-Jaros, A.; Malkowska-Lanzafame, A.; Siodla, E.; Kaczmarek, E. Expression of Angiogenesis-Stimulating Factors (VEGF, CD31, CD105) and Angiogenetic Index in Gingivae of Patients with Chronic Periodontitis. *Folia Histochem. Cytobiol.* **2012**, *50* (4), 554–564.

(282) Taylor, B. D.; Ness, R. B.; Klebanoff, M. A.; Tang, G.; Roberts, J. M.; Hougaard, D. M.; Skogstrand, K.; Haggerty, C. L. The Impact of Female Fetal Sex on Preeclampsia and the Maternal Immune Milieu. *Pregnancy Hypertens.* **2018**, *12*, 53–57.
(283) Shiozaki, A.; Matsuda, Y.; Satoh, S.; Saito, S. Impact of Fetal Sex in Pregnancy-Induced Hypertension and Preeclampsia in Japan. *J. Reprod. Immunol.* **2011**, *89* (2), 133–139.
(284) Elsmén, E.; Källén, K.; Marsál, K.; Hellström-Westas, L. Fetal Gender and Gestational-Age-Related Incidence of Pre-Eclampsia. *Acta Obstet. Gynecol. Scand.* **2006**, *85* (11), 1285–1291.
(285) Global Pregnancy Collaboration:; Schalekamp-Timmermans, S.; Arends, L. R.; Alsaker, E.; Chappell, L.; Hansson, S.; Harsem, N. K.; Jälmby, M.; Jeyabalan, A.; Laivuori, H.; et al. Fetal Sex-Specific Differences in Gestational Age at Delivery in Pre-Eclampsia: A Meta-Analysis. *Int. J. Epidemiol.* **2017**, *46* (2), 632–642.
(286) Baun, M.; Hay-Schmidt, A.; Edvinsson, L.; Olesen, J.; Jansen-Olesen, I. Pharmacological Characterization and Expression of VIP and PACAP Receptors in Isolated Cranial Arteries of the Rat. *Eur. J. Pharmacol.* **2011**, *670* (1), 186–194.
(287) Choi, H.-K.; Choi, B. C.; Lee, S.-H.; Kim, J. W.; Cha, K. Y.; Baek, K.-H. Expression of Angiogenesis- and Apoptosis-Related Genes in Chorionic Villi Derived from Recurrent Pregnancy Loss Patients. *Mol. Reprod. Dev.* **2003**, *66* (1), 24–31.
(288) Chen, J.; Khalil, R. A. Matrix Metalloproteinases in Normal Pregnancy and Preeclampsia. *Prog. Mol. Biol. Transl. Sci.* **2017**, *148*, 87–165.
(289) Binet, F.; Sapieha, P. ER Stress and Angiogenesis. *Cell Metab.* **2015**, *22* (4), 560–575.
(290) Milkiewicz, M.; Hudlicka, O.; Shiner, R.; Egginton, S.; Brown, M. D. Vascular Endothelial Growth Factor mRNA and Protein Do Not Change in Parallel during Non-Inflammatory Skeletal Muscle Ischaemia in Rat. *J. Physiol.* **2006**, *577* (Pt 2), 671–678.
(291) Forsythe, J. A.; Jiang, B. H.; Iyer, N. V.; Agani, F.; Leung, S. W.; Koos, R. D.; Semenza, G. L. Activation of Vascular Endothelial Growth Factor Gene Transcription by Hypoxia-Inducible Factor 1. *Mol. Cell. Biol.* **1996**, *16* (9), 4604–4613.
(292) Wong, M. K.; Nicholson, C. J.; Holloway, A. C.; Hardy, D. B. Maternal Nicotine Exposure Leads to Impaired Disulfide Bond Formation and Augmented Endoplasmic Reticulum Stress in the Rat Placenta. *PLoS One* **2015**, *10* (3), e0122295.
(293) Wang, M.; Wey, S.; Zhang, Y.; Ye, R.; Lee, A. S. Role of the Unfolded Protein Response Regulator GRP78/BiP in Development, Cancer, and Neurological Disorders. *Antioxid. Redox Signal.* **2009**, *11* (9), 2307–2316.
(294) Wu, W.-S.; Chien, C.-C.; Chen, Y.-C.; Chiu, W.-T. Protein Kinase RNA-Like Endoplasmic Reticulum Kinase-Mediated Bcl-2 Protein Phosphorylation Contributes to Evodiamine-Induced Apoptosis of Human Renal Cell Carcinoma Cells. *PLoS One* **2016**, *11* (8), e0160484.
(295) Sasabe, E.; Tatemoto, Y.; Li, D.; Yamamoto, T.; Osaki, T. Mechanism of HIF-1alpha-Dependent Suppression of Hypoxia-Induced Apoptosis in Squamous Cell Carcinoma Cells. *Cancer Sci.* **2005**, *96* (7), 394–402.
(296) Choi, S. H.; Park, J. Y. Erratum to: Regulation of the Hypoxic Tumor Environment in Hepatocellular Carcinoma Using RNA Interference. *Cancer Cell Int.* **2017**, *17*, 69.
(297) Sabet, J. A.; Park, L. K.; Iyer, L. K.; Tai, A. K.; Koh, G. Y.; Pfalzer, A. C.; Parnell, L. D.; Mason, J. B.; Liu, Z.; Byun, A. J.; et al. Paternal B Vitamin Intake Is a Determinant of Growth, Hepatic Lipid Metabolism and Intestinal Tumor Volume in Female Apc1638N

Mouse Offspring. *PLoS One* **2016**, *11* (3), e0151579.
(298) Sanchez-Delgado, M.; Court, F.; Vidal, E.; Medrano, J.; Monteagudo-Sánchez, A.; Martin-Trujillo, A.; Tayama, C.; Iglesias-Platas, I.; Kondova, I.; Bontrop, R.; et al. Human Oocyte-Derived Methylation Differences Persist in the Placenta Revealing Widespread Transient Imprinting. *PLoS Genet.* **2016**, *12* (11), e1006427.
(299) Constância, M.; Hemberger, M.; Hughes, J.; Dean, W.; Ferguson-Smith, A.; Fundele, R.; Stewart, F.; Kelsey, G.; Fowden, A.; Sibley, C.; et al. Placental-Specific IGF-II Is a Major Modulator of Placental and Fetal Growth. *Nature* **2002**, *417* (6892), 945–948.
(300) Yang, B.; Wagner, J.; Damaschke, N.; Yao, T.; Wuerzberger-Davis, S. M.; Lee, M.-H.; Svaren, J.; Miyamoto, S.; Jarrard, D. F. A Novel Pathway Links Oxidative Stress to Loss of Insulin Growth Factor-2 (IGF2) Imprinting through NF-κB Activation. *PLoS One* **2014**, *9* (2), e88052.
(301) Miki, H.; Yamauchi, T.; Suzuki, R.; Komeda, K.; Tsuchida, A.; Kubota, N.; Terauchi, Y.; Kamon, J.; Kaburagi, Y.; Matsui, J.; et al. Essential Role of Insulin Receptor Substrate 1 (IRS-1) and IRS-2 in Adipocyte Differentiation. *Mol. Cell. Biol.* **2001**, *21* (7), 2521–2532.
(302) Siddle, K. Molecular Basis of Signaling Specificity of Insulin and IGF Receptors: Neglected Corners and Recent Advances. *Front. Endocrinol.* **2012**, *3*, 34.
(303) Bacus, S. S.; Altomare, D. A.; Lyass, L.; Chin, D. M.; Farrell, M. P.; Gurova, K.; Gudkov, A.; Testa, J. R. AKT2 Is Frequently Upregulated in HER-2/neu-Positive Breast Cancers and May Contribute to Tumor Aggressiveness by Enhancing Cell Survival. *Oncogene* **2002**, *21* (22), 3532–3540.
(304) Ueno, H.; Kondo, E.; Yamamoto-Honda, R.; Tobe, K.; Nakamoto, T.; Sasaki, K.; Mitani, K.; Furusaka, A.; Tanaka, T.; Tsujimoto, Y.; et al. Association of Insulin Receptor Substrate Proteins with Bcl-2 and Their Effects on Its Phosphorylation and Antiapoptotic Function. *Mol. Biol. Cell* **2000**, *11* (2), 735–746.
(305) Folkman, J. Angiogenesis and Apoptosis. *Semin. Cancer Biol.* **2003**, *13* (2), 159–167.
(306) Mardilovich, K.; Shaw, L. M. Hypoxia Regulates Insulin Receptor Substrate-2 Expression to Promote Breast Carcinoma Cell Survival and Invasion. *Cancer Res.* **2009**, *69* (23), 8894–8901.
(307) Copps, K. D.; White, M. F. Regulation of Insulin Sensitivity by Serine/threonine Phosphorylation of Insulin Receptor Substrate Proteins IRS1 and IRS2. *Diabetologia* **2012**, *55* (10), 2565–2582.
(308) Zhou, Y.; Yu, S.; Cai, C.; Zhong, L.; Yu, H.; Shen, W. LXRα Participates in the mTOR/S6K1/SREBP-1c Signaling Pathway during Sodium Palmitate-Induced Lipogenesis in HepG2 Cells. *Nutr. Metab.* **2018**, *15*, 31.
(309) Liu, H.; Zhong, H.; Leng, L.; Jiang, Z. Effects of Soy Isoflavone on Hepatic Steatosis in High Fat-Induced Rats. *J. Clin. Biochem. Nutr.* **2017**, *61* (2), 85–90.
(310) Jensen, M. N.; Ritskes-Hoitinga, M. How Isoflavone Levels in Common Rodent Diets Can Interfere with the Value of Animal Models and with Experimental Results. *Lab. Anim.* **2007**, *41* (1), 1–18.
(311) Andreoli, M. F.; Stoker, C.; Rossetti, M. F.; Alzamendi, A.; Castrogiovanni, D.; Luque, E. H.; Ramos, J. G. Withdrawal of Dietary Phytoestrogens in Adult Male Rats Affects Hypothalamic Regulation of Food Intake, Induces Obesity and Alters Glucose Metabolism. *Mol. Cell. Endocrinol.* **2015**, *401*, 111–119.

Chapter 9.0 Appendix

9.1 Supplemental figures and tables

Appendix Table 9.1.1: Control mouse dietary contents.

Macronutrients		
Crude Protein	%	22.0
Fat (ether extract) [a]	%	5.5
Carbohydrate (available) [b]	%	40.6
Crude Fiber	%	3.9
Neutral Detergent Fiber [c]	%	12.8
Ash	%	8.1
Energy Density [d]	kcal/g (kJ/g)	3.0 (12.6)
Calories from Protein	%	29
Calories from Fat	%	17
Calories from Carbohydrate	%	54
Minerals		
Calcium	%	1.1
Phosphorus	%	0.9
Non-Phytate Phosphorus	%	0.6
Sodium	%	0.4
Potassium	%	1.0
Chloride	%	0.7
Magnesium	%	0.2
Zinc	mg/kg	77
Manganese	mg/kg	102
Copper	mg/kg	24
Iodine	mg/kg	3
Iron	mg/kg	280
Selenium	mg/kg	0.27
Amino Acids		
Aspartic Acid	%	2.1
Glutamic Acid	%	3.6
Alanine	%	1.2
Glycine	%	1.1
Threonine	%	0.9
Proline	%	1.4
Serine	%	1.4
Leucine	%	1.7
Isoleucine	%	1.0
Valine	%	1.1
Phenylalanine	%	1.1
Tyrosine	%	0.9
Methionine	%	0.4
Cystine	%	0.3
Lysine	%	1.2
Histidine	%	0.6
Arginine	%	1.4
Tryptophan	%	0.3

Teklad Diets are designed and manufactured for research purposes only.

Standard Product Form: **Pellet**

Vitamins		
Vitamin A [e, f]	IU/g	15.8
Vitamin D_3 [e, g]	IU/g	3.0
Vitamin E	IU/kg	150
Vitamin K_3 (menadione)	mg/kg	50
Vitamin B_1 (thiamin)	mg/kg	32
Vitamin B_2 (riboflavin)	mg/kg	9
Niacin (nicotinic acid)	mg/kg	66
Vitamin B_6 (pyridoxine)	mg/kg	14
Pantothenic Acid	mg/kg	23
Vitamin B_{12} (cyanocobalamin)	mg/kg	0.06
Biotin	mg/kg	0.41
Folate	mg/kg	3
Choline	mg/kg	2380
Fatty Acids		
C16:0 Palmitic	%	0.7
C18:0 Stearic	%	0.2
C18:1ω9 Oleic	%	1.1
C18:2ω6 Linoleic	%	2.5
C18:3ω3 Linolenic	%	0.2
Total Saturated	%	0.9
Total Monounsaturated	%	1.2
Total Polyunsaturated	%	2.7
Other		
Cholesterol	mg/kg	30

[a] Ether extract is used to measure fat in pelleted diets, while an acid hydrolysis method is required to recover fat in extruded diets. Compared to ether extract, the fat value for acid hydrolysis will be approximately 1% point higher.

[b] Carbohydrate (available) is calculated by subtracting neutral detergent fiber from total carbohydrates.

[c] Neutral detergent fiber is an estimate of insoluble fiber, including cellulose, hemicellulose, and lignin. Crude fiber methodology underestimates total fiber.

[d] Energy density is a calculated estimate of *metabolizable energy* based on the Atwater factors assigning 4 kcal/g to protein, 9 kcal/g to fat, and 4 kcal/g to available carbohydrate.

[e] Indicates added amount but does not account for contribution from other ingredients.

[f] 1 IU vitamin A = 0.3 µg retinol

[g] 1 IU vitamin D = 25 ng cholecalciferol

For nutrients not listed, insufficient data is available to quantify.

Nutrient data represent the best information available, calculated from published values and direct analytical testing of raw materials and finished product. Nutrient values may vary due to the natural variations in the ingredients, analysis, and effects of processing.

0915

Appendix Table 9.1.2: High fat mouse dietary contents.

Product #	D12492	
	gm%	*kcal%*
Protein	26	*20.0*
Carbohydrate	26	*20.0*
Fat	35	*60.0*
Total		*100.0*
kcal/gm	5.24	
Ingredient	**gm**	***kcal***
Casein, 30 Mesh	200	*800*
L-Cystine	3	*12*
Corn Starch	0	*0*
Maltodextrin 10	125	*500*
Sucrose	68.8	*275*
Cellulose, BW200	50	*0*
Soybean Oil	25	*225*
Lard	245	*2205*
Mineral Mix S10026	10	*0*
DiCalcium Phosphate	13	*0*
Calcium Carbonate	5.5	*0*
Potassium Citrate, 1 H2O	16.5	*0*
Vitamin Mix V10001	10	*40*
Choline Bitartrate	2	*0*
FD&C Red Dye #40	0	*0*
FD&C Blue Dye #1	0.05	*0*
Total	**773.85**	***4057***

* Typical analysis of cholesterol in lard = 72 mg per 100 gram.

D12451
Cholesterol (mg)/4057 kcal = 167.8
Cholesterol (mg)/kg = 195.5

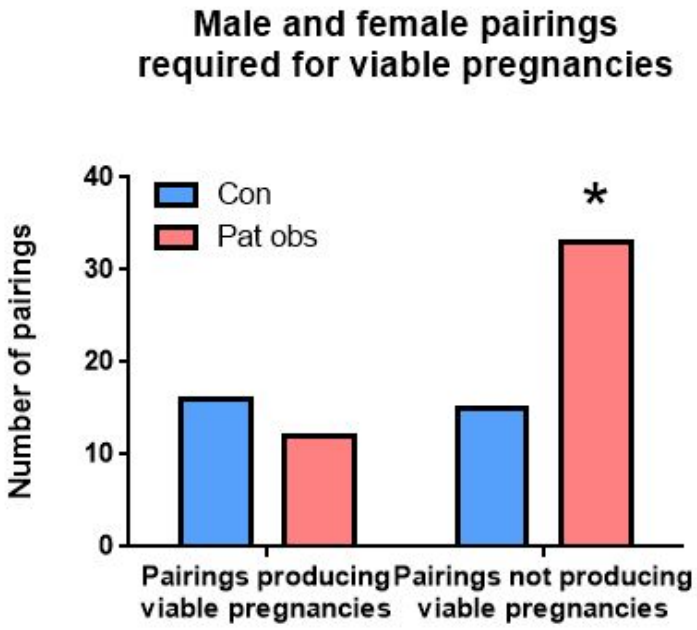

Appendix Figure 9.1.1: Paternal obesity is associated with increased number of matings required to produce similar numbers of viable pregnancies. Male mice were mated with control-fed females, and pairings were classified as producing a viable pregnancy, or not. Data are presented as total number of pairings across all males of each group. * denotes $p<0.05$, after Fisher's exact test was used to compare data between groups. Control-fed males (Con, n=15, blue), HF-fed males (Pat obs, n=15, pink).

9.2 Awards

FHS Research Plenary Excellence in Oral Presentation Award

McMaster University, Hamilton, ON, May 2018

9.3 Conference presentations

Presented a poster titled "Maternal and Paternal obesity negatively influence placental development in a sex-specific manner in mice" at the Southern Ontario Reproductive Biology Conference held in April 2016 at Queen's University, Kingston, ON

Abstract accepted for an oral presentation titled "The effects of paternal obesity on fetoplacental development" at the 4th annual Canadian National Perinatal Research Meeting held in February 2017 at the Fairmont hotel, Montebello, QC

Presented a poster titled "Paternal obesity reduces Bcl2-mediated apoptosis in term placentae in a murine model" at the Faculty of Health Sciences Research Plenary held in May 2017 at McMaster University, Hamilton, ON

Presented a poster titled "Paternal obesity reduces Bcl2-mediated apoptosis in term placentae in a murine model" at the Southern Ontario Reproductive Biology Conference held in April 2017 at Western University, London, ON

Gave an oral presentation titled "Paternal obesity disrupts placental development and is associated with fetal hepatic ER stress in a murine model" at the 5th annual Canadian National Perinatal Research Meeting held in February 2018 at the Banff Centre, Banff, AB

Gave an oral presentation titled “Paternal obesity impairs fetal liver development and is associated with ER stress in a mouse model at mid-gestation” at the Faculty of Health Sciences Research Plenary held in May 2018 at McMaster University, Hamilton, ON